

Aus dem Pharmakologischen Institut
Geschäftsführender Direktor: Prof. Dr. Thomas Worzfeld
des Fachbereichs Medizin der Philipps-Universität Marburg

Expression and Function of Plexin-B Ligands in the Intestinal Epithelium

Inaugural-Dissertation zur Erlangung des Doktorgrades
der Naturwissenschaften (Dr. rer. nat.)
dem Fachbereich Medizin der Philipps-Universität Marburg
vorgelegt von

Florian Till Hub aus Schwäbisch Hall

Marburg, 2020

Angenommen vom Fachbereich Medizin der Philipps-Universität Marburg
am: 04.11.2020

Gedruckt mit Genehmigung des Fachbereichs.

Dekan i.V. der Prodekan: Prof. Dr. R. Müller

Referent: Prof. Dr. T. Worzfeld

1. Korreferent: Prof. Dr. R. Jacob

Table of Contents

List of Figures.....	x
List of Tables	xii
Summary.....	1
Zusammenfassung.....	2
1 Introduction.....	3
1.1 The gastrointestinal tract	3
1.1.1 Anatomy and function of the small and large intestine.....	3
1.1.2 The intestinal epithelium	4
1.1.3 Colorectal cancer.....	9
1.2 The semaphorin-plexin system.....	10
1.2.1 Ligands of the semaphorin-plexin system.....	11
1.2.2 Plexins.....	16
1.3 Use of the Cre- <i>loxP</i> system to study cell type-specific gene function in the intestine.....	18
1.3.1 Bacterial artificial chromosome recombination	19
1.4 The intestinal organoid model.....	21
2 Aim of the study.....	23
3 Materials	24
3.1 Laboratory consumables	24
3.2 Technical equipment and devices.....	24
3.3 Cell culture.....	25
3.4 Chemicals.....	26
3.5 Kits.....	28
3.6 Bacteria	29
3.7 PCR and cloning reagents.....	29
3.8 Enzymes.....	29
3.9 Plasmids	30
3.10 Bacterial artificial chromosomes	31
3.11 Oligonucleotides	31
3.12 Primary antibodies	34
3.13 Secondary antibodies	34
3.14 smRNA FISH probes	34

3.15	Buffers and solutions	35
3.15.1	Bacterial media	35
3.15.2	Plasmid and BAC DNA	36
3.15.3	<i>lacZ</i> reporter staining solutions	37
3.15.4	Immunostaining and FISH solutions	38
3.15.5	Cell culture media and solutions	38
3.15.6	Organoid culture media and solutions	39
4	Methods	43
4.1	Cell culture	43
4.1.1	Mouse intestinal crypt isolation and culture	43
4.1.2	Human intestinal crypt isolation and culture	44
4.1.3	Organoid passaging	45
4.1.4	Organoid freezing and thawing	46
4.1.5	Lentiviral transduction of intestinal organoids	46
4.1.6	Functional organoid experiments	48
4.1.7	Cultivation of cell lines	48
4.2	Molecular biology techniques	50
4.2.1	Plasmid cloning of shRNA constructs	50
4.2.2	Recombination of bacterial artificial chromosomes	52
4.2.3	Bacterial cultures	58
4.2.4	Preparation of electrocompetent bacteria	59
4.2.5	Electroporation of plasmid DNA into bacteria	59
4.2.6	Colony PCR	59
4.2.7	Plasmid and BAC DNA isolation	60
4.2.8	Diagnostic restriction digests of BACs	61
4.2.9	RNA isolation	62
4.2.10	Real-time quantitative polymerase chain reaction	62
4.2.11	Dual-luciferase assay	64
4.3	Histological and immunohistochemical methods	66
4.3.1	Swiss rolling of small Intestine and colon samples	66
4.3.2	Preparation of cryosections	66
4.3.3	Preparation of paraffin sections	67
4.3.4	<i>lacZ</i> reporter staining	68
4.3.5	Immunofluorescence staining	68

4.3.6	Single-molecule RNA fluorescence <i>in situ</i> hybridization	69
4.4	Imaging techniques.....	71
4.4.1	Imaging and quantification of IF stainings and smRNA-FISH	71
4.4.2	Live cell imaging of intestinal organoids	72
4.4.3	Computational analysis of organoid images	72
4.4.4	Statistical analysis of imaging data	72
4.5	Single cell RNA sequencing data and analysis.....	73
5	Results.....	74
5.1	Expression analysis of semaphorins and plexins in the intestinal epithelium.....	74
5.1.1	Sema4A, 4B, 4C and angiogenin are expressed in the intestinal epithelium	74
5.1.2	Sema4B and 4D display distinct expression patterns	77
5.1.3	Sema4A, 4G and angiogenin expression partially overlaps in the intestine	78
5.1.4	Plexin B1 is expressed in the entire intestinal epithelium	82
5.1.5	scRNA sequencing of human intestinal epithelial cells confirms expression analysis in mouse tissues.....	83
5.2	Generation of a novel <i>Alpi-Cre2</i> BAC through homologous BAC recombination	87
5.2.1	A <i>Cre2</i> cassette was recombined into the <i>Alpi</i> gene of a BAC	87
5.2.2	Preparation of the <i>Alpi-Cre2</i> BAC for oocyte injection	90
5.2.3	<i>Cre</i> recombinase is expressed and functional in transgenic <i>Alpi-Cre2⁺ mT/mG⁺</i> reporter mice	90
5.3	Function of class 4 semaphorins and B-plexins in the intestinal epithelium	93
5.3.1	<i>Sema4B</i> single knockout and <i>plexin B1/B2</i> double knockout organoids display intestinal stem cell defects	93
5.3.2	Lowered <i>Lgr5</i> expression in the intestines of angiogenin knockout mice points to a possible loss of stem cells	96
5.4	Establishment of lentiviral transductions of intestinal organoids	97
5.4.1	shRNA-mediated knockdown in organoids is a powerful tool to study gene function	100

5.4.2	Semaphorin 4A shRNAi reduces expression in CMT-93, but not murine intestinal organoids	106
5.5	Establishment of human colonic organoid cultures from normal and tumor tissue.....	108
6	Discussion	111
6.1	Potential redundant and non-redundant functions of B-plexins and their ligands in the intestinal epithelium	111
6.2	Generating mouse lines through BAC recombination	120
6.3	Intestinal organoids in the study of intestinal epithelial function.....	123
	References	i
	Academic Teachers.....	xxi
	Danksagung	xxii

List of Abbreviations

2D.....	Two-dimensional
3D.....	Three-dimensional
ALPI	alkaline phosphatase, intestinal
ANG	angiogenin
APC.....	APC regulator of WNT signaling pathway
ASCL2.....	achaete-scute complex homolog 2
ATOH1	atonal bHLH transcription factor 1
BAC	Bacterial artificial chromosome
BBS	BES-buffered saline
BMI1	polycomb protein B lymphoma Mo-MLV insertion region 1 homolog
BMP	bone morphogenetic protein
BSA	Bovine serum albumin
CBC.....	Crypt base columnar cell
CCS.....	Crypt chelation solution
CHGA.....	Chromogranin-A
CRC	Colorectal cancer
DAB.....	3,3'-Diaminobenzidine, 3,3'-Diaminobenzidine
DCLK1.....	doublecortin-like kinase 1
DEPC	Diethyl pyrocarbonate
DKO	Double knockout
DLL1.....	delta-like canonical notch ligand 1
DLL4.....	delta-like canonical notch ligand 4
DMEM	Dulbecco's modified eagle medium
DMSO	Dimethylsulfoxide
DSB.....	Double-strand-breaks
EDOF	Extended depth of field
EDTA.....	Ethylene diamine tetraacetic acid disodium salt dihydrate
EEC	Enteroendocrine cell
EGF	epidermal growth factor
EGTA	Ethylene glycol tetraacetic acid
EMT.....	Epithelial-to-mesenchymal transition
FAP	Familial adenomatous polyposis

FBS	Fetal bovine serum, Fetal bovine serum
FGF	Fibroblast growth factor
FLP	Flippase
FRT	Flippase recognition target
GAP	GTPase-activating protein
GFP	Green fluorescent protein
GI	Gastrointestinal
HEK-293T	Human embryonic kidney 293T
HES1	hes family bHLH transcription factor 1
HNPCC	Hereditary non-polyposis colorectal cancer
HOPX	homeobox-only protein
IF	Immunofluorescence
IGF-1	Insulin-like growth factor 1
IRES	Internal ribosomal entry sites
ISC	Intestinal stem cell
KGF-1	keratinocyte growth factor-1
LAS X	Leica Application Suite X
LB	Lysogeny broth
LGR5	leucin-rich-repeat-containing G-protein-coupled receptor 5
LSM	Laser scanning microscope
LYZ1	lysozyme
Muc2	mucin-2
OLFM4	olfactomedin 4
PBS	Phosphate buffered saline
PCI	Phenol-chloroform-isoamyl alcohol
PDTX	Patient-derived tumor xenografts
PFA	Paraformaldehyde
PGE-2	Prostaglandin E2
PLXNB1	plexin B1
PLXNB2	plexin B2
PSI	Plexin-semaphorin-integrin
RBD	RHO-GTPase-binding domain
rISC	Reserve intestinal stem cell
rRNA	Ribosomal RNA

scRNA	Single cell RNA
SDS	Sodium dodecyl sulfate
Sema4A	semaphorin 4A
Sema4B	semaphorin 4B
Sema4C	semaphorin 4C
Sema4D	semaphorin 4D
Sema4G	semaphorin 4G
shRNA	Short hairpin RNA
SI	Small intestine
smRNA FISH	Single-molecule RNA fluorescence <i>in situ</i> hybridization
SOB	Super Optimal Broth
SOC	Super Optimal Broth with catabolite repression
TA	Transit-amplifying
TAM	Tumor-associated macrophage
TBST	Tris-buffered saline with Tween
T-PMT	Transmitted light photomultiplier
TRC	The RNAi Consortium
TTL	Tubulin tyrosine ligase
VEGF	vascular endothelial growth factor

List of Figures

Figure 1 The intestinal epithelium.....	5
Figure 2 Intestinal epithelial lineages.	7
Figure 3 Class 4 semaphorins, angiogenin and their plexin receptors.	11
Figure 4 Schematic of BAC recombination steps.	20
Figure 5 Structure of oligonucleotides used in shRNA cloning.	50
Figure 6 Schematic of BAC recombination steps.	53
Figure 7 Sepharose-based gel permeation chromatography column.	58
Figure 8 lacZ reporter stainings reveal ligand expression patterns in the small intestine.	75
Figure 9 lacZ reporter stainings reveal ligand expression patterns in the large intestine.	76
Figure 10 Immunofluorescence stainings of Sema4B and Sema4D.	77
Figure 11 Semaphorin 4A is widely expressed in both small and large intestine.	79
Figure 12 Semaphorin 4G is expressed in the TA zone.	80
Figure 13 Angiogenin is expressed weakly, but widespread.	81
Figure 14 Plexin B1 is widely expressed in both small and large intestine.	83
Figure 15 scRNA sequencing of human colonic epithelial cells reveal lineage-specific clusters.	84
Figure 16 Class 4 semaphorins and B-plexins are expressed in the human colonic epithelium.	86
Figure 17 Successful integration of the Cre2 insert by homologous recombination.	88
Figure 18 Successful removal of AmpR by FLPase recombination.	89
Figure 19 Preparation of the Alpi-Cre2 BAC for oocyte injection.	90
Figure 20 Basic principle of the mT/mG reporter locus.	91
Figure 21 Analysis of intestinal Alpi-Cre2 expression in mT/mG reporter mice.	92
Figure 22 Workflow of functional organoid experiments.	93
Figure 23 Intestinal stem cell function is reduced in Sema4B single knockout and plexin B1/B2 double knockout organoids.	94
Figure 24 RTqPCR reveals reduction of stem cells in angiogenin knockout tissue.	96

Figure 25 Lentiviral transductions of intestinal organoids.....	97
Figure 26 Lentiviral transduction yields a high number of transduced intestinal organoids.....	99
Figure 27 TTL expression is reduced in shTTL-expressing intestinal organoids.	100
Figure 28 TTL knockdown strikingly changes intestinal organoid morphology.	101
Figure 29 Knockdown of TTL reduces intestinal organoid size.	102
Figure 30 Morphological complexity of TTL knockdown organoids is reduced.	103
Figure 31 Expression analysis of intestinal epithelial marker genes in TTL knockdown organoids.....	105
Figure 32 Lentiviral shSema4A constructs reduce Sema4A mRNA expression in CMT-93, but not intestinal organoids.....	107
Figure 33 Establishment of human colonic organoid cultures.	108
Figure 34 Ligands display distinct expression patterns in the intestinal epithelium.	112

List of Tables

Table 1 Laboratory consumables	24
Table 2 Technical equipment and devices	24
Table 3 Cell culture materials	25
Table 4 Chemicals.....	26
Table 5 Kits	28
Table 6 Bacterial strains.....	29
Table 7 PCR and cloning reagents.....	29
Table 8 Enzymes.....	29
Table 9 Plasmids.....	30
Table 10 Bacterial artificial chromosomes	31
Table 11 PCR and sequencing primers.....	31
Table 12 RTqPCR primers	32
Table 13 shRNA plasmid cloning inserts.....	33
Table 14 Primary antibodies.....	34
Table 15 Secondary antibodies	34
Table 16 smRNA FISH probes	34
Table 17 Bacterial antibiotic stock solutions.....	36
Table 18 Medium compositions used in conditioned media production.....	39
Table 19 shRNA oligonucleotide annealing reaction	51
Table 20 Linearization reaction of LT3GEPIR for shRNA cloning	51
Table 21 shRNA oligonucleotide ligation reaction	51
Table 22 BAC linearization reaction	57
Table 23 Working concentrations of bacterial antibiotics.....	58
Table 24 Colony PCR master mix	60
Table 25 Colony PCR protocol	60
Table 26 Diagnostic BAC digest.....	61
Table 27 Reverse transcription master mix	62
Table 28 Reverse transcription thermocycler protocol	63
Table 29 RTqPCR master mix.....	63
Table 30 RTqPCR protocol	63
Table 31 Plasmid mixes for dual-luciferase assay reporter cell transfection	64

Summary

The gastrointestinal tract is of central importance, due to its role in digestion, nutrient uptake and as a first line of defense against microbial and parasitic food contaminants. The intestine is the longest section, in which these processes take place. Its inner lining, the intestinal epithelium is a complex tissue with highly diverse cell types. The cellular turnover is the fastest in the human body, the entire epithelium completely renews itself every 4 to 7 days. Consequently, intestinal epithelial proliferation and differentiation need to be carefully balanced to maintain homeostasis, a process in which intestinal stem cells play a crucial role. Once disturbed, a plethora of intestinal diseases develop, including colorectal cancers, which account for 10 % of new cancer cases every year. The semaphorin-plexin system consists of a family of ligands, the semaphorins and their corresponding receptors, the plexins. These molecules have been described to play an important role in epithelial homeostasis in other organs and are known to be involved in cancer development. Since plexins B1 and B2 are known to be expressed in the intestine, the expression of their class 4 semaphorin ligands and angiogenin in the intestinal epithelium was systematically analyzed. These experiments revealed the ligands to be expressed in partially overlapping patterns. Next, a bacterial artificial chromosome was constructed to express Cre under the enterocyte-specific *Alpi* promoter. This construct enabled the generation of a novel *Alpi-Cre* mouse line for future breeding of enterocyte-specific knockout mice. Studying stem cell function, intestinal crypts were isolated from *Plexin B1/B2* knockout mice and analyzed for their ability to form organoids. Organoid formation was reduced, pointing to a defect in stem cell function. To identify the relevant ligands, semaphorin knockout organoids were analyzed in the same manner, but failed to replicate the receptor knockout phenotype. To target multiple ligands simultaneously by inducible RNAi, a lentiviral transduction method was established for future organoid studies. To explore the role of semaphorins in human intestinal physiology and disease, colonic organoids from normal and tumor tissue samples of patients were established. These results precisely lay out the overlapping expression patterns of B-plexin ligands in the intestinal epithelium, highlight their redundancies, and enable further functional studies, including translational research in the human intestinal epithelium.

Zusammenfassung

Der Gastrointestinaltrakt ist aufgrund seiner Rolle in der Verdauung und Absorption von Nährstoffen und als erste Verteidigung gegen mikrobielle und parasitische Krankheitserreger von zentraler Wichtigkeit. Der Darm ist der längste Abschnitt und erfüllt diese Aufgaben. Sein Epithel ist ein komplexes Gewebe mit diversen Zelltypen, das sich in 4 bis 7 Tagen vollständig erneuert. Um dessen Homöostase zu wahren, müssen Proliferation und Differenzierung im Gleichgewicht sein, wobei die intestinalen Stammzellen eine zentrale Rolle spielen. Wird die Homöostase gestört, entwickeln sich Krankheiten, u. a. kolorektale Tumore, die jährlich 10 % aller neuen Krebserkrankungen ausmachen. Das Semaphorin-Plexin-System besteht aus einer Liganden-Familie, den Semaphorinen und deren Rezeptoren, den Plexinen. Dieses System ist ein Regulator epithelialer Homöostase in anderen Organen, sowie in der Tumorentstehung. Da Plexin B1 und B2 im Darm exprimiert sind, wurde die Expression relevanter Klasse-4-Semaphorin-Liganden, sowie von Angiogenin im Darmepithel systematisch analysiert. Hierbei wurden sich überschneidende Expressionsmuster entdeckt. Weiterhin wurde ein bakterielles artifizielles Chromosom konstruiert, um Cre-Rekombinase unter der Kontrolle des enterozyten-spezifischen *Alpi*-Promotors zu exprimieren. Dieses Konstrukt ermöglichte die Zucht eines neuen *Alpi-Cre* Mausstamms, mit dem Ziel, zukünftig enterozyten-spezifische Knockout-Mäuse zu generieren. Die Funktion intestinaler Stammzellen wurde analysiert, indem Darmkrypten von Plexin B1/B2 Doppelknockout-Mäusen isoliert und in Kultur genommen wurden. Deren reduzierte Fähigkeit, Organoide auszubilden, wies auf einen Defekt der Stammzell-Funktion hin. Semaphorin-Knockout-Organoide wurden analysiert, um die zugehörigen Liganden zu identifizieren, replizierten den Phänotyp des Rezeptor-Knockouts allerdings nicht. Zudem wurde die lentivirale Transduktion von Organoiden etabliert, um mittels RNAi die Expression mehrerer Liganden gleichzeitig reduzieren zu können. Ferner wurden Kolon-Organoide aus gesundem Gewebe und Tumorproben von Patienten etabliert, um die Funktion der Semaphorine in menschlichem Darmepithel und dessen Erkrankungen zu untersuchen. Diese Ergebnisse zeigen überlappende Expressionsmuster der B-Plexin-Liganden im Darm, legen deren Redundanz dar und ermöglichen weitere funktionelle Experimente, inklusive der Untersuchung des menschlichen Darmepithels.

1 Introduction

1.1 The gastrointestinal tract

The gastrointestinal (GI) tract is the body's organ system tasked with the mechanical and chemical breakdown of food into single-molecule nutrients that it absorbs through the epithelium (H. Karasov & Douglas, 2013). It is structured as a tubular series of organs, starting at the oral cavity, continuing through the esophagus, the stomach, the small intestine, the large intestine or colon, and terminates at the anus, where the remains of the digestive process are excreted. Beyond providing nutrients, the GI tract presents a border for pathogens entering the body, regulates the body's metabolism through hormones, and directly interacts with the nervous system. Most of the GI tract is structured in four major histological layers. The *mucosa* forms the innermost layer lining the organ's lumen. It consists of a simple columnar epithelium sitting on a layer of connective tissue, the *lamina propria* and a layer of muscle, the *lamina muscularis mucosae*. The epithelium comes into direct contact with the intestine's contents and fulfills a multitude of functions of which the most prominent is the absorption of nutrients from the intestinal contents. The submucosa is a layer of connective tissue and blood vessels located beneath the mucosa and facilitates the supply of oxygen to the epithelium and the transport of most absorbed substances from the intestine into the rest of the body. Furthermore, the submucosal or Meissner's plexus innervates the inner intestinal wall, communicating with both epithelial cells and the muscularis mucosae. Next, the muscularis provides contractility to the GI tract: Two layers of smooth muscle, one concentric and one longitudinal, allow for the contraction of the organs in peristaltic movement, pushing intestinal contents along. Motor control of these muscles is provided by the myenteric or Auerbach's plexus, consisting of a network of ganglia, that is part of the enteric nervous system. Finally, the GI tract's outermost layer is formed by either the adventitia or serosa, both layers of connective tissue.

1.1.1 Anatomy and function of the small and large intestine

The GI tract's longest sections are the small and large intestine. At the proximal end, the small intestine (SI) connects to the stomach's pyloric region and is structured into three sections from proximal to distal, termed the *duodenum*, *jejunum*,

and *ileum*. At its distal end, the ileocecal valve marks the transition into the large intestine, which is sectioned into the *cecum*, the ascending colon, transverse colon, descending colon, sigmoid colon, and *rectum*, before it terminates at the *anus*. Both small and large intestine are characterized by intestinal crypts or crypts of Lieberkühn, glandular structures initially described by Jonathan Nathanael Lieberkühn (Lieberkühn, 1745). Lined with epithelium, they extend into the *submucosa* of the intestinal wall and provide the intestinal stem cell niche. Functionally, in the *duodenum* proteins, lipids, and carbohydrates are prepared for absorption by enzymatic breakdown. The *jejunum* is the section of the small intestine where most absorption of nutrients takes place. A special role in this task falls to the *villi*, finger-like protrusions extending into the lumen: They vastly extend the intestine's luminal surface area and house both capillaries and lymphatic vessels that transport absorbed molecules into the body (Clevers, 2013). Importantly, vitamin B12 is absorbed in the *ileum* (LeBlanc et al., 2013). The colon is tasked with the absorption of water and bile salts from the intestinal contents. In addition, vitamin K produced by colonizing microbiota is absorbed here (Hill, 1997). Through these processes, the intestinal contents solidify, are gathered in the *rectum*, and ultimately excreted through the *anus*.

1.1.2 The intestinal epithelium

The intestinal epithelium is a simple columnar epithelium, lining the lumen of the small and large intestine and serves as the first barrier to all contents passing through the intestine. Due to the stresses the epithelium endures, both physical and chemical, it is the tissue with the highest cellular turnover in the human body, the entire epithelial layer completely renews itself within four to seven days (Stevens & Leblond, 1947).

To fulfill the intestine's multitude of duties, the organ relies on a quickly proliferating, highly dynamic, and diverse population of epithelial cells that originate from the crypts of Lieberkühn where the intestinal stem cell pool is located (Barker et al., 2007). As these cells divide once every day, excess cells are randomly pushed out of the stem cell niche, thus migrating upwards (Snippert et al., 2010). These progenitor cells form the transit-amplifying (TA) zone, where they divide 4-5 times before committing to the absorptive or secretory lineage and differentiate

into a number of highly specialized cell types (Figure 1) (Spit et al., 2018; van der Flier & Clevers, 2009). As they mature, the cells continue moving towards the villus tip where they become apoptotic and are shed into the intestinal lumen (Hall et al., 1994).

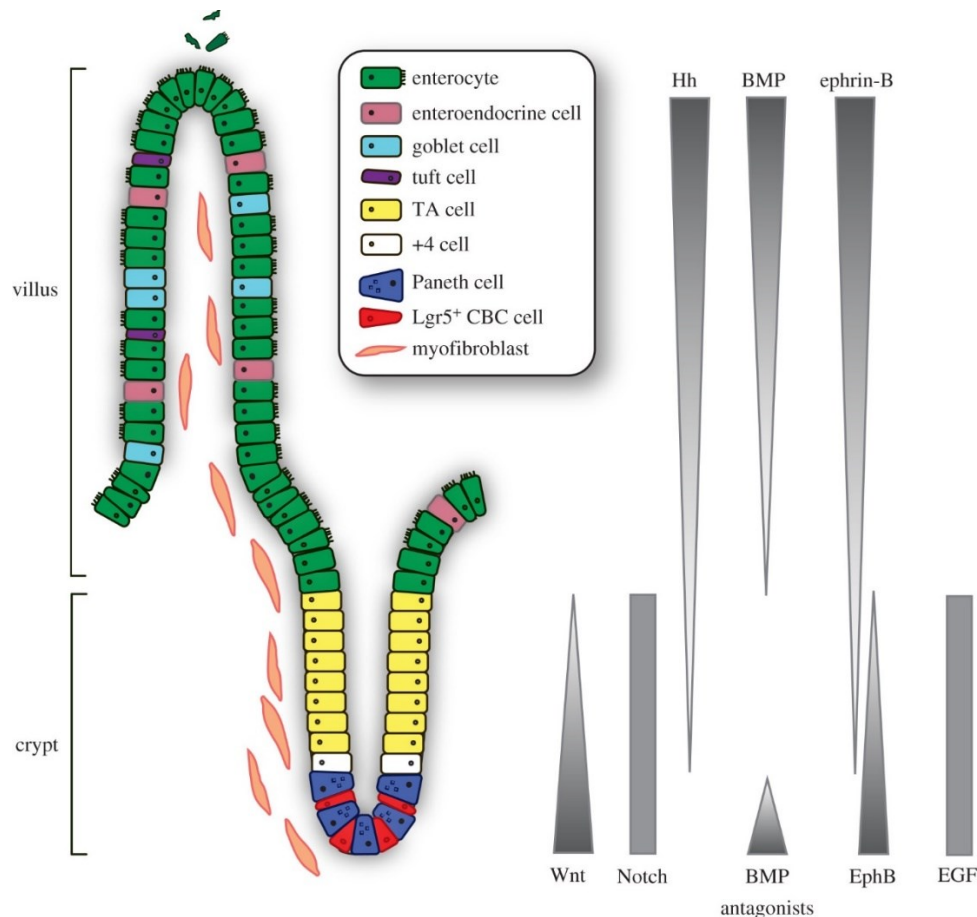


Figure 1 The intestinal epithelium. From (Spit et al., 2018), licensed under CC BY (<https://creativecommons.org/licenses/by/4.0/>).

1.1.2.1 The intestinal stem cell niche

At the crypt's bottom the intestinal stem cells (ISCs), also called crypt base columnar cells (CBCs), are interspersed with Paneth cells to form the stem cell niche (Bjerknes & Cheng, 1981; Cheng & Leblond, 1974). Under homeostatic conditions, all intestinal epithelial cells originate from these ISCs (Barker et al., 2007). The intestinal stem cell niche is supported by multiple cell types, Paneth cells contribute crucial nutrients and growth factors like Wnt, epidermal growth factor (EGF), and delta-like canonical notch ligand 4 (DLL4), which are required

for the maintenance of the stem cell pool (Rodríguez-Colman et al., 2017; Sato, van Es, et al., 2011). In addition, subepithelial telocytes and myofibroblasts also produce Wnt ligands preserving stemness (Shoshkes-Carmel et al., 2018; Valenta et al., 2016). Further niche factors include R-Spondins, which are Wnt pathway activators and Noggin, an inhibitor of bone morphogenetic protein (BMP)-mediated differentiation (Haramis et al., 2004; Spit et al., 2018). ISCs are identified by the expression of leucine-rich-repeat-containing G-protein-coupled receptor 5 (LGR5) and give rise to all cells required for homeostatic renewal of the entire intestinal epithelium (Barker et al., 2007). Other marker genes associated with ISCs include the Notch target gene olfactomedin 4 (OLFM4) and achaete-scute complex homolog 2 (ASCL2), a key Wnt target gene regulating stemness (Schuijers et al., 2015; van der Flier et al., 2009). The crypt's stem cell population undergoes symmetrical divisions governed by neutral drift dynamics, ultimately producing crypts consisting of a single clone's offspring (Lopez-Garcia et al., 2010; Snippert et al., 2010). As ISCs regularly divide, but space at the crypt bottom is limited, excess cells are pushed upwards and out of the stem cell niche to become progenitor cells for the two epithelial lineages (Snippert et al., 2010). The apical border of the stem cell niche is formed by reserve intestinal stem cells (rISCs) in the +4 nuclear position, named after their location within the crypt, counting upwards from the bottom-most nucleus (Bankaitis et al., 2018). Within the ISC pool, these largely quiescent rISCs represent a more damage resistant population marked by the expression of polycomb protein B lymphoma Mo-MLV insertion region 1 homolog (BMI1) (Sangiorgi & Capecchi, 2008; K. S. Yan et al., 2012). Other biomarkers have since been associated with reserve stem cells, including homeobox-only protein (HOPX) in a study by Takeda et al., that demonstrated reserve and actively cycling ISCs to be interconvertible (Takeda et al., 2011). These reserve stem cells are non- or slowly proliferating under homeostatic conditions but contribute a large number of epithelial cells after injury, crucially including LGR5-positive ISCs, demonstrating their ability to fully restore the intestinal epithelium (Sangiorgi & Capecchi, 2008; Takeda et al., 2011; Tian et al., 2011; K. S. Yan et al., 2012). In addition, a wide range of intestinal cell types have been demonstrated to be capable of contributing to intestinal regeneration, e.g., delta-like canonical notch ligand 1 (DLL1) or SOX9-positive progenitors, Paneth and enteroendocrine cells, comprehensively reviewed by Bankaitis et al.

(Bankaitis et al., 2018). Furthermore, absorptive progenitors expressing the enterocyte marker alkaline phosphatase, intestinal (ALPI), but not terminally differentiated enterocytes are able to repopulate the intestinal stem cell niche after injury and give rise to cells expressing stem or Paneth cell signatures (Tetteh et al., 2016).

1.1.2.2 Intestinal epithelial differentiation

All intestinal epithelial cells originate from ISC at the crypt base and undergo differentiation into specialized cell types as they migrate upwards (Spit et al., 2018). Two main lineages govern differentiation in the intestinal epithelium, the absorptive and the secretory lineage (Figure 2) (Schepers & Clevers, 2012). Cell fate determination is largely regulated by the Notch pathway: The transcription factor hes family bHLH transcription factor 1 (HES1) is a Notch target gene and inhibits the strongly pro-secretory transcription factor atonal bHLH transcription factor 1 (ATOH1) (Jensen et al., 2000; Yang et al., 2001). Thus, activation of Notch reduces differentiation into the secretory lineage, while inhibition of Notch increases the number of secretory cells in the epithelium (Fre et al., 2005; Milano et al., 2004; J. H. van Es et al., 2005).

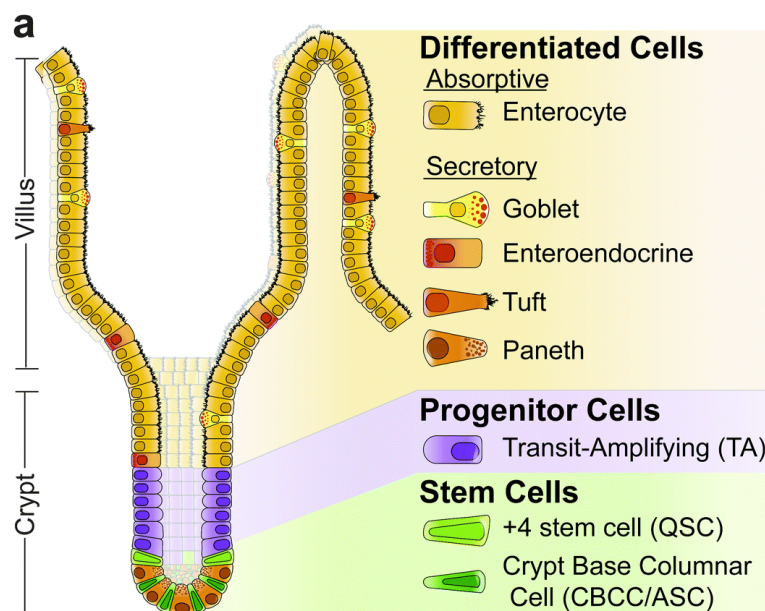


Figure 2 Intestinal epithelial lineages. Adapted from (Carulli et al., 2014) licensed under CC BY (<https://creativecommons.org/licenses/by/3.0/>).

The absorptive enterocytes are the most numerous cell type and take up nutrients from the chymus, while also interacting with the intestine's immune cells (Miron & Cristea, 2012; Snoeck et al., 2005). The cells of the secretory lineage are fewer in number but tasked with a plethora of specialized functions: Paneth cells are crucial in maintaining the ISC pool and provide nutrients, EGF, Wnt and Notch ligands, and secrete antimicrobial peptides like defensins and lysozyme (LYZ1) (Porter et al., 2002; Rodríguez-Colman et al., 2017; Sato, van Es, et al., 2011). Consequently, they migrate towards the crypt base to become part of the intestinal stem cell niche (Bjerknes & Cheng, 1981; Ireland et al., 2005). Differentiation into Paneth cells requires expression of the Wnt pathway target gene *Sox9*, making it a key regulator of the secretory lineage (Bastide et al., 2007). Goblet cells secrete mucin-2 (MUC2) into the intestinal lumen, a component of the mucus that protects the epithelium from enzymes, chemical stresses and prevents microorganisms from coming into direct contact with the epithelium (Pelaseyed et al., 2014). Enteroendocrine cells (EECs) are derived from neurogenin3-positive progenitor cells (Jenny et al., 2002). They differentiate into several specialized, hormone-secreting cell types, involving them directly in the local and systemic regulation of digestion and metabolism (Gribble & Reimann, 2016). Despite their diversity, chromogranin-A (CHGA) is considered a universally expressed marker for EECs (Varndell et al., 1985). Additionally, they form the epithelium's link to the nervous system, directly interacting with afferent neurons (Bohórquez et al., 2015). Tuft cells are diverse, chemosensory cells, named after their apical tuft of microvilli and are present along the entire small and large intestine (McKinley et al., 2017). The expression of doublecortin-like kinase 1 (DCLK1) is generally used as a marker to identify these cells (Gerbe et al., 2009). While the function of tuft cells is incompletely understood, multiple studies assigned them a central role in the body's immune response to parasitic infection (Gerbe et al., 2016; Howitt et al., 2016; von Moltke et al., 2016).

1.1.3 Colorectal cancer

Colorectal cancer (CRC) is the most common cancer of the GI tract and originates in the colon and rectum. Most tumors are of epithelial origin, forming adenocarcinomas. In 2018, CRC accounted for 10.2 % of new cancer cases worldwide, making it the third-most common cancer behind lung and breast cancer. In the same year, it caused 881,000 deaths, 9.2 % of cancer-related mortality and second only to lung cancer. Its incidence positively correlates with the human development index, meaning CRC is most common in more-developed regions, i.e., Australia and New Zealand, Europe, and North America (Bray et al., 2018). People over the age of 60 are most strongly affected, representing 80 % of sporadic colon cancer patients at diagnosis (Kuipers et al., 2015). While both genetic and environmental factors play a role in colorectal cancer, most cases are sporadic, with 75 % of patients having a negative family history. Typical environmental risk factors are lifestyle factors associated with several tumors: Smoking, alcohol consumption, increased body weight, intake of processed food stuffs and red meat contribute to a risk increase (World Cancer Research Fund, 2018). The two most common hereditary causes of colorectal cancer are hereditary non-polyposis colorectal cancer (HNPCC), also known as Lynch syndrome, and familial adenomatous polyposis (FAP). Together they account for ca. 5-10 % of cases. While HNPCC is caused by defects in DNA mismatch-repair genes, FAP is caused by loss-of-function mutations in the gene APC regulator of WNT signaling pathway (APC), a negative regulator of the Wnt pathway (Lynch & de la Chapelle, 2003). Both syndromes lead to an early onset in tumor formation and a greatly increased lifetime risk. Since tumor tissue of different stages is often available from the same patient, the progression of CRC has been studied extensively: Generally, development of CRC is understood to be caused by an accumulation of mutations, commonly referred to as the adenoma-carcinoma sequence (Fearon & Vogelstein, 1990; Vogelstein et al., 1988). Initiation of tumor development is most commonly linked to a loss-of-function in the *APC* gene, followed by gain-of-function mutations affecting the EGFR pathway (e.g., *RAS* or *PIK3CA* mutations), inactivation of BMP signaling (e.g., *SMAD4* mutations) and p53, ultimately facilitating the progression from a benign adenoma to a malign and possibly metastatic carcinoma. The development of methods to recapitulate CRC outside of the

patient has been the subject of research for a long time and the first patient-derived tumor xenografts (PDX) were established in the early 1950s (Toolan, 1953). The method has been advanced substantially since then and offers the advantage of providing the tumor microenvironment as well, but also has its drawbacks. Since only small amounts of tissue can be transplanted, a tumor's heterogeneity might not be fully captured and some studies reported additional mutations in the xenograft, that were not present in the original tumor (Bleijs et al., 2019; Morgan et al., 2017). Furthermore, engraftment rates depend on the parent tumor's staging and as xenografts are passaged, clonal selection of tumors takes place and the patient's stroma will eventually be lost (Bleijs et al., 2019). Lastly, PDXs rely on the use of laboratory animals, making this method to replicate patient-derived tumors relatively complex. More recently, the development of organoid cultures derived from human intestinal tissues has opened new avenues in the study of CRC, as patient-derived tissues can be cultured and manipulated *ex vivo* without the reliance on animal models (Sato et al., 2009; Sato, Stange, et al., 2011). A more detailed introduction to organoids is provided in section 1.4.

1.2 The semaphorin-plexin system

The semaphorin-plexin system consists of two families of cell-cell signaling proteins first discovered in the nervous system: Semaphorins represent the ligands, and plexins the receptors (Bamberg et al., 1999). The functions assigned to these molecules have vastly expanded since: Among others, they are important in organ development of the brain and kidney, epithelial homeostasis, immune system, and bone turnover and have been described to be involved in pathological processes, including cancer (Worzfeld & Offermanns, 2014). More recently, angiogenin (ANG) has been described to be a ligand to plexin B2, expanding an already complex signaling system (W. Yu et al., 2017).

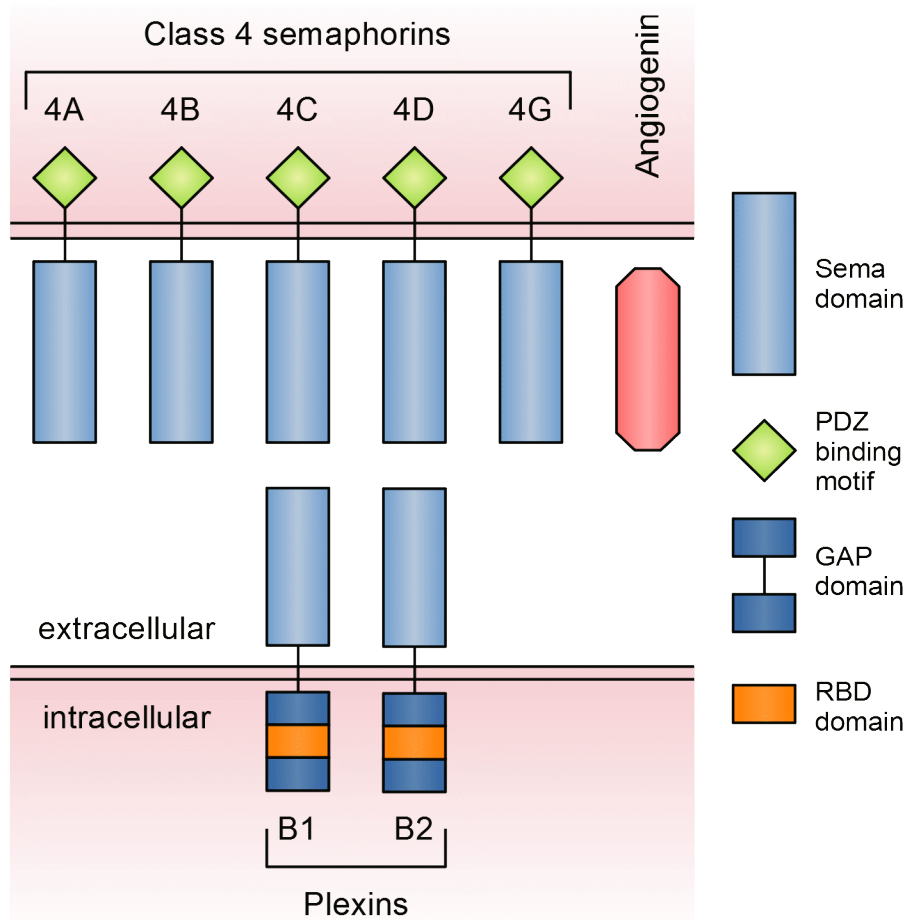


Figure 3 Class 4 semaphorins, angiogenin and their plexin receptors.

1.2.1 Ligands of the semaphorin-plexin system

Semaphorins are a large family of transmembrane and secreted ligands, organized in eight classes, 1-7 and V, of which classes 1 and 2 appear in invertebrates, 3 to 7 are present in vertebrates and class V semaphorins were discovered in viruses (Bamberg et al., 1999). All semaphorins are characterized by a common structural property, the ca. 500 amino acid N-terminal sema domain, and the plexin-semaphorin-integrin (PSI) domain, both of which are located extracellularly (Figure 3) (Kolodkin et al., 1993). The sema domain is essential for semaphorin-plexin signaling: First, it enables the homodimerization of semaphorins (Klostermann et al., 1998; Love et al., 2003). Second, it mediates plexin receptor binding: Semaphorin homodimers bind two monomeric plexin molecules via their sema domain, bring them into proximity and activate intracellular signaling (Janssen et al., 2010; Nogi et al., 2010). In class 3 semaphorins, the

semaphorin homodimer binds two receptor heterodimers consisting of a plexin and a neuropilin co-receptor (Janssen et al., 2012). While semaphorin-plexin interactions often take place between membrane-bound molecules, there are exceptions to that rule: Class 3 semaphorins are secreted ligands, and the extracellular domain of class 4 semaphorins may be liberated by proteolytic cleavage, enabling them to act as soluble ligands (Elhabazi et al., 2001; Hemming et al., 2009; Nakatsuji et al., 2012; Xiaosong Wang et al., 2001). Beyond their roles as ligands, semaphorins can also function as receptors (Gurrapu et al., 2019; Sun et al., 2017). Semaphorins regulate a wide range of physiological processes in the nervous and immune system, epithelial architecture, as well as angiogenesis (C. Gu & Giraud, 2013; Kumanogoh & Kikutani, 2013; Neufeld et al., 2012; Pasterkamp, 2012; Potiron et al., 2007; Xia et al., 2015). Furthermore, semaphorins play a role in pathological mechanisms as well, influencing tumor growth directly by acting on the malignant cell, or indirectly e.g., by regulating angiogenesis (Neufeld et al., 2012, 2016). Previous publications, as well as unpublished data from another doctoral candidate, Ivana Matković, showed the receptors plexin B1 (PLXNB1) and plexin B2 (PLXNB2) to be highly expressed in the intestinal epithelium (Meehan et al., 2014; Xia et al., 2015). Consequently, the focus of this thesis lies on B-plexin ligands, namely semaphorins 4A, B, C, D, G, and angiogenin.

Semaphorin 4A (Sema4A) is a membrane-bound ligand to B-plexins, plexin D1 and TIM2 (Worzfeld & Offermanns, 2014). Originally, it was discovered together with several other semaphorins in the developing nervous system of mouse embryos and named SemB (Püschel et al., 1995). Since its discovery, Sema4A has been found to be a key regulator in the immune system, and thus been termed an “immune semaphorin”, but also plays a role in angiogenesis (Ito & Kumanogoh, 2016). In the immune system, Sema4A is expressed on dendritic cells and required for efficient T-cell activation, as *Sema4A*-deficient mice showed reduced immune responses (Kumanogoh et al., 2005). Signaling through plexin B2, Sema4A contributes to the activation and differentiation of CD8+ T cells (Ito et al., 2015). In patients suffering from multiple sclerosis, Sema4A was found to be highly expressed in dendritic cells from which its extracellular domain was proteolytically cleaved, resulting in increased serum levels which were linked to a worse clinical outcome (Nakatsuji et al., 2012). Expressed in endothelial

cells, *Sema4A* inhibits vascular endothelial growth factor (VEGF)-mediated migration and proliferation of endothelial cells and thus angiogenesis by signaling through plexin D1 (Toyofuku et al., 2007). In the retina, *Sema4A* was reportedly required for the exosomal release of anti-apoptotic prosaposin, preventing the loss of retinal pigment epithelial cells induced by oxidative stress and regulated the transport of retinoid binding proteins (Toyofuku et al., 2012). Interestingly, no receptor was necessary for *Sema4A* to exert its effects: Instead, *Sema4A* was identified as a regulator of endosomal transport mechanisms. In addition to its role as a ligand, *Sema4A* has been described to act as a receptor to plexin B1 as well, increasing migratory behavior of several cancer cell lines (Sun et al., 2017). In familial colorectal cancer type X, a hereditary non-polyposis colorectal cancer, germline mutations of the *SEMA4A* gene were discovered to increase MAPK/Erk signaling (Schulz et al., 2014).

Semaphorin 4B (*Sema4B*), initially named SemC, was originally discovered in the central nervous system (Püschel et al., 1995), although no functional role was assigned to it at that time. Later, an expression analysis found *Sema4B*, among others, to be expressed in the developing and regenerating olfactory epithelium (Williams-Hogarth et al., 2000). Like *Sema4A*, it has since been assigned a role in the immune system: *Sema4B* is expressed on T cells and inhibits basophil-mediated immune responses (Nakagawa et al., 2011). In the kidney, Xia et al. discovered *Sema4B* to be expressed in tubular epithelial cells and identified plexin B2 as its receptor (Xia et al., 2015). They further found *Sema4B*, together with *Sema4D* and *Sema4G*, to be required for tubular epithelial repair upon ischemic injury. Some publications also linked *Sema4B* to lung cancer, in which it inhibits proliferation, tumor cell motility, and metastasis (Jian et al., 2014, 2015; Nagai et al., 2007).

Semaphorin 4C (*Sema4C*) was first described to be expressed in the brain, kidney, liver, heart, lung, and spleen of adult mice, although still named SemF at the time (Adams et al., 1996). Since then *Sema4C* has been found to be central in organ development: In the cerebellum, where it signals through plexin B2, *Sema4C*-deficient mice suffered exencephaly (Maier et al., 2011). In the kidney, *Sema4C* is required for ureteric branching (Perälä et al., 2011). Inflammatory hypersensitivity to pain mediated by peripheral sensory neurons also depended on *Sema4C*-plexin B2 signaling (Paldy et al., 2017). *Sema4C* is further a substrate

to γ -secretase, that mediates proteolytic cleavage of its extracellular domain (Hemming et al., 2009). In the immune system, Sema4C signals through plexin B2 to efficiently generate plasma cells (H. Yan et al., 2017). Additional roles have been described in cancer: In breast cancer models, Gurrapu et al. described Sema4C signaling through plexin B2 to be required to maintain proliferation in breast cancer cells (Gurrapu et al., 2018). In a separate publication, the same group reported that Sema4C also increased metastasis by reverse signaling, in which plexins B1 and B2 serve as ligands (Gurrapu et al., 2019). Similar functions were described by Smeester et al. in osteosarcomas, where Sema4C increased tumor growth (Smeester et al., 2020).

Semaphorin 4D (Sema4D), also known as CD100, is expressed on cells of the immune and nervous system, osteoclasts, in the kidney, and on tumor-associated macrophages (TAMs) (Worzfeld & Offermanns, 2014). Like other class 4 semaphorins, it can be cleaved proteolytically (Xiaosong Wang et al., 2001). Under physiological conditions, Sema4D promotes angiogenesis through its receptor plexin B1 (Basile et al., 2006). As mentioned previously, Sema4B, Sema4D, and Sema4G facilitate renal tubular epithelial repair by concertedly signaling through plexins B1 and B2 (Xia et al., 2015). Furthermore, a study by Meehan et al. found all epithelial cells of the colon to be plexin B2-positive and intraepithelial $\gamma\delta$ T lymphocytes in the colon to be Sema4D-positive. This signaling axis proved to be important, as *Sema4D*-knockout mice were more strongly affected by DSS-induced colitis (Meehan et al., 2014). This phenotype was attributed to a loss of keratinocyte growth factor-1 (KGF1) production, an epithelial growth factor that was previously shown to be protective against colitis (Chen et al., 2002). In tumors, Sema4D was generally found to promote disease progression: In *Sema4D* knockout mice, angiogenesis, growth and metastasis of xenograft tumors was reduced (Sierra et al., 2008). Consequently, an antibody blocking Sema4D is being investigated as a treatment option in tumors (e.g., drug VX15/2503; clinical trials.gov). A study by Ikeya et al. found the high expression levels of Sema4D and plexin B1 in colorectal cancers to predict worse survival in patients (Ikeya et al., 2016). Finally, Zhou et al. linked reverse signaling of plexin B1 through Sema4D to disease progression in oral squamous cell carcinoma (Zhou et al., 2017).

Semaphorin 4G (Sema4G) was initially identified by Li et al. and found to be expressed in the brain, kidney and liver of adult mice (H. Li et al., 1999). Little is known regarding its functions, outside of its role in cerebellar development, where Sema4G signals through plexin B2, albeit in a redundant manner with Sema4C (Maier et al., 2011). In the kidney Sema4G, together with Sema4B and Sema4D, is required for the repair of the tubular epithelium upon ischemic injury (Xia et al., 2015). Few reports exist about the role of Sema4G in cancer: These studies correlate low expression of Sema4G with improved clinical outcomes in glioma and colorectal cancer, although further studies will be needed to corroborate these findings (Xiaoliang Wang et al., 2008; Xiao et al., 2020).

Beyond the class 4 semaphorins described above, semaphorins have additional functions in the intestine: Stromal fibroblasts have been shown to secrete class 3 semaphorins, that support the growth of intestinal organoids by signaling through neuropilin receptors, demonstrating a role in intestinal epithelial homeostasis (Karpus et al., 2019).

Angiogenin (ANG) is a secreted ribonuclease, initially isolated from the supernatant of HT-29, a human adenocarcinoma cell line. In the same work, the authors identified its capability to induce angiogenesis, one of its core functions (Fett et al., 1985). Early studies revealed angiogenin mRNA to be predominantly expressed in the liver, but also in the small and large intestine of adult rats (Weiner et al., 1987). Beyond its role in angiogenesis, it fulfills a variety of other functions, including the regulation of hematopoietic stem cell growth and survival, neurogenesis and innate immunity (Goncalves et al., 2016; Hooper et al., 2003; S. Li & Hu, 2012; Subramanian & Feng, 2007). ANG serves as a ligand that undergoes receptor-mediated endocytosis and exerts its functions in a context-dependent manner. Under conditions favoring growth, ANG is translocated to the nucleus, where it serves as a transcription factor increasing ribosomal RNA (rRNA) expression (Moroianu & Riordan, 1994; Tsuji et al., 2005). In stressed cells, it locates to the cytoplasm and inhibits translation for most mRNA species, excluding those with strong internal ribosomal entry sites (IRES), which are usually present in transcripts of anti-apoptotic and pro-survival genes (Ivanov et al., 2011). ANG was recently described to signal through plexin B2 (W. Yu et al., 2017). The authors demonstrate plexin B2 to be both required and sufficient to mediate its functions, i.e., proliferation, phosphorylation of MAP and ERK, protection from

apoptosis, nuclear translocation of ANG, and the production of rRNA. Furthermore, W. Yu et al. found treatment with an antibody directed against the ANG binding site of plexin B2 to reduce the size and angiogenesis of xenograft tumors in mice. In another study, preventing ANG from translocating to the nucleus by neomycin treatment reduced the growth of xenograft tumors in mice (Yoshioka et al., 2006). ANG was reported to be expressed in most CRCs and high levels of ANG mRNA were associated with a poor prognosis (Etoh et al., 2000; D. Li et al., 1994). In a study investigating colitis, ANG secreted by myeloid cells was found to be protective for intestinal epithelial cells (Bai et al., 2020). These findings highlight a role in the intestine and a therapeutic potential of ANG inhibition in cancers and substitution in e.g., colitis. Finally, loss-of-function mutations have been observed in some neurodegenerative diseases like amyotrophic lateral sclerosis or Parkinson's disease (Greenway et al., 2006; M. A. van Es et al., 2011).

1.2.2 Plexins

Plexins are a family of membrane-bound receptors, subdivided into classes A through D, that interact with semaphorins and in the case of class 3 semaphorins with neuropilins as co-receptors (Janssen et al., 2012; Takahashi et al., 1999; Tamagnone et al., 1999; Winberg et al., 1998). Furthermore, the receptor tyrosine kinases MET and ERBB2 can serve as co-receptors with B-plexins (Giordano et al., 2002; Swiercz et al., 2004). Recent evidence further indicates, that plexins can act as ligands to semaphorins e.g., plexin B1 to Sema4A and plexins B1 and B2 to Sema4C (Gurrapu et al., 2019; Sun et al., 2017). Binding between plexins and semaphorins is mediated by an N-terminal, extracellular sema domain (Tamagnone et al., 1999). In their inactive state, plexins form autoinhibited monomers through a closed formation of their intracellular C-terminus (He et al., 2009). Upon binding of a semaphorin homodimer, two plexin monomers are brought into close proximity, leading to the activation of downstream signaling, most notably the intracellular GTPase-activating protein (GAP) domain, that acts on Rap proteins, which regulate important processes like proliferation, cellular junctions, and cell polarity (Gloerich & Bos, 2011; Y. Wang et al., 2013), and the RHO-GTPase-binding domain (RBD), that activates RhoA and RhoC (Figure 3) (Pascoe et al., 2015; Y. Wang et al., 2013).

Previous publications, as well as unpublished data from another doctoral candidate, Ivana Matković, showed the receptors plexin B1 and B2 to be highly expressed in the intestinal epithelium (Meehan et al., 2014; Xia et al., 2015). Consequently, this thesis focuses on plexins B1 and B2. Both are activated by class 4 semaphorins, specifically Sema4A and Sema4D in the case of plexin B1 and Sema4A, Sema4B, Sema4C, Sema4D, Sema4G, and ANG in the case of plexin B2, as summarized in previous publications (Worzfeld & Offermanns, 2014; Xia et al., 2015; W. Yu et al., 2017). Plexin B2 has been assigned a central role in the developing nervous system: In the cerebellum, plexin B2 is the receptor to Sema4C and Sema4G (Maier et al., 2011), and is needed for immature granule cell migration and proliferation (Deng et al., 2007; Friedel et al., 2007). In the kidney, plexin B2 is required for ureteric branching, making it an important regulator of organ development (Perälä et al., 2011). Xia et al. later demonstrated, that plexin B1/B2 double-deficient mice displayed renal tubular epithelial defects, further supporting a role in the developing kidney. Upon ischemic injury, they further showed plexin B2 to be essential for the repair of the renal tubular epithelium. Knockout mice suffered a loss of epithelial architecture, that was attributed to a failure to properly align the mitotic spindle of dividing cells (Xia et al., 2015), highlighting an important role in epithelial regulation. Plexin B2 is further expressed on keratinocytes and crucially involved in epidermal damage repair, as it activates $\gamma\delta$ T cells through Sema4D and blocking this interaction delayed wound healing (Witherden et al., 2012). In the skin, plexins B1 and B2 were recently described to act as mechanosensors regulating stem cell divisions through homophilic interactions (Jiang et al., 2020). In cancer, plexin B1 fills opposing roles, with its effect depending on genetic context and the type of tumor: For example in ERBB2-overexpressing breast tumors, low plexin B1 expression indicated a better prognosis, while the opposite was true in ERBB2-negative breast cancer (Worzfeld et al., 2012). Plexin B2 promotes glioma invasion (Le et al., 2015), and the stemness of cancer stem cells in the prostate (S. Li et al., 2020). Furthermore, the angiogenin-plexin-B2 axis protects epithelial cells in the colon from colitis (Bai et al., 2020).

1.3 Use of the Cre-*loxP* system to study cell type-specific gene function in the intestine

The Cre-*loxP* system was initially described in the P1 bacteriophage by Sternberg and Hamilton (Sternberg & Hamilton, 1981). It depends on two components, the Cre recombinase and a genetic locus flanked by *loxP* DNA motifs, often referred to as “floxed” (Sauer & Henderson, 1988). Once Cre is expressed and active, the floxed locus is excised by the recombinase. By now, the Cre-*loxP* system is frequently used to generate transgenic mice, e.g., gene knockout animals, a useful tool in studying a wide variety of physiological and pathological processes (McLellan et al., 2017). To obtain these transgenic animals, both Cre recombinase, as well as the floxed DNA loci must be integrated into the genome. This can be achieved through the injection of modified DNA templates into mouse oocytes, that then grow into the transgenic animals (Vintersten et al., 2008). In many cases either spatial or temporal control over the activity of Cre is desired. Gu et al. demonstrated that cell type-specific Cre activity can be achieved by tying its expression to the activity of a cell-type specific promoter (H. Gu et al., 1994), enabling targeted, non-systemic knockouts. To provide temporal control over recombination activity, Cre recombinase can be coupled to a mutated estrogen receptor (CreER), that leads to the sequestration of Cre from the nucleus (Hayashi & McMahon, 2002). To relocate the fused recombinase to the nucleus, the animals or cells are treated with tamoxifen, a process that might have undesirable influence on several biological processes and may only work partially. In addition, a certain level of unspecific activation of CreER might also occur. Therefore, constitutive expression of Cre may be preferable in some experimental settings.

To generate transgenic mouse lines expressing Cre in a controlled manner, homologous bacterial artificial chromosome (BAC) recombination can be used to integrate Cre into a section of genomic DNA at a specific location. Subsequently, the modified BACs are injected into mouse oocytes where they integrate into the genome and give rise to transgenic mice carrying the desired genetic modification. Several mouse lines exist, that express Cre in the intestinal epithelium or one of its cell types, including an inducible *Alpi-CreER* mouse line, that expresses Cre in enterocytes upon treatment with tamoxifen (Tetteh et al., 2016). However, no constitutive *Alpi-Cre* mouse line has been described to date. Given the fast

turnover of the intestinal epithelium, conditional modification of the genome might not be sufficient, as modified cells are quickly lost from the epithelium, thus masking potential effects of the genetic modification. Consequently, constitutively active, enterocyte-specific Cre mouse lines would be a useful tool in the study of intestinal epithelial dynamics. As part of this thesis, a bacterial artificial chromosome (BAC) was recombined to constitutively express Cre recombinase under the control of the enterocyte-specific *Alpi* promoter. The BAC was furthermore prepared for the injection into mouse oocytes with the goal of breeding a novel *Alpi-Cre* mouse line. Lastly, the expression of Cre in these mice was analyzed in collaboration with Josina Großmann as part of her bachelor thesis.

1.3.1 Bacterial artificial chromosome recombination

Bacterial artificial chromosomes (BACs) are a tool that originated from the Human Genome Project, during which the entire human genome was sequenced. Their main function was to make fragments of genomic DNA easier to maintain and manipulate. These fragments were integrated into plasmid backbones containing *E. coli*'s F factor, making it possible to amplify and maintain DNA sequences of up to 300 kb in *E. coli* (Shizuya et al., 1992). Utilizing these BACs, genomic DNA sequences can be modified by homologous or Red/ET recombination. This process is mediated by the Red α /Red β recombination proteins derived from the λ phage (Muyrers et al., 1999; Youming et al., 1998; D. Yu et al., 2000). The method can be used to insert, delete, or replace parts of genomic DNA in the BAC. Plasmids are employed to express the required recombination proteins in the BAC-carrying bacteria. In addition, the desired insert is provided as a linear DNA molecule flanked by homology arms that correspond to the target site in the BAC. Efficient homologous recombination relies on the formation of double-strand-breaks (DSBs) in the targeted DNA molecule, for which Red α /Red β mediate DSB repair (Thaler et al., 1987). Red α serves as a 5'-3' exonuclease, digesting one of the strands at the DSB, leaving a single-strand 3' overhang, to which the DNA annealing protein Red β attaches. It facilitates the alignment with the homology arm of the linear template DNA sequence, for which the 3' overhang serves as a primer, thus allowing for the replication of the targeted DNA molecule together with the insert. For the experiments described here, the plasmids provided with

the Counter-Selection BAC Modification Kit (Gene Bridges) were used, namely pSC101-BAD-gbaATet or pRED/ET for short. This plasmid carries the *red $\alpha\beta$* operon, coding the recombination proteins under the control of the L-arabinose-inducible *pBAD* promoter (Guzman et al., 1995). The protein AraC is expressed from the same plasmid and in the absence of L-arabinose, forms dimers which inhibit transcription at the *pBAD* promoter and thus of the Red α /Red β recombination proteins. As soon as L-arabinose is added, AraC binds it, the transcriptional inhibition is lifted and the Red α /Red β recombination proteins are expressed, making the bacteria recombination-competent. Another site-directed recombination method used here is the flippase-flippase recognition target (FLP-FRT) recombination method, that functions similarly to Cre recombination (Buchholz, 1996). Once FLPase is expressed, it recognizes FRT sites, which direct its activity. Modified BACs can then be used to generate transgenic mouse lines and intestinal organoids (Schwank, Andersson-Rolf, et al., 2013).

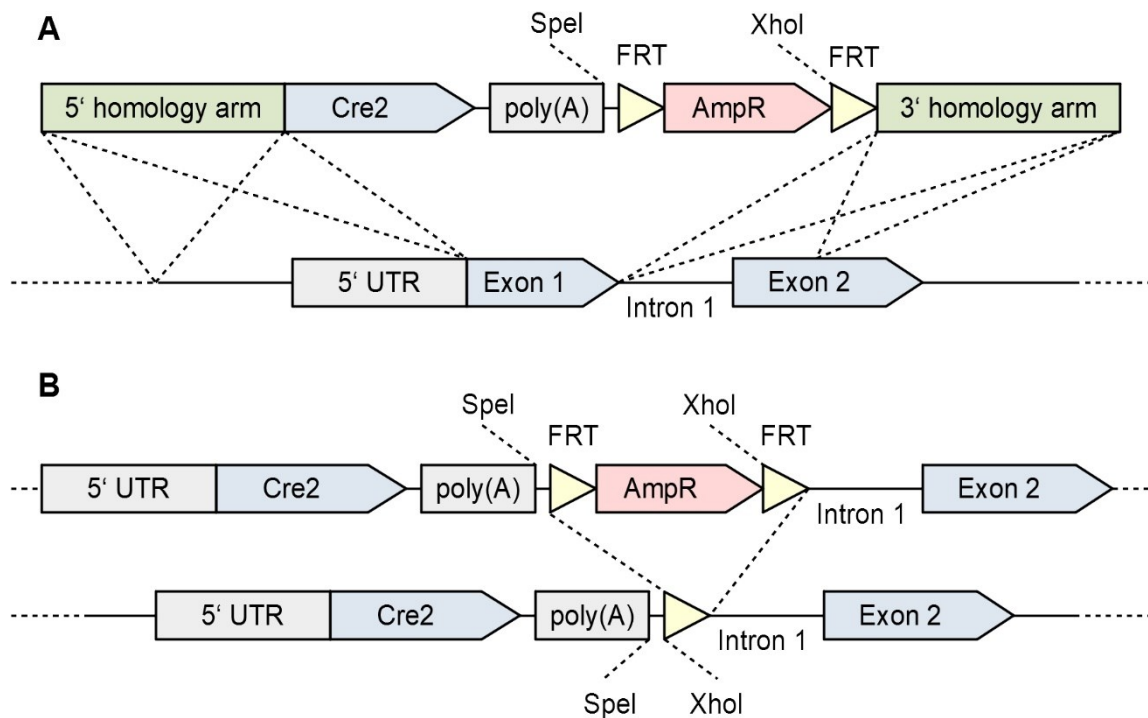


Figure 4 Schematic of BAC recombination steps. **(A)** pRED/ET-mediated homologous recombination of the *Cre2* insert into the *Alpi* BAC. **(B)** FLPase-mediated removal of the ampicillin resistance selection marker.

In the experiments described in this thesis, Cre2-recombinase was integrated into the *Alpi* gene by homology-directed BAC recombination and FLP-FRT (Figure 4). The final FLPase-modified BAC was injected into mouse oocytes by

collaborators, generating a mouse line expressing the Cre2-recombinase under the control of the *Alpi* promoter (Vintersten et al., 2008).

1.4 The intestinal organoid model

Intestinal organoids are a primary three-dimensional (3D) cell culture model, closely resembling the intestinal epithelium. Single LGR5+ ISCs or intestinal crypts are isolated and seeded into a protein matrix where they grow into complex structures. They recapitulate the crypt-villus architecture and contain all epithelial cell types (Sato et al., 2009). In this manner they can not only be propagated for extended periods, but also cryopreserved and manipulated in different ways, making them a powerful tool in the study of the intestinal epithelium and its diseases. Under the right culture conditions ISCs form small spheroids that are still largely homogeneous in their cell composition. After ca. 72 h of culture, cellular symmetry is broken by the formation of the first stem cell niche, consisting of both Paneth and LGR5+ ISCs (Serra et al., 2019). From there, organoids start to grow “buds”, that extend outwards, forming finger-like structures that recapitulate the intestinal crypt. The stem cell niche remains located at the outermost tip, while differentiated cells are located towards the central part of the organoid, mimicking the *in vivo* crypt-villus architecture elegantly. Intestinal organoids depend on niche factors that maintain its stem cell pool and promote proliferation. As the Wnt pathway is a core regulator of stemness in the intestine, its activation is crucial. To that end, culture media typically contain the LGR5 ligand R-Spondin1, a positive regulator of Wnt signaling. While in mouse small intestinal organoids intrinsic production of Wnt ligand is sufficient, colonic cultures, as well as human intestinal organoids require exogenous Wnt as well. In addition, EGF is added as a general promoter of proliferation and important factor in the maintenance of the intestinal stem cell niche. Furthermore, BMP signaling is inhibited by Noggin, as it would otherwise increase differentiation of epithelial cells (Sato et al., 2013). As mentioned earlier, intestinal organoids are cultured in a protein matrix, very frequently Matrigel (Corning) is used. This substrate is manufactured from proteins secreted by Engelbreth-Holm-Swarm mouse sarcoma cells. It is rich in laminin and collagen and provides a growth environment that closely imitates the basal lamina underlying the epithelium. While the medium components required for

organoid culture are well defined, the exact composition of extracellular matrices is still unclear as they are produced from cell cultures (Kleinman & Martin, 2005). Utilizing the organoid model, primary intestinal cells become accessible to manipulation by a wide variety of methods. Their gene expression can be modified by transfection, electroporation or viral transduction with plasmids and BACs (M. Fujii et al., 2015; Koo et al., 2012; Schwank, Andersson-Rolf, et al., 2013). These engineered organoids can then be studied extensively, characterizing e.g. changes in morphology, differentiation, or function. Some of these methods have already been used to model diseases like cystic fibrosis or intestinal cancer *ex vivo*, using patient-derived organoids in conjunction with genome modification methods like CRISPR-Cas9 (X. Li et al., 2014; Matano et al., 2015; Schwank, Koo, et al., 2013). As organoids can easily be treated with biologically active compounds, patient-derived organoids have also been used for high-throughput drug screenings, providing invaluable information on the efficacy in the targeted tissue without having to rely on model organisms. This method bridges the gap between two-dimensional (2D) cell culture and e.g. PDTXs or the application of compounds to an entire organism in drug development. Beyond that, patient-derived organoids have been demonstrated to model their parent tumor's treatment response, highlighting a useful role in the personalization of medical treatment (Vlachogiannis et al., 2018). As intestinal organoids only consist of epithelial cells, they do not recapitulate stromal interactions as e.g. PDTXs do. To fill this gap, organoids have been co-cultured e.g. with neurons and myofibroblasts (Bohórquez et al., 2015; Pastuła et al., 2016). While this approach may not fully replicate the situation *in vivo*, it does however enable the controlled introduction of stromal cells and thus focused studies of the role of certain stromal elements. To better characterize host-pathogen interactions, organoid co-cultures with microbial or viral pathogens have been established, allowing for the study of infectious GI tract diseases as well (Dutta & Clevers, 2017). Furthermore, cells derived from organoids can be used in single-cell sequencing, providing highly detailed information about e.g. gene expression without the risk of stromal contamination of the samples. Like this, even rare cell types in the intestinal epithelium can be examined closely (Grün et al., 2015). One key aspect of intestinal epithelial function is the ability of ISCs to efficiently generate appropriately differentiated daughter cells, a process that can be modeled by organoids *ex vivo*.

2 Aim of the study

This study aims to analyze the expression and function of Plexin-B ligands in the intestinal epithelium.

3 Materials

Single-use lab ware for general use and cell culture was obtained from Greiner Bio-One, Sarstedt, USA Scientific, and ibidi. Specifically required materials are listed below.

3.1 Laboratory consumables

Table 1 Laboratory consumables

Material	Manufacturer
Austerlitz Insect Pins Minutiens	Fine Science Tools
Electroporation cuvettes, 1 mm	Carl Roth
Embedding Cassette	Carl Roth
Immedge hydrophobic barrier PAP pen	Vector Laboratories
Membrane filter, 0.025 µm pore size	Millipore
Superfrost Ultra Plus glass slides	Thermo Scientific
Vacuum Filter Filtropur V 25; 0.45 µm	Sarstedt

3.2 Technical equipment and devices

Table 2 Technical equipment and devices

Device	Manufacturer
Accu-Cut SRM Microtome	Sakura
Biofuge pico	Heraeus
Biofuge stratos	Heraeus
Centrifuge 5417R	Eppendorf
CFX Connect Real-Time PCR Detection System	Biorad
Cryostat	Leica
Electrophoresis Chamber	University workshop
Embedding Machine TES99	Melite
FlexCycler ²	Biometra
Gel iX20 Imager Gel Documentation	Intas Science Imaging
Genova Bio Spectrophotometer	Jenway
Heracell 150	Heraeus
Herasafe	Heraeus
HybEZ II Oven	ACD Bio

Device	Manufacturer
Leica DM750 Light Microscope	Leica
Leica ICC50W Camera	Leica
Leica Thunder Imaging Microscope	Leica
Luminoskan Ascent Luminometer	Thermo Scientific
MaxQ4000	Thermo Scientific
MicroPulser Electroporator	Biorad
NanoDrop 1000	PEQLAB
S20 SevenEasy pH meter	Mettler Toledo
Sorvall RC 5B Plus	DuPont
Thermomixer compact	Eppendorf
Zeiss Axio Vert.A1 microscope	Zeiss
Zeiss Laser Scanning Microscope (LSM) 700	Zeiss

3.3 Cell culture

Table 3 Cell culture materials

Medium/Reagents	Supplier
A83-01	Sigma-Aldrich
Accumax	Sigma-Aldrich
Advanced DMEM/F12	Thermo Fisher Scientific
B27 supplement	Thermo Fisher Scientific
BES	Sigma-Aldrich
Bovine serum albumin (BSA)	Sigma-Aldrich
Dulbecco's modified eagle medium (DMEM)	Capricorn Scientific
Epidermal Growth Factor (EGF)	Promokine
Fetal bovine serum (FBS)	Gibco
Fugene HD	Promega
Gastrin I	Sigma-Aldrich
Gentamicin/Amphotericin B, 100x	Gibco
GSK-3 Inhibitor XVI CHIR99021	Millipore
HEPES Buffer Solution	Capricorn
Matrigel	Corning

Medium/Reagents	Supplier
N-2 supplement	Thermo Fisher Scientific
N-Acetylcysteine	Sigma-Aldrich
Penicillin-Streptomycin	Capricorn Scientific
Phosphate buffered saline (PBS)	Capricorn Scientific
Polybrene	Sigma-Aldrich
Prostaglandin E2 (PGE-2)	Tocris
Puromycin	Invitrogen
rhFGF-basic	Peprtech
rhIGF-1	Biozol
rmNoggin	Peprtech
Stable Glutamine 200 mM	Capricorn Scientific
Trypsin-EDTA (0.05 %, 0.02 % in PBS)	Capricorn Scientific
Valproic acid	Sigma-Aldrich
Y-27632 ROCK Inhibitor	Sigma-Aldrich
Zeocin	Invitrogen

3.4 Chemicals

Table 4 Chemicals

Chemical	Supplier
Acetic acid, 96 %	Carl Roth
Agar, bacteriological	Carl Roth
Agar, NEEO ultra-quality	Carl Roth
Ampicillin sodium salt	Carl Roth
Chloramphenicol	Carl Roth
D-sorbitol	Carl Roth
Diethyl pyrocarbonate (DEPC)	Sigma-Aldrich
Dimethylformamide	Sigma-Aldrich
Dimethylsulfoxide (DMSO)	Carl Roth
Disodium phosphate	Carl Roth
Eosin 1 %, alcoholic	Morphisto
Ethanol	Carl Roth

Chemical	Supplier
Ethidumbromide	Carl Roth
Ethylene diamine tetraacetic acid disodium salt dihydrate (EDTA)	Carl Roth
Ethylene glycol tetraacetic acid (EGTA)	Carl Roth
Glucose	Carl Roth
Glutaraldehyde	Carl Roth
Glycerol, 86 %	Carl Roth
Hydrochloric acid	Carl Roth
Isopropyl alcohol	Carl Roth
Kanamycin	Sigma-Aldrich
L-arabinose	Sigma-Aldrich
Magnesium chloride (hexahydrate)	Carl Roth
Magnesium sulfate (heptahydrate)	J. T. Baker
Monopotassium phosphate	Carl Roth
Mounting Medium Pertex	Histolab
Nicotinamide	Sigma-Aldrich
NP-40 Alternative	Millipore
Paraffin, 50-52 °C	Carl Roth
Paraformaldehyde	Sigma
Phenol-chloroform-isoamyl alcohol (PCI)	Carl Roth
Potassium acetate	Carl Roth
Potassium chloride	Carl Roth
Potassium ferricyanide	Carl Roth
Potassium ferrocyanide	Carl Roth
Sepharose CL-4B	Sigma-Aldrich
Sodium acetate	Carl Roth
Sodium chloride	Carl Roth
Sodium deoxycholate	Carl Roth
Sodium dihydrogen phosphate	Carl Roth
Sodium dodecyl sulfate (SDS)	Carl Roth
Sodium hydrogen phosphate (heptahydrate)	Carl Roth
Sodium hydroxide	Carl Roth

Chemical	Supplier
Spermidine	Sigma-Aldrich
Streptomycin	Sigma-Aldrich
Sucrose	Carl Roth
Tetracycline	Sigma-Aldrich
Tris	Carl Roth
Triton X-100	Carl Roth
Tryptone	Carl Roth
X-Gal	Sigma-Aldrich
Xylene	Carl Roth
Yeast extract	Carl Roth

3.5 Kits

Table 5 Kits

Kit	Supplier
Alexa Fluor 488 Tyramide Superboost kit, Streptavidin	Thermo Fisher Scientific
Avidin/Biotin Blocking Kit	Vector
Counter-Selection BAC Modification Kit	Gene Bridges
Direct-zol RNA MiniPrep kit	Zymo Research
Dual-Luciferase Reporter Assay	Promega
NucleoBond Xtra Midi	Macherey-Nagel
NucleoSpin Gel and PCR Clean-up	Macherey-Nagel
NucleoSpin Plasmid	Macherey-Nagel
RNAscope 2.5 HD Reagent Kit Brown	ACD Bio
RNAscope 2.5 HD Reagent Kit Red	ACD Bio
TriFast	peqGOLD

3.6 Bacteria

Table 6 Bacterial strains

Bacterial Strain	Supplier
DH10B <i>E. coli</i>	BACPAC CHORI
NEB-10 beta electrocompetent <i>E. coli</i>	NEB

3.7 PCR and cloning reagents

Table 7 PCR and cloning reagents

Reagent	Supplier
100x BSA	NEB
10x Taq buffer with KCl	Thermo Scientific
DNA ligase buffer, 10x	Thermo Scientific
dNTP mix, 10 mM	Thermo Scientific
GC buffer, 5x	Thermo Scientific
Gene Ruler 100 bp Plus DNA ladder	Thermo Scientific
Generuler 1 kb DNA ladder	Thermo Scientific
HF buffer, 5x	Thermo Scientific
Loading dye, 6x	Thermo Scientific
MgCl ₂ ; 25 mM	Thermo Scientific
Polynucleotide kinase buffer A, 10x	Thermo Scientific
Random hexamer primer	Thermo Scientific
SybrGreen	Biorad

3.8 Enzymes

Table 8 Enzymes

Enzyme	Supplier
BamHI	Thermo Scientific
BcuI (SpeI)	Thermo Scientific
EcoRI	Thermo Scientific
HindIII	Thermo Scientific
NheI	Thermo Scientific
NotI	Thermo Scientific

Enzyme	Supplier
Phusion HS II polymerase	Thermo Scientific
Sall	Thermo Scientific
T4 Polynucleotide kinase	Thermo Scientific
T7 DNA ligase	Thermo Scientific
Taq DNA polymerase	Thermo Scientific
XhoI	Thermo Scientific

3.9 Plasmids

Table 9 Plasmids

Plasmid	Insert
LT3GEPIR (Fellmann et al., 2013)	empty vector
LT3GEPIR_mS4A_sh1	mSema4A shRNA 1
LT3GEPIR_mS4A_sh4	mSema4A shRNA 1
LT3GEPIR_mTTL_sh2	mTTL shRNA 2
p706-FLP (Gene Bridges)	FLPase
pCS2 β -CateninS33A	constitutive active β -Catenin mutant
pGL4.10[luc2]_FOP10 (Promega)	Firefly luciferase
pGL4.10[luc2]_TOP10 (Promega)	Firefly luciferase
phCre2-ERT2.pA.FRTN1ampFRT	Cre2-ERT2
pMDG.2	Lentiviral envelope plasmid
pRL-CMV	Renilla luciferase
pSC101-BAD-gbaATet (pRED/ET), (Gene Bridges)	BAC recombination proteins
psPAX2	Lentiviral packaging plasmid

3.10 Bacterial artificial chromosomes

BACs were sourced from the BACPAC Resources Center (<https://bacpacresources.org>).

Table 10 Bacterial artificial chromosomes

Clone Name	Description
RP23-173D12	BAC spanning the murine <i>Alpi</i> gene
RP23-173L11	BAC spanning the murine <i>Alpi</i> gene
RP23-437G2	BAC spanning the murine <i>Alpi</i> gene
RP23-49020	BAC spanning the murine <i>Alpi</i> gene

3.11 Oligonucleotides

Table 11 PCR and sequencing primers

Oligonucleotide name	Sequence
#145/HindIII_EcoRI_Cre_fwd	ATATATAAGCTTGAATTCGGTACCGTCCACCATG
#146/Cre_STOP_BamHI_rev	ATATATGGATCCTCTTAATCGCCATCTTCGAGCAG
#147/Seq_phCre2_fwd	CGGTGGGAGGTCTATATAAG
#148/Seq_phCre2_rev	ACAGTGGGAGTGGCACCTTC
#149/us_hm_NheI_fwd	ATATATGCTAGCGGTCTCCTCTTCAGCTGG
#149b/us_hm_NheI_fwd	ATATATGCTAGCCTCTGAGGCCTGTTAATACCC
#150/us_hm_NheI_rev	ATATATGCTAGCGTAAGAAGGTTCCCTTTCTGACTCC
#151/ds_hm_EcoRI_fwd	ATATATGAATTCGGTTGGGGTACTGATGG
#152/ds_hm_HindIII_rev	ATATATAAGCTTTAGCCAGGGACAAAGTCCAT
#152b/ds_hm_HindIII_rev	ATATATAAGCTTGGATTCCAGCAGCATAACAG
#153/Seq_phCre2_rev2	ACACAGGAAACAGCTATGAC
#168/Cre_BAC_5'PCR_rev	GATTAAGAGGATCCACTAGTTCTAGAAG
#169/Alpi_BAC_seq_fwd	GGGTACTTGGAGTACAAGGGCTG
#170/Alpi_BAC_seq_rev	ACCCAACCTGCAGGAGACATAG

Table 12 RTqPCR primers

Oligonucleotide name	Sequence
mAlpi_fwd	AGGATCCATCTGTCCTTTGGT
mAlpi_rev	CAGCTGCCTTCTTGTTCCA
mAng_fwd	GCCAGCTTTGGAATCTCTGTTGG
mAng_fwd_MM	AGCGAATGGAAGCCCTTACA
mAng_rev	ACATCTTTGCAGGGTGAGGTTAGG
mAng_rev_MM	TCATCGAAGTGGACAGGCA
mChgA_fwd	ATCCTCTCTATCCTGCGACAC
mChgA_rev	GGGCTCTGGTTCTCAAACACT
mDclk1_fwd	GAGAAGGCACAGCTTGCAG
mDclk1_rev	GTTATTGTGGCAGGAATCTGG
mDefa6_fwd	CCAGGCTGATCCTATCCAAA
mDefa6_rev	CAATAGCATACCAGATCTCTCAATG
mHes1_fwd	ACACCGGACAAACCAAAGAC
mHes1_rev	CGCCTCTTCTCCATGATAGG
mKi67_qfwd	AGGGTAACTCGTGGAACCAA
mKi67_qrev	TCTTAACTTCTTGGTGCATACAATG
mLgr5_fwd	CTTCACTCGGTGCAGTGCT
mLgr5_rev	GATCAGCCAGCTACCAAATAGG
mLyz1_fwd	GAGACCGAAGCACCGACTATG
mLyz1_rev	CGGTTTTGACATTGTGTTTCGC
mMuc2_fwd	CCCTCTACACCCCAATCCACATC
mMuc2_rev	GAGGAGATTACCCCCACAGTGGA
mRetnlB_fwd	GGAAGCTCTCAGTCGTCAAGA
mRetnlB_rev	GCACATCCAGTGACAACCAT
mTrpm5_fwd	AACAGCCCTGAGCCTCAAT
mTrpm5_rev	CTCTGGGTTGTTTGCATGG
mTtl_fwd1	CGACGAGAATAGCAGCGTCT
mTtl_rev1	AGGCTCGTGACCTAGTCTCC
mYwhaz_fwd	TTACTTGGCCGAGGTTGCT
mYwhaz_rev	TGCTGTGACTGGTCCACAAT

shRNA plasmid cloning inserts

Targeting sequences are highlighted as bold text in the full oligo sequence.

Table 13 shRNA plasmid cloning inserts

Oligonucleotide	Broad Institute Clone ID	Full oligo sequence
mTTL_sh1_fwd	TRCN0000191436	TCGAGAAGGTATATTGCTGTTGACAGT GAGCG CGTATGTGATTTATCCA ACTAT AGTGAAGCCACAGATGTAT AGTTGGAT AAATCACATACG TGCCTACTGCCTCGG
mTTL_sh1_rev	TRCN0000191436	AATTCCGAGGCAGTAGGCAC CGTATGTG ATTTATCCA ACTATACATCTGTGGCTT CACTA TAGTTGGATA AAATCACATACGC GCTCACTGTCAACAGCAATATACTTC
mTTL_sh2_fwd	TRCN0000190258	TCGAGAAGGTATATTGCTGTTGACAGT GAGCG CTCCAGAGGAAAGAGAGAGAA T AGTGAAGCCACAGATGTAT TTCTCTCTC TTTCTCTGGAG TGCCTACTGCCTCGG
mTTL_sh2_rev	TRCN0000190258	AATTCCGAGGCAGTAGGCAC CTCCAGAG GAAAGAGAGAGAA TACATCTGTGGCTT CACTA TTCTCTCTCTTTCTCTGGAGC GCTCACTGTCAACAGCAATATACTTC
S4A_sh1_fwd	TRCN0000067438	TCGAGAAGGTATATTGCTGTTGACAGT GAGCG CCTGGCCTTGAATATCCAGAA T AGTGAAGCCACAGATGTAT TTCTGGATA TTCAAGGCCAGG TGCCTACTGCCTCGG
S4A_sh1_rev	TRCN0000067438	AATTCCGAGGCAGTAGGCAC CCTGGCCT TGAATATCCAGAA TACATCTGTGGCTT CACTA TTCTGGATATTCAAGGCCAGGC GCTCACTGTCAACAGCAATATACTTC
S4A_sh4_fwd	TRCN0000067441	TCGAGAAGGTATATTGCTGTTGACAGT GAGCG GCTTATCTCGTGGAGGAGATTT AGTGAAGCCACAGATGTAA AATCTCCTC CACGAGATAAGC TGCCTACTGCCTCGG

Oligonucleotide	Broad Institute Clone ID	Full oligo sequence
S4A_sh4_rev	TRCN0000067441	AATCCGAGGCAGTAGGCAG GCTTATCT CGTGGAGGAGATT TACATCTGTGGCTT CACTAA AATCTCCTCCACGAGATAAGCC GCTCACTGTCAACAGCAATATACCTTC

3.12 Primary antibodies

Table 14 Primary antibodies

Antibody	Species	Supplier, Cat. number	Dilution
anti-hLyz1	rabbit	DAKO; A0099	1:400
anti-mAngiogenin	mouse	abcam; 10600	1:400
anti-mOlfm4	rabbit	Cell signaling; 39141S	1:400
anti-mSema4B	sheep	R&D; AF6239	1:200
anti-mSema4D	rat	Invitrogen; 14-1001-82	1:400

3.13 Secondary antibodies

Table 15 Secondary antibodies

Antibody	Species	Supplier, Cat. number	Dilution
anti-mouse AlexaFluor 555	goat	Invitrogen; A28180	1:500
anti-rabbit AlexaFluor 488	goat	Invitrogen; A11034	1:400
anti-rat AlexaFluor 488	goat	Invitrogen; A11006	1:200
anti-rat AlexaFluor 555	goat	Invitrogen; A21434	1:200
anti-sheep AlexaFluor 546	donkey	Invitrogen; A21098	1:400

3.14 smRNA FISH probes

Table 16 smRNA FISH probes

Target transcript	Supplier	Catalog Number
<i>mAng</i>	ACD Bio	463971
<i>mPlxnb1</i>	ACD Bio	469241
<i>mSema4A</i>	ACD Bio	498371
<i>mSema4G</i>	ACD Bio	461391

3.15 Buffers and solutions

3.15.1 Bacterial media

Lysogeny broth (LB, bacterial medium)

- 10 g/l Tryptone
- 5 g/l yeast extract
- 10 g/l sodium chloride

LB agar (bacteriological plates)

- 10 g/l Tryptone
- 5 g/l yeast extract
- 10 g/l sodium chloride
- 15 g bacteriological agar per liter medium

Super Optimal Broth (SOB, bacterial medium)

- 20 g/l Tryptone
- 5 g/l yeast extract
- 0.6 g/l sodium chloride
- 0.2 g/l potassium chloride

The resulting solution is autoclaved 20 minutes at 121 °C. Before use, 20 mM Mg^{2+} is added by preparing a 1 M Mg^{2+} solution: Equal volumes of 1 M $MgCl_2 \cdot 6H_2O$ and 1 M $MgSO_4 \cdot 7H_2O$ are mixed and 20 ml/l of the resulting solution are added to the SOB medium.

Super Optimal Broth with catabolite repression (SOC, bacterial medium)

SOC medium is prepared like SOB medium (see above) before 20 mM glucose is added to finalize the medium.

Bacterial freezing medium

- 65 % glycerol
- 0.1 M magnesium sulfate
- 20 mM Tris, pH 7.7

Bacterial antibiotic stocks

Antibiotic stock solutions were protected from light and stored at -20 °C when stored for extended periods. Working aliquots were kept at 4 °C and in the dark to prevent degradation.

Table 17 Bacterial antibiotic stock solutions

Antibiotic	Stock concentrations	Solvent
Ampicillin	100 mg/ml	ddH ₂ O
Chloramphenicol	30 mg/ml	100 % ethanol
Tetracycline	10 mg/ml	75 % ethanol
Kanamycin	30 mg/ml	ddH ₂ O
Streptomycin	50 mg/ml	ddH ₂ O

3.15.2 Plasmid and BAC DNA

Small alkaline quickies (DNA isolation)

Resuspension buffer S1

- 50 mM Tris, pH 8.0
- 10 mM EDTA
- 0.1 mg/ml RNase A

Lysis buffer S2

- 0.2 M NaOH
- 1 % Sodium dodecyl sulfate

Neutralization buffer S3

- 3 M Potassium acetate
- 96 % Acetic acid (Add until the solution's pH value reaches 5.5)

10x Annealing buffer

- 1 M NaCl
- 100 mM Tris (stock solution: pH 7.4)

Oocyte injection buffer

- 10 mM Tris (stock solution: pH 7.5)
- 0.1 mM EDTA (stock solution: pH 8.0)
- 100 mM NaCl

The solution was sterile filtered prior to use.

3.15.3 *lacZ* reporter staining solutions

Solution A

- 0.2 M $\text{NaH}_2\text{PO}_4 \cdot \text{H}_2\text{O}$

Solution B

- 0.2 M $\text{Na}_2\text{HPO}_4 \cdot 7\text{H}_2\text{O}$

Solution C

115 ml of solution A are mixed with 385 ml solution B and filled to 1 l with H_2O .

Solution D

1 liter of solution C is supplemented with 5 mM EGTA and 2 mM MgCl_2 .

Fixation buffer

200 ml of solution D are mixed with glutaraldehyde to a concentration of 0.2 %.

Washing buffer

800 ml of solution D are mixed with sodium deoxycholate to a final concentration of 0.01 % and NP-40 to a concentration of 0.02 %.

Staining buffer

200 ml of washing buffer are supplemented with potassium ferricyanide to 10 mM, potassium ferrocyanide to 10 mM and 0.1 g X-gal dissolved in 2 ml of dimethylformamide.

3.15.4 Immunostaining and FISH solutions

Permeabilization and blocking buffer

- PBS
- 0.1 % v/v Triton X-100
- 5 % v/v horse serum

Tris -buffered saline with Tween (TBST)

- 6,05 % w/v Tris
- 8,5 % w/v NaCl

The solution's pH was set to 7.5-7.6. Before use, 200 µl of Tween were added per 100 ml of buffer.

3.15.5 Cell culture media and solutions

3.15.5.1 Cell culture solutions

2x BES-buffered saline (BBS)

- 50 mM BES
- 1.5 mM Na₂HPO₄
- 280 mM NaCl

The substances were dissolved in ddH₂O, the pH was adjusted to 6.95 and sterile filtered. Aliquots were stored at 4 °C.

Calcium chloride solution

CaCl₂ was dissolved in ddH₂O to a concentration of 2 M and sterile filtered.

3.15.5.2 Cell culture media for the generation of conditioned media

Table 18 Medium compositions used in conditioned media production

Wnt3a-conditioned medium	R-Spondin1-conditioned medium
Basal growth medium <ul style="list-style-type: none"> • DMEM • 10 % v/v FBS • 1x Penicillin-Streptomycin 	Basal growth medium <ul style="list-style-type: none"> • DMEM • 10 % v/v FBS • 1x GlutaMAX • 1x Penicillin-Streptomycin
Selection medium <ul style="list-style-type: none"> • Basal growth medium • 100 mg/ml Zeocin 	
Conditioning medium <ul style="list-style-type: none"> • DMEM • 10 % v/v FBS • 1x Penicillin-Streptomycin 	Conditioning medium <ul style="list-style-type: none"> • Advanced DMEM/F12 • 10 mM HEPES • 1x GlutaMAX
Freezing medium <ul style="list-style-type: none"> • DMEM • 15 % v/v FBS • 10 %v/v DMSO 	

3.15.6 Organoid culture media and solutions

Crypt chelation solution (CCS)

Chemicals are dissolved in H₂O to make a 5x stock solution and stored at 4 °C:

- 28 mM Na₂HPO₄
- 40 mM KH₂PO₄
- 480 mM NaCl
- 8 mM KCl
- 220 mM Sucrose
- 274 mM D-sorbitol

To obtain the working solution, the 5x stock was diluted in PBS and supplemented with EDTA to of 5 mM. Before use, 0.5 mM DTT was added to the solution.

BSA-PBS

A 1 % w/v BSA solution in PBS was prepared as a 10x stock solution for the use in organoid culture. The working solution was prepared by diluting one volume of 10x stock in nine volumes of PBS and adding 1x Penicillin-Streptomycin.

Basal medium

- Advanced DMEM/F12
- 10 mM HEPES
- 2 mM L-Glutamine
- 1x Penicillin/Streptomycin

Organoid freezing medium

- Basal Medium
- 10 % v/v FBS
- 10 % v/v DMSO

3.15.6.1 Human colonic organoid media

Human colonic organoid medium

3 ml basal medium were supplemented as follows:

- 5 ml Wnt3a-conditioned medium
- 2 ml R-Spondin1-conditioned medium
- 1x B27 supplement
- 10 nm Gastrin I
- 1 mM N-Acetylcysteine
- 2.5 μ M PGE-2
- 100 ng/ml rmNoggin
- 50 ng/ml EGF
- 100 ng/ml rhIGF-1
- 50 ng/ml rhFGF-basic
- 500 nM A83-01

Human colonic cancer organoid medium

8 ml basal medium were supplemented as follows:

- 2 ml R-Spondin1-conditioned medium
- 1x B27 supplement
- 10 nm Gastrin I
- 1 mM N-Acetylcysteine
- 2.5 μ M PGE-2
- 100 ng/ml rmNoggin
- 50 ng/ml EGF
- 100 ng/ml rhIGF-1
- 50 ng/ml rhFGF-basic
- 500 nM A83-01

3.15.6.2 Mouse organoid culture media

Crypt culture medium

9 ml Basal Medium were supplemented with the following components:

- 1 ml R-Spondin1 conditioned medium
- 1x N-2 supplement
- 1x B27 supplement
- 1 mM N-Acetylcysteine
- 100 ng/ml rmNoggin
- 50 ng/ml EGF
- 1 mM Valproic acid
- 10 μ M CHIR-99021

Stimulation medium

4 ml Basal Medium were supplemented with the following components:

- 5 ml Wnt3a conditioned medium
- 1 ml R-Spondin1 conditioned medium
- 1x N-2 supplement
- 1x B27 supplement
- 10 mM Nicotinamide
- 1 mM N-Acetylcysteine
- 100 ng/ml rmNoggin
- 50 ng/ml EGF
- 1 mM Valproic acid
- 10 μ M CHIR-99021

Organoid infection medium

To prepare medium for lentiviral transductions of murine intestinal organoids, stimulation medium was supplemented with 8 μ g/ml polybrene.

4 Methods

4.1 Cell culture

4.1.1 Mouse intestinal crypt isolation and culture

Mice were sacrificed, the small intestine was removed and placed in a petri dish with PBS. Intestinal contents were flushed out with PBS by placing the proximal end over the opening of a single-use plastic Pasteur pipette and carefully pressing PBS through the intestine. The intestine was then opened longitudinally, washed with PBS and cut into ca. 3-5 mm long pieces. The tissue pieces were then washed in a 50 ml centrifuge tube containing 20 ml PBS by gently rocking the tube and replacing the PBS ca. 2-3 times. Dissociation of the tissue was done by incubating the tissue with 5 mM EDTA in PBS for 5 minutes on a rocking shaker. The tissue was picked up with a 25 ml pipette and the remaining liquid was discarded. The pieces were pipetted up and down ca. 10 times, placed back in the centrifuge tube and washed with ca. 20 ml PBS 2-3 times. EDTA treatment and PBS washes were repeated up to 4 times in total before crypts were released mechanically by vigorous shaking of the tube for 30 seconds. The tissue pieces were then allowed to settle and 10 ml of the supernatant containing the crypts were immediately transferred to a 15 ml centrifuge tube coated with BSA-PBS, followed by centrifugation for 5 minutes at 500 g. From here on, the samples were kept on ice whenever possible. The supernatant was removed, and the pellet was resuspended in an appropriate volume of BSA-PBS, depending on the pellet size. For the use in cell culture, the number of crypts per ml was then determined by placing 10 μ l of crypt suspension on a microscopy slide and counting the number of intact crypts. The desired number of crypts was transferred to a 1.5 ml tube coated with BSA-PBS and resuspended in basal medium and centrifuged for 3 minutes at 300 g. The supernatant was removed, and the pellet was resuspended in Matrigel. 25 μ l crypt-Matrigel suspension was then placed as droplets into the wells of a prewarmed 48-well plate. Matrigel was polymerized by incubation in a humidified cell culture incubator at 37 °C and 5 % CO₂ for 10 to 25 minutes. Cells isolated for normal cell culture received 250 μ l of crypt culture medium (CCM) per well supplemented with ROCK inhibitor for the first 48 h of culture. All organoids were cultured in a humidified atmosphere at 37 °C and 5 % CO₂.

4.1.2 Human intestinal crypt isolation and culture

Human normal and tumor tissue from the intestine and colon was acquired in cooperation with the Department of Visceral, Thoracic and Vascular Surgery and the Department of Pathology of the University Clinic Gießen and Marburg as part of the study “Organoid-Kulturen des normalen Darmepithels und maligner Darmtumoren” with the patient’s consent. Resected human small intestine or colon was sent to the Department of Pathology without prior fixation. Tissue required for diagnostic analysis in the Department of Pharmacology was taken by a pathologist before any tissue was taken for organoid cultures. Ca. 3 cm² of normal mucosa were taken with a distance of at least 10 cm from pathological lesions. If possible, 1 cm² of epithelial tumor tissue was cut. Both samples were placed in chilled PBS for transport on ice. Intestinal epithelial cells were isolated for the establishment of human intestinal organoid cultures following a protocol provided by the group of Kim Jensen (BRIC, Copenhagen). All steps were performed on ice. The resected tissue was washed 3 times in PBS supplemented with 1x Gentamicin/Amphotericin B by light shaking in a 50 ml centrifuge tube. The buffer was removed, and the tissue placed in a petri dish. The tissue was subdivided for multiple applications: One piece of epithelial tissue was snap-frozen for RNA-isolation, another piece was fixed in 0.2 % paraformaldehyde (PFA) for histological analysis. 10-15 pieces of ca. 1 mm² were cut from the epithelial section of the sample and placed in a 15 ml centrifuge tube coated with 0.1 % BSA-PBS. Mucus and debris were removed by vigorous shaking. The tissue was transferred to a fresh 15 ml centrifuge tube with 2 ml of Crypt Chelation Solution (CCS) and incubated for 15 minutes on ice. To mechanically release the crypts from the tissue, 3-4 mm of a 1,000 µl pipette tip were cut off and the tissue was pipette dup and down ca. 20 times. The tissue pieces were settled by gravity, and the supernatant was pipetted into a fresh 15 ml centrifuge tube coated with BSA-PBS. Fresh CCS was pipetted on the tissue. The CCS incubation and mechanical release of crypts was repeated up to five times in total. The crypt suspensions were immediately centrifuged for 3 minutes at 300 g and 4 °C and the supernatant removed. The pellet was resuspended in 1 ml BSA-PBS and kept on ice until all isolation samples were prepared this way. All samples were then centrifuged for 3 minutes at 500 g and 4 °C, the supernatant was removed, and the

pellet resuspended in the appropriate amount of Matrigel. 25 μ l crypt-Matrigel suspension was then placed as droplets into the wells of a prewarmed 48-well plate. Matrigel was polymerized by incubation in a humidified cell culture incubator at 37 °C and 5 % CO₂ for 10 to 25 minutes. Cells isolated from normal tissue received 250 μ l of human colonic organoid medium per well, cells isolated from tumor tissue received 250 μ l of human colonic tumor medium per well. All culture media were supplemented with ROCK inhibitor for the first 48 h of culture. All organoids were cultured in a humidified atmosphere at 37 °C and 5 % CO₂.

4.1.3 Organoid passaging

All steps were performed on ice. To passage both human and murine intestinal organoids, the culture medium was removed. 500 μ l of ice-cold BSA-PBS was added to each well, Matrigel droplets were scraped off with a 1,000 μ l pipette and pipetted up and down ca. 3-5 times to break down the Matrigel. The resulting suspensions of up to 5 wells were collected in 15 ml centrifuge tubes coated with BSA-PBS and centrifuged 3 minutes at 300 g. The supernatant was removed, and the pellet resuspended in 900 μ l BSA-PBS. To break down the organoids mechanically, the suspension was pipetted up and down ca. 20 times with the pipette tip opening pressed against the bottom of the centrifuge tube. Another 900 μ l of BSA-PBS was used to wash down any cells stuck to the walls of the tube, followed by another centrifugation for 3 minutes at 300 g. BSA-PBS washes and mechanical breaking of the organoids was repeated ca. 2-4 times, but at least until all remaining Matrigel was removed from the cell pellets. The resulting cell pellet was resuspended in 2 ml of basal medium and centrifuged for 3 minutes at 500 g. The supernatant was removed, and the pellet resuspended in the desired volume of Matrigel. Typical subcultivating ratios ranged from 1:2 to 1:5. 25 μ l per well of the cell-Matrigel suspension were then seeded into each well of a prewarmed 48-well plate. The Matrigel was polymerized by incubation in a humidified cell culture incubator at 37 °C and 5 % CO₂ for 10 to 25 minutes. Cells received 250 μ l of the appropriate culture medium per well supplemented with ROCK inhibitor for the first 48 h of culture. All organoids were cultured in a humidified atmosphere at 37 °C and 5 % CO₂.

4.1.4 Organoid freezing and thawing

For extended storage, organoids were frozen in liquid nitrogen as follows: 3 to 5 days after the last passage the medium was removed from 2 wells of a 48-well cell culture plate. 500 μ l of freshly prepared organoid freezing medium were added to each well, followed by mechanical disruption of the Matrigel using the tip of a 1,000 μ l pipette. After pipetting the cells up and down ca. 5 times, the organoid suspension of both wells was pooled into a freezing vial and placed in a freezing container at -80 °C overnight. The next day the frozen organoids were transferred to liquid nitrogen storage. To thaw frozen organoids, one vial of frozen cells was placed in a water bath at 37 °C until the freezing medium was completely liquefied. The suspension was then immediately added dropwise to 5 ml of prewarmed basal medium in a 15 ml centrifuge tube. The cells were centrifuged for 3 minutes at 500 g. The supernatant was removed, and the pellet re-suspended in the desired volume of Matrigel. 25 μ l per well of the cell-Matrigel suspension were then seeded into each well of a prewarmed 48-well plate. The Matrigel was polymerized by incubation in a humidified cell culture incubator at 37 °C and 5 % CO₂ for 10 to 25 minutes. Cells received 250 μ l of the appropriate culture medium per well supplemented with ROCK inhibitor for the first 48 h of culture.

4.1.5 Lentiviral transduction of intestinal organoids

For lentiviral infection of intestinal organoids, 9 days prior to the day of transduction one well of organoids was seeded and cultivated in CCM for each viral construct that was going to be transduced. To generate the lentiviral particles, 5 days before the transduction date one 150 cm² dish of human embryonic kidney 293T cells (HEK-293T) was seeded for each construct, followed by calcium phosphate transfection as follows: The construct that was to be transduced was mixed with the two packaging plasmids pMDG.2 and psPAX2 at a ratio of 1:2:2, usually 11:22:22 μ g for a 150 cm² dish and the volume was adjusted to 1,012 μ l with sterile H₂O. 2x BBS was shaken vigorously and 1,125 μ l were added to the plasmid mix, immediately followed by 113 μ l of 2 M calcium chloride solution that was added dropwise. The final transfection mix was incubated 20 minutes at room temperature and then dripped onto the previously seeded dish of HEK-293T cells,

that were then incubated normally for 3 hours before the culture medium was exchanged. The cells were then incubated undisturbed until the lentiviral supernatant was harvested for the infection. Two days prior to transduction, organoids were passaged 1:2 as described above and cultured in stimulation medium. To collect the first batch of lentivirus, the medium on the virus-producing HEK-293T cells was collected and replaced with fresh medium. The supernatant was centrifuged for 5 minutes at 1,000 g, sterile filtered using a 0.22 μm syringe filter and stored at 4 °C overnight. The following day, another batch of lentivirus was collected following the same protocol, pooling both batches after sterile filtration. To concentrate the virus, the filtrate was centrifuged at 4 °C and 8,000 g overnight, usually ca. 14 hours. On the day of transduction, the supernatant of the viral filtrate was discarded, and the resulting pellet was resuspended in organoid infection medium. The stimulated organoids were collected and broken up as described for passaging up to the last BSA-PBS wash. The cells were then washed with PBS and a single-cell suspension was prepared by incubating the cell pellet with AccuMAX for up to 10 minutes at room temperature, pipetting up and down every 2-3 minutes and inspecting the cells microscopically. To quench Accutase activity, 5 ml of basal medium were added to the cells, followed by centrifugation for 3 minutes at 1,000 g. After removing the supernatant, the cell pellet was resuspended in the desired volume of infection medium, usually 100 μl per original well of organoids. 100 μl of cell suspension were mixed with 250 μl of viral suspension and placed in a well of a 48-well plate. The cells were then “spinoculated” for 60 minutes at 600 g in a plate centrifuge, followed by 6 hours of incubation in a cell culture incubator with a humidified atmosphere at 37 °C and 5 % CO_2 . The cells were then collected in BSA-PBS-coated 1.5 ml centrifuge tubes using 1 ml of BSA-PBS, centrifuged for 5 minutes at 1,000 g and seeded in Matrigel as described for regular organoid culture. For 72 h after transduction, infection medium supplemented with 10 μM Y-27632 was used, followed by CCM with added antibiotics to select for transduced cells. 0.5 $\mu\text{g/ml}$ puromycin or 1.5 $\mu\text{g/ml}$ blasticidin were applied until the organoids grew back and regained their crypt-villus architecture.

4.1.6 Functional organoid experiments

To investigate ISC function in knockout organoids, intestinal crypts of knockout and control animals were isolated as described in section 4.1.1. Crypts were counted prior to seeding and 400 intestinal crypts per well of a 48-well plate were seeded and cultivated for 5 days, changing medium every second day. For the morphological analysis, the plate was imaged using the Zeiss LSM 700 confocal microscope's transmitted light photomultiplier (T-PMT) to obtain 2D-images of the entire wells. The number of organoids and their morphology was then analyzed using the OrganoSeg software as described in section 4.4.3. To investigate ISC function in knockdown organoids, inducible shRNA-expressing organoids were generated by lentiviral transduction as described in section 4.1.5. Organoids were prepared for seeding as detailed in section 4.1.3. 25 μ l of cell-Matrigel suspension were seeded into each well of an ibidi 8-well μ -Slide and covered with medium. Expression of the shRNA constructs was induced immediately by adding 1 μ g/ml doxycycline. Imaging experiments were performed as detailed in section 4.4.2, once immediately after seeding and then every 24 h for up to 168 h. After concluding the imaging experiment, organoid RNA was harvested as detailed in section 4.2.9.

4.1.7 Cultivation of cell lines

All cell lines were cultured in a humidified atmosphere at 37 °C and 5 % CO₂. HA-R-Spondin1-Fc 293T cells were cultivated using DMEM medium containing 10 % v/v fetal bovine serum (FBS) and 1x Penicillin-Streptomycin. Cells were passaged every 2-3 days by removing the culture medium, washing the flask with PBS and incubating the cells with Trypsin-EDTA solution for 5 minutes or until all cells detached. Culture medium was then added to quench trypsin activity, followed by splitting the cells in a 1:4 to 1:6 ratio. The appropriate volume of culture medium was added according to the culture flask's size. Wnt3a-L-cells were cultivated using DMEM medium containing 10 % v/v FBS and 1x Penicillin-Streptomycin. Cells were passaged every 2-3 days by removing the culture medium, washing the flask with PBS and incubating the cells with Trypsin-EDTA solution for 5 minutes or until all cells detached. Culture medium was then added to quench trypsin activity, followed by splitting the cells in a 1:4 to 1:6 ratio.

The appropriate volume of culture medium was added according to the culture flask's size. HEK-293T and CMT-93 were cultivated using DMEM medium containing 10 % v/v and 1x Penicillin-Streptomycin. Cells were passaged every 2-3 days by removing the culture medium, washing the flask with PBS and incubating the cells with Trypsin-EDTA solution for 5 minutes or until all cells detached. Culture medium was then added to quench trypsin activity, followed by splitting the cells in a 1:10 to 1:20 ratio. The appropriate volume of culture medium was added according to the culture flask's size.

4.1.7.1 Generation of R-Spondin1-conditioned medium

R-Spondin1-conditioned medium for the culture of intestinal organoids was generated from HA-R-Spondin1-Fc 293T cells. HA-R-Spondin1-Fc 293T cells were thawed and expanded in basal growth medium, followed by selection for 5 days, ensuring the presence of the R-Spondin1 construct in all cells. The cells were passaged when they reached 80-90 % confluence and usually split at ratios of 1:4 and 1:6, maintaining confluence of ca. 40-90 %. For R-Spondin1-conditioning, 3 T175 cell culture flasks were seeded with cells and expanded until they reached 80 % confluence. The culture medium was then changed to conditioning medium, followed by 7 days of culture without another medium change or passaging of the cells. The medium was then collected and centrifuged for 15 minutes at 3,000 g and 4 °C. The supernatant was passed through a 0.45 µm vacuum filter and divided into 5 ml aliquots in 15 ml centrifuge tubes for storage at -80 °C.

4.1.7.2 Generation of Wnt3a-conditioned medium

Wnt3a-conditioned medium for the culture of intestinal organoids was generated from Wnt3a-L-cells. Wnt3a-L-cells were thawed and expanded in basal growth medium, followed by selection for 5 days, ensuring the presence of the Wnt3a construct in all cells. The cells were passaged when they reached 80-90 % confluence and usually split at ratios of 1:4 and 1:6, maintaining confluence of ca. 40-90 %. For Wnt3a-conditioning, 3 T175 cell culture flasks were seeded with cells and expanded until they reached 80 % confluence. The culture medium was then changed to conditioning medium, followed by 7 days of culture without

another medium change or passaging of the cells. The medium was then collected and centrifuged for 15 minutes at 3,000 g and 4 °C. The supernatant was passed through a 0.45 µm vacuum filter and divided into 5 ml aliquots in 15 ml centrifuge tubes for storage at -80 °C.

4.2 Molecular biology techniques

4.2.1 Plasmid cloning of shRNA constructs

The lentiviral inducible shRNA expression plasmids were designed and cloned as follows: Sequences targeting the genes of interest were selected from the database provided by the RNAi Consortium (TRC) and tested in shRNA-expressing pLKO1 plasmids available from Sigma-Aldrich's Mission shRNA library. The targeting sequence's ability to reduce mRNA expression in CMT-93 cells was tested by transfection of the plasmids, RNA isolation and quantification of target gene mRNA levels using RTqPCR. The screening experiments up to this point were done in collaboration with Inga Shcheglova as part of her bachelor's thesis.

Generally, the two most effective sequences for each gene were selected for cloning into the lentiviral doxycycline-inducible shRNA expression plasmid LT3GEPIR (Fellmann et al., 2013). To that end, two oligonucleotides, the forward and reverse strand, were designed following the general structure displayed in Figure 5.

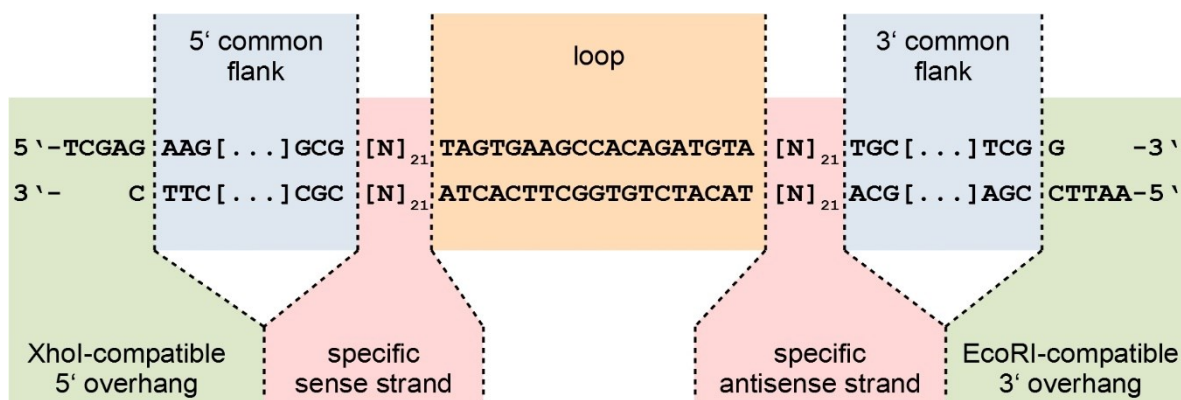


Figure 5 Structure of oligonucleotides used in shRNA cloning.

The full oligonucleotide sequences used for each target gene are listed in Table 13. First, the complementary oligonucleotides were annealed. To that end, a 1:1 mix of both oligonucleotides was prepared as detailed in Table 19.

Table 19 shRNA oligonucleotide annealing reaction

Reagent	Volume per reaction
Forward strand oligo (10 μ M)	11.25 μ l
Reverse strand oligo (10 μ M)	11.25 μ l
10x Annealing buffer	2.5 μ l

The annealing mix was then placed in a water bath of ca. 1 liter at 95 °C and left to cool until it reached room temperature, followed by 1:400 dilution in 0.5x annealing buffer. In parallel, the target vector was linearized using restriction digest with both XhoI and EcoRI. The reactions were set up as described in the table below and incubated for 1 hour at 37 °C.

Table 20 Linearization reaction of LT3GPIR for shRNA cloning

Reagent	Volume per reaction
LT3GPIR (1 μ g/ μ l)	4 μ l
10x Tango buffer	8 μ l
XhoI	1 μ l
EcoRI	1 μ l
ddH ₂ O	to 40 μ l

The digest reactions were then separated using agarose gel electrophoresis and the plasmid backbone fragment was isolated by gel cleanup, utilizing the Macherey-Nagel NucleoSpin Gel and PCR Clean-up kit according to the manufacturer's instructions. Subsequently, the reactions ligating the double-stranded oligonucleotides into the linearized plasmid backbone were set up as described below and incubated for 1 to 3 hours at room temperature.

Table 21 shRNA oligonucleotide ligation reaction

Reagent	Volume per reaction
Annealed oligonucleotide dilution	1 μ l
Linearized plasmid	1 μ l (10-20 ng)
10x Ligation buffer	1 μ l
T4 DNA ligase	1 μ l
ddH ₂ O	to 10 μ l

Transformation of up to 5 µl of each ligation reaction was performed as described in 4.2.5. Single colonies were selected and screened for plasmid carrying the correct insert. To that end, each colony was used to inoculate a backup LB agar plate, a colony PCR reaction as described in 4.2.6 and a 1.5 ml LB overnight culture for plasmid isolation as described in 4.2.7. Isolated plasmid DNA underwent restriction digests to confirm structural integrity of the DNA construct, as well as sequencing to confirm the sequence of the insert. Plasmids for which correct ligation could be confirmed were then used for further experiments.

4.2.2 Recombination of bacterial artificial chromosomes

4.2.2.1 Donor plasmid cloning

To insert an ampicillin selectable Cre construct into a BAC containing the *Alpi* gene, first a donor plasmid was generated from phCre2-ERT2.pA.FRTN1ampFRT. To that end, the present Cre2-ERT2 insert was replaced with a Cre2 insert. First, the Cre2-ERT2 insert was removed by restriction digest using HindIII and BamHI. Simultaneously, the new Cre2 insert was PCR-amplified from phCre2-ERT2.pA.FRTN1ampFRT utilizing primers #145 and #146, that added a 5' EcoRI restriction site and a 3' STOP codon to the Cre2 insert. Subsequent ligation of that insert yielded the desired plasmid phCre2.pA.FRTN1ampFRT. For the homologous recombination into the BAC, additional homology arms were added both 5' and 3' of the cassette that was to be inserted into the BAC. The homology arms were PCR-amplified using primers #149/150 (5') and #151/152 (3') from the target BAC. Both homology arms were inserted into the donor plasmid by restriction digest and subsequent ligation. EcoRI and HindIII were used for the 5' homology arm, NheI for the 3' homology arm. Colony PCRs and sequencing of all intermediate steps was done using primers #147/148.

4.2.2.2 BAC recombination

In short, insertion of the ampicillin selectable Cre2 construct was performed utilizing Red/ET recombination. Bacteria containing the target BAC were made recombination-competent by transformation of pRED/ET. The intended insert was PCR-amplified from the previously cloned donor plasmid

phCre2.pA.FRTN1ampFRT, cleaned up after agarose gel separation and transformed into the newly recombination-competent bacteria (Figure 6 A). After confirmation of successful recombination of the insert into the BAC, the ampicillin selection cassette was removed by FLPase recombination (Figure 6 B).

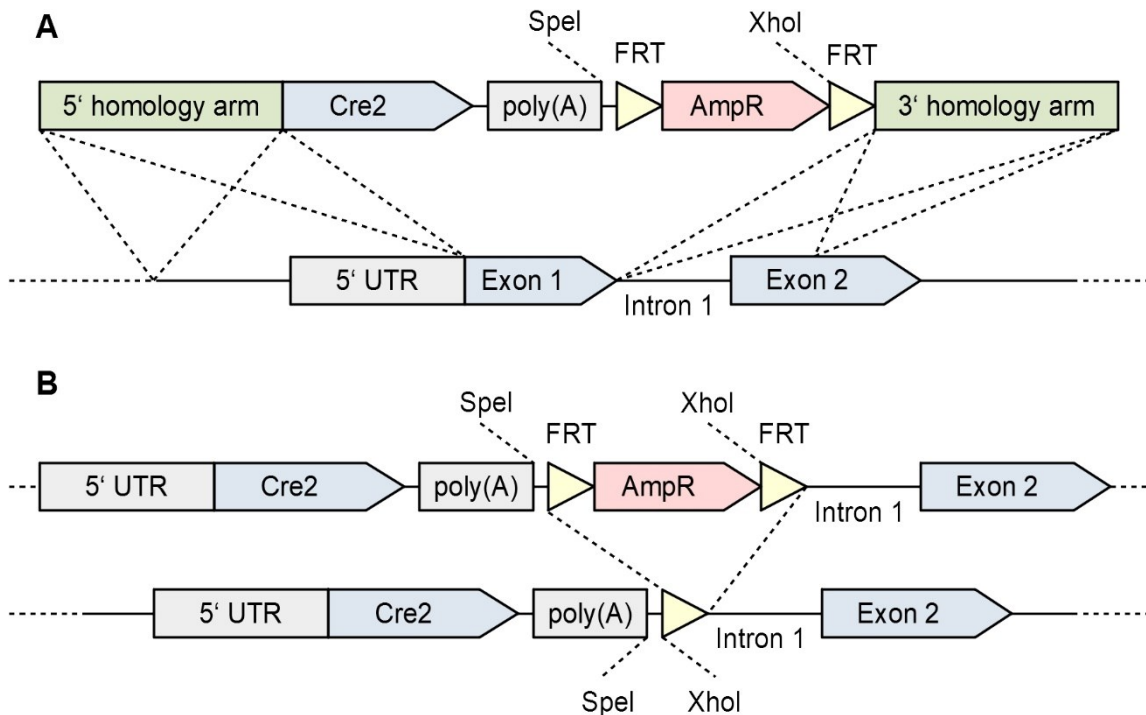


Figure 6 Schematic of BAC recombination steps. (A) pRED/ET-mediated homologous recombination of the Cre2 insert into the *Alpi* BAC. (B) FLPase-mediated removal of the ampicillin resistance selection marker.

To that end, an expression plasmid containing FLPase was transformed into bacteria containing the BAC that was to be modified. Successful FLPase recombination was confirmed by both test digest and PCR and correctly modified BACs were injected into mouse oocytes. In detail, the following protocol was used:

Transformation of pRED/ET into *E. Coli*

To make the bacteria containing the BAC recombination-competent, they were transformed with the plasmid pRED/ET. To that end, the day before the transformation, the bacteria were spread on a LB agar plate containing streptomycin to ensure their sensitivity to the antibiotic. In addition, a pre-culture of 1 ml LB medium with chloramphenicol was inoculated and incubated at 37 °C and 1,000 rpm in a shaking heat block overnight. The following day, three reaction tubes with 1.4 ml of LB with chloramphenicol were inoculated with 30 µl of the preculture

and cultivated 2-3 h at 37 °C and 1,000 rpm in a shaking heat block, followed by centrifugation for 30 seconds at 11,000 rpm and 2 °C. All further steps were performed on ice. The supernatant was discarded, and the resulting pellet was washed three times by resuspending the bacteria in autoclaved ddH₂O and centrifuging as before. After the last wash step, the supernatant was discarded by pouring off, leaving ca. 20-30 µl to remain in the reaction tube, in which the pellet of bacteria was resuspended by flicking the tube. 1 µl of 20 ng/µl pRED/ET was added to two of the three bacterial suspensions, which were subsequently transferred to electroporation cuvettes, followed by electroporation using the *E. coli* 1 standard protocol of the Biorad Micropulser. The bacteria were washed out of the cuvettes with 1 ml of LB medium without antibiotics and transferred to 1.5 ml reaction tubes. One of the cultures, that received the plasmid was cultured at 37 °C, the other together with the control culture without plasmid at 30 °C and 1,000 rpm for 70 minutes. 100 µl of each preculture were streaked on an LB agar plate containing both chloramphenicol and tetracycline to select for the BAC and pRED/ET respectively, followed by overnight incubation at 30 °C protected from light.

Insertion of the *Cre2-AmpR* cassette into the BAC

The following day, a preculture of 1 ml LB medium with chloramphenicol and tetracycline was inoculated with pRED/ET-positive bacteria and incubated at 30 °C and 1,000 rpm in a shaking heat block overnight. Four 1.5 ml reaction tubes were prepared with 1.4 ml of LB medium with chloramphenicol and tetracycline and inoculated with 30 µl of overnight preculture, followed by incubation at 30 °C and 1,000 rpm until optical density at 600 nm reached 0.3, usually for ca. 2 hours. Two tubes were then stimulated with 50 µl of 10 % L-arabinose solution, the other two were left unstimulated as controls and culture continued for another 45 to 60 minutes at 37 °C and 1,000 rpm. Preparation of bacterial pellets for transformation was then performed by centrifugation for 30 seconds at 11,000 rpm and 2 °C. All further steps were performed on ice. The supernatant was discarded, and the resulting pellet was washed three times by resuspending the bacteria in autoclaved ddH₂O and centrifuging as before. After the last wash step, the supernatant was discarded by pouring off, leaving ca. 20-30 µl to remain in the reaction tube, in which the pellet of bacteria was resuspended by flicking the tube. 2-3 µl of the previously PCR-amplified *Cre2* insert (primers #149/152) were

added to one arabinose-stimulated and one unstimulated tube of bacteria. All bacteria were then electroporated as described above, followed by a preculture in 1 ml of LB without antibiotics for 70 minutes at 37 °C and 1,000 rpm. 100 µl of these cultures were streaked on an LB agar plate containing both chloramphenicol and ampicillin to select for the BAC and the insertion of the *Cre2* cassette. Tetracycline was omitted from the agar so bacteria would lose the pRED/ET recombination plasmid. Correct recombination was verified by PCR of both recombination sites (5': primers #149b/168; 3': #146/152b) and restriction digest (BcuI; XhoI) of the BAC that resulted from the homologous recombination.

FLPase-mediated removal of the *Cre2* insert's ampicillin resistance

For each BAC clone tested successfully for the insertion of the *Cre2-AmpR* insert the following preparations were made for their transformation with the p706-FLP recombination plasmid. An overnight preculture was inoculated with a single clone in a 1.5 ml reaction tube containing 1.4 ml of LB medium with chloramphenicol and ampicillin and cultured at 37 °C and 1,000 rpm. The following day, two 1.5 ml reaction tubes with LB containing chloramphenicol and ampicillin were inoculated with 30 µl of the overnight preculture each and cultivated at 37 °C and 1,000 rpm for 2-3 hours. Preparation of bacterial pellets for transformation was then performed by centrifugation for 30 seconds at 11,000 rpm and 2 °C. All further steps were performed on ice. The supernatant was discarded, and the resulting pellet was washed three times by resuspending the bacteria in autoclaved ddH₂O and centrifuging as before. After the last wash step, the supernatant was discarded by pouring off, leaving ca. 20-30 µl to remain in the reaction tube, in which the pellet of bacteria was resuspended by flicking the tube. To one of the tubes, 2 µl of 20 ng/µl p706-FLP was added and both bacterial suspensions were electroporated as described above, followed by a preculture in 1 ml of LB without antibiotics for 70 minutes at 30 °C and 1,000 rpm. 100 µl of each bacterial culture was streaked on LB agar plates containing chloramphenicol and tetracycline and incubated protected from light at 30 °C overnight. Single tetracycline-resistant colonies were then selected for the induction of FLPase recombination. A preculture of 200 µl LB with chloramphenicol and tetracycline in a 1.5 ml reaction tube was inoculated with a single colony and cultivated for 2 hours at 30 °C and 1,000 rpm. The resulting bacterial suspension was streaked on LB agar plates

with chloramphenicol but without tetracycline resulting in the loss of p706-FLP, and incubated overnight at 37 °C, which induces expression of the FLPase. On the following day, single colonies were used to inoculate an LB agar backup plate containing chloramphenicol, and 2 1.5 ml reaction tubes, one with LB containing only chloramphenicol, the second with LB containing chloramphenicol and ampicillin, which were incubated overnight at 37 °C and 1,000 rpm. Clones were selected for analysis if bacteria did not grow in the culture with ampicillin, indicating successful FLPase-mediated removal of the ampicillin resistance in the *Cre2* insert. Correct modification was confirmed by PCR of the recombination sites (5': primers #149b/168; 3': #146/152b) and restriction digest of BAC DNA (*BcuI*; *XhoI*). In addition, the entire insert was PCR-amplified (primers #149b/152b) and sent for sequencing (primers #149/152/169/170).

4.2.2.3 Preparation of BAC DNA for oocyte injection

BAC DNA for oocyte injection was obtained by growing out the bacteria overnight in an Erlenmeyer flask with 300 ml of LB medium with chloramphenicol. BAC DNA was then prepared as follows: Bacterial overnight cultures were centrifuged 10 minutes at 5,000 rpm and 4 °C. The supernatant was discarded, and the resulting pellet was resuspended, lysed and neutralized using 12 ml each of the respective Macherey-Nagel NucleoBond Xtra Midi kit buffers. The samples were centrifuged 15 minutes at 4,000 rpm and 4 °C and the supernatant transferred to a 15 ml centrifuge tube. 2 ml of phenol-chloroform-isoamyl alcohol (PCI) were then mixed with the sample, followed by centrifugation for 15 minutes at 4,000 rpm and 4 °C. The supernatant was transferred to a new 15 ml centrifuge tube and precipitated with isopropyl alcohol and centrifuged for 60 minutes at 4,000 rpm and 4 °C. After discarding the supernatant, the pellet was dissolved in 1 ml 10 mM Tris and mixed with 20 ml chloroform. The solution was centrifuged for 15 minutes at 4,000 rpm and 4 °C, the aqueous phase transferred to a new reaction tube and again mixed with chloroform at a ratio of 1:1. The samples were centrifuged for 10 minutes at maximum speed and room temperature in a micro-centrifuge. The aqueous phase was transferred to a new reaction tube again and precipitated with isopropyl alcohol as before. The supernatant was discarded, and the DNA pellet dissolved in 10 mM Tris solution. Prior to the oocyte injection of the DNA, the BAC's structural integrity was confirmed by restriction digest,

PCRs and sequencing of the full insert as described before. A clone that gave positive results in all tests was selected and linearized by restriction digest, removing the pBACe3.6 plasmid backbone:

Table 22 BAC linearization reaction

Reagent	Volume per reaction
BAC DNA (2.5 µg/µl)	50 µl
10x Buffer O	50 µl
100x BSA	5 µl
100 mM Spermidine	12.5 µl
NotI	20 µl
ddH ₂ O	to 500 µl

Samples were incubated overnight at 37 °C and the restriction enzyme was heat inactivated at 65 °C for 20 minutes. Separation of the resulting DNA fragments was done by Sepharose gel permeation chromatography. To construct the column, a sterile 5 ml cell culture pipette was used (Figure 7). The filter string from the top end of the pipette was removed, pulled apart and part of it was placed in the pipette's tip. Sepharose was then resuspended in its original container and added in small steps to prevent air from getting trapped in the column until the pipette was almost filled. A 12 ml syringe without a plunger was then placed on top of the pipette and fixed to it using strips of Parafilm to serve as a buffer reservoir. Whenever necessary, the flow of buffer through the column was stopped by closing the tip of the 5 ml pipette with a micropipette tip that had its tip closed by melting it shut. To equilibrate the stationary phase of the column, 30 ml of oocyte injection buffer were passed through the column over the course of ca. 5 hours and 40 minutes. To load the BAC digest reaction onto the column, it was mixed with the appropriate volume of 6x loading dye, the buffer reservoir was temporarily removed, and the digest reaction was slowly pipetted on top of the Sepharose without disturbing it. The sample entered the Sepharose column before the buffer reservoir was replaced and 10 ml of oocyte injection buffer were added. Starting at that time point, 20 500 µl fractions were collected. To confirm complete linearization, and identify the fractions with the highest concentration, 45 µl of each fraction were separated using agarose gel electrophoresis as described for the diagnostic BAC restriction digests. The fractions showing the

highest band intensity at the appropriate size were selected for oocyte injection and handed over to collaborators at the Max-Planck Institute for Heart and Lung Research (Bad Nauheim), who performed the oocyte injection and mouse husbandry.

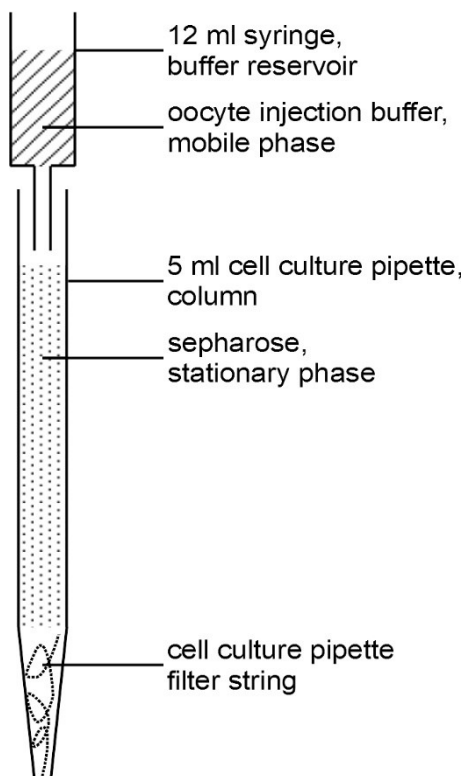


Figure 7 Sepharose-based gel permeation chromatography column. Schematic of the Sepharose column assembly used to separate the linearized BAC from its plasmid backbone; dimensions not to scale.

4.2.3 Bacterial cultures

Bacteria were cultured in LB or on LB agar plates at 37 °C where not indicated otherwise. Antibiotics working concentrations are indicated in Table 23.

Table 23 Working concentrations of bacterial antibiotics

Antibiotic	Working concentrations
Ampicillin	100 µg/ml
Chloramphenicol	15 µg/ml
Tetracycline	3 µg/ml
Kanamycin	15 µg/ml
Streptomycin	50 µg/ml

4.2.4 Preparation of electrocompetent bacteria

Bacteria from a previous preparation or a tube of bought bacteria were streaked on an LB agar plate using a three-phase streaking pattern (T-streak) and cultivated overnight at 37 °C. A single colony from this plate was used to inoculate a 10 ml SOB preculture in an Erlenmeyer flask and incubated 16-18 h at 37 °C and 200 rpm in a shaking incubator. Subsequently, 6 Erlenmeyer flasks containing 200 ml of prewarmed SOB were inoculated with 2 drops of preculture each, followed by incubation at 37 °C and 200 rpm. Optical density of the cultures was measured regularly at a wavelength of 600 nm until it reached 0.5-0.7. The bacterial cultures were then transferred to centrifuge cups and placed on ice for 15 minutes followed by centrifugation for 10 minutes at 5,000 rpm and 4 °C. The supernatant was removed, and the resulting pellet was resuspended in 200 ml of 10 % v/v glycerol dissolved in distilled water per cup. Centrifugation and resuspension in glycerol were repeated, followed by another centrifugation step. The supernatant was then poured off and the pellets were resuspended in the residual glycerol by pipetting up and down. Finally, the resulting bacteria suspension was aliquoted to 100 µl and stored at -80 °C.

4.2.5 Electroporation of plasmid DNA into bacteria

Electrocompetent bacteria were thawed on ice and 50 µl were aliquoted into 1.5 ml reaction tubes for each transformation reaction. Up to 5 µl of any DNA solution were added to the bacteria and mixed by flicking the tube. The entire volume was then transferred to an electroporation cuvette and electroporated using the *E. coli* 1 protocol of the Biorad Micropulser. 1 ml LB medium without antibiotics was used to resuspend the bacteria and incubated for 1 hour at 37 °C and 1,000 rpm on a shaking heat block. To obtain single colonies, 250 µl of this preculture were streaked on LB agar plates containing the appropriate antibiotic to select for the transformed DNA molecule and incubated overnight at 37 °C.

4.2.6 Colony PCR

To identify bacterial colonies that carry the desired DNA construct after plasmid cloning or BAC recombination, colony PCR was used. A PCR master mix was prepared using the volumes indicated in Table 24.

Table 24 Colony PCR master mix

Reagent	Volume per reaction
10x Taq buffer with KCl	5 μ l
MgCl ₂	8 μ l
dNTPs; 10 mM	1 μ l
DMSO	1.5 μ l
Forward primer; 10 μ M	1 μ l
Reverse primer; 10 μ M	1 μ l
Taq DNA polymerase	0.2 μ l
ddH ₂ O	to 50 μ l

Each reaction was inoculated with a single bacterial colony by tapping the colony with a pipette tip and then suspending the bacteria in the mix by pipetting up and down. When further expansion of the bacteria was required, the same tip was used to inoculate a LB backup plate as well as a small LB overnight culture. The colony PCR reaction was run in a thermocycler with the protocol in Table 25.

Table 25 Colony PCR protocol

PCR step	Temperature [°C]	Duration [s]	
Initial denaturation	95	180	
Denaturation	95	30	x30
Annealing	[T _a = T _m - 5]	30	
Extension	72	[product length in kb * 60]	
Final extension	72	300	
Hold	4	∞	

The resulting PCR products were separated using agarose gel electrophoresis to determine if a bacterial clone contained the desired construct.

4.2.7 Plasmid and BAC DNA isolation

Small alkaline quickies

To isolate plasmid or BAC DNA from bacteria, overnight cultures of 2 ml LB in a 2 ml reaction tube were inoculated with the desired bacterial clone and incubated at 37 °C on a shaking incubator. The following day, cultures were centrifuged at 13,000 rpm for 5 minutes and the supernatant was removed. The bacterial pellet

was resuspended in 200 µl of buffer S1 by pulse vortexing. 200 µl of buffer S2 were added to each reaction and mixed by inverting. 200 µl of buffer S3 were added and samples were incubated on ice for 5 minutes and centrifuged at 13,000 rpm for 10 minutes. The supernatant was transferred to a fresh 1.5 ml reaction tube, 500 µl PCI were added and the samples were mixed by vigorous shaking for 30 seconds, followed by centrifugation at 13,000 rpm for 5 minutes. The supernatant was again transferred to a new 1.5 ml reaction tube and DNA was precipitated by addition of 500 µl of isopropyl alcohol. Samples were placed at -20 °C for 10 minutes, centrifuged at 13,000 rpm for 10 minutes and the supernatant was removed. The resulting pellet was washed with 500 µl 70 % ethanol, air-dried and dissolved in ddH₂O.

4.2.8 Diagnostic restriction digests of BACs

The structural integrity and sequence identity of BACs was tested using restriction digests of BAC DNA. For this, fragment sizes were predicted by in silico digest using the ApE software (Davis, 2020). The digest reactions were then set up as follows:

Table 26 Diagnostic BAC digest

Reagent	Volume per reaction
10x Enzyme buffer	5 µl
Restriction enzyme	2 µl
BAC DNA	35 µl
ddH ₂ O	to 50 µl

Samples were incubated for 1 hour at 37 °C, mixed with 6x loading dye and separated in an agarose gel at 4 °C and 45 V over 24 hours with images of the gel being taken at varying intervals to document smaller DNA fragments. If necessary, the gel run was extended beyond 24 hours to also be able to better differentiate between large DNA fragments.

4.2.9 RNA isolation

RNA-isolation of both 2D cell cultures and organoids was done by first removing the culture medium, washing the cells with PBS and adding the appropriate volume of TriFast to each well, e.g. 250 μ l for each well in a 48-well plate. After 2 minutes of incubation, the reagent was pipetted up and down to dissolve the cells and the resulting solution was collected in 1.5 ml reaction tubes. 50 μ l of chloroform were added to each tube, the samples were shaken vigorously for 15 seconds and incubated 10 minutes at room temperature. The samples were then centrifuged for 5 minutes at 12,000 g and the aqueous supernatant was transferred to a new 1,5 ml reaction tube and the remaining sample discarded. 125 μ l of isopropyl alcohol were added to each sample, the tubes were inverted to mix the solution and chilled for 10 minutes at -20 °C, before precipitation by centrifugation for 10 minutes at 4 °C and 12,000 g. The supernatant was discarded two wash steps were done as follows: 500 μ l of 70 % ethanol were added to each tube, and the samples were centrifuged for 5 minutes at 12,000 g. The supernatant was discarded and after the second wash step the pellets were air-dried and dissolved in 20 μ l of nuclease-free H₂O.

4.2.10 Real-time quantitative polymerase chain reaction

Reverse transcription

Following RNA isolation, reverse transcription was performed to yield cDNA for the use in RTqPCR. For this, the desired amount of RNA per sample was mixed with 1 μ l of random hexamer primer, filled to 12.5 μ l with nuclease-free H₂O and incubated at 65 °C in a thermocycler for 5 minutes. The samples were then mixed with 7.5 μ l of the following master mix:

Table 27 Reverse transcription master mix

Reagent	Volume per reaction
5x Reaction buffer for RT	4 μ l
Ribolock RNase inhibitor	0.5 μ l
dNTPs	2 μ l
Reverse transcriptase	1 μ l

Reverse transcription was done following the protocol in Table 28.

Table 28 Reverse transcription thermocycler protocol

Temperature	Duration [minutes]
25 °C	10
42 °C	60
70 °C	10
4 °C	∞

The finished cDNA samples were then diluted to a final concentration of 2 ng per μl sample and stored at $-20\text{ }^{\circ}\text{C}$ or used immediately for analysis in qPCR.

Real-time quantitative PCR

Real-Time quantitative PCR was performed by preparing a master mix for each primer pair to be used in the reactions according to Table 29.

Table 29 RTqPCR master mix

Reagent	Volume per reaction
SybrGreen	12.5 μl
nuclease-free H ₂ O	7 μl
Primer mix, 10 μM	0.5 μl

20 μl of this master mix was distributed to each well of a 96-well PCR plate and mixed with 5 μl of diluted cDNA solution, containing 10 ng of cDNA per reaction. The RTqPCR was then run in a CFX Connect Real-Time PCR Detection System qPCR machine using the following protocol:

Table 30 RTqPCR protocol

PCR step	Temperature [$^{\circ}\text{C}$]	Duration [s]	
Denaturation	95	300	
Denaturation	95	15	x39
Annealing	58	30	
Extension	72	30	
Melting curve	65 to 95 in 0.5 increments	5 per step	

mRNA expression levels were calculated using the $\Delta\Delta\text{Ct}$ method, normalizing to the housekeeping gene *Ywhaz*.

4.2.11 Dual-luciferase assay

Reporter cell transfection and stimulation

To determine Wnt pathway activation capability of the Wnt3a-conditioned and R-Spondin1-conditioned media, a Dual Luciferase Assay was performed using the Dual-Luciferase Reporter Assay Kit by Promega. HEK-293T cells were transfected for use as reporter cells in a 24-well plate, for which the following plasmid mixes were prepared in DMEM:

Table 31 Plasmid mixes for dual-luciferase assay reporter cell transfection

Plasmid mix	Plasmid concentrations
TOP	<ul style="list-style-type: none">• pGL4.10[luc2]_TOP10; 100 ng per well• pRL-CMV; 10 ng per well
FOP	<ul style="list-style-type: none">• pGL4.10[luc2]_FOP10; 100 ng per well• pRL-CMV; 10 ng per well
TOP β -Cat	<ul style="list-style-type: none">• pGL4.10[luc2]_TOP10; 100 ng per well• pCS2 β-CateninS33A; 50 ng per well• pRL-CMV; 10 ng per well
FOP β -Cat	<ul style="list-style-type: none">• pGL4.10[luc2]_FOP10; 100 ng per well• pCS2 β-CateninS33A; 50 ng per well• pRL-CMV; 10 ng per well

Additionally, 0.5 μ l of Fugene HD transfection reagent per well were mixed with 100 μ l of DMEM per well. 100 μ l per well of this mix were added to each plasmid mix, followed by 15 minutes of incubation at room temperature. In the meantime, HEK-293T cells were trypsinized and counted. 30,000 cells per well were then added to each of the plasmid mixes and the final volume of all mixes was adjusted to 0.5 ml per well by adding DMEM culture medium. The transfection mixes containing the cells were then seeded into the wells of a 24-well cell culture plate and incubated in a humidified cell culture incubator at 37 °C and 5 % CO₂. The following day, the cell culture medium was exchanged to stimulation medium, consisting of a mix of regular DMEM cell culture medium and 10 % R-Spondin1- or 50 % Wnt3a-conditioned medium generated previously. For each stimulation condition, 2 wells of the TOP-transfected cells, as well as 2 wells of the FOP-transfected cells were treated with stimulation medium. As a positive control

condition, 2 wells of the TOP β -Cat-transfected cells, as well as 2 wells of the FOP β -Cat-transfected cells received regular culture medium mixed with non-conditioned conditioning medium used in the generation of R-Spondin1 and Wnt3a-conditioned media. As a negative control, 2 wells of the TOP-transfected cells, as well as 2 wells of the FOP-transfected cells received regular culture medium mixed with non-conditioned conditioning medium used in the generation of R-Spondin1 and Wnt3a-conditioned media. Stimulation was done for 24 hours in a humidified cell culture incubator at 37 °C and 5 % CO₂. Cells were then washed with PBS and 100 μ l of 1x passive lysis buffer prepared according to the manufacturer's directions were pipetted into each well of the cell culture plate followed by 15 minutes of incubation at room temperature on an orbital shaker. Lysates were then transferred to 1.5 ml reaction tubes and cleared by centrifugation for 30 seconds at maximum speed. The supernatants were transferred to new 1.5 ml reaction tubes and stored at -20 °C or used immediately to measure luciferase activity.

Measurement

The Luciferase assay reagent and Stop & Glo reagent were prepared according to the manufacturer's instructions. 20 μ l of each sample were pipetted into a well of an opaque, white 96-well plate. Before the measurement, 100 μ l of luciferase assay reagent were added to all samples and firefly luciferase was measured immediately using the luminometer. To measure renilla luciferase activity, 100 μ l of Stop & Glo reagent were added to each sample and renilla luciferase activity was recorded using the luminometer. Wnt pathway activation was quantified by first dividing firefly luciferase luminescence to renilla luciferase luminescence for each sample for both TOP and FOP wells and then subsequently dividing the resulting TOP and FOP values:

$$\frac{\left(\frac{\text{firefly TOP}}{\text{renilla TOP}}\right)}{\left(\frac{\text{firefly FOP}}{\text{renilla FOP}}\right)} = \text{Wnt activation}$$

4.3 Histological and immunohistochemical methods

4.3.1 Swiss rolling of small Intestine and colon samples

Mice were sacrificed and the small and large intestine removed as required for analysis. The organs were placed in a glass petri dish with a 15 cm diameter, of which the bottom was filled with clear silicon and covered with PBS to wash the tissue. The distal end of the intestines was pinned to the silicon using 0.2 mm diameter minuten pins and opened longitudinally from the proximal end following the line where the mesentery was attached, pinning the sides of the tissue to the silicon as well. Remaining blood and intestinal contents were washed away with PBS, before replacing it with either 0.2 % PFA if the tissue was to be cryosectioned or 4 % PFA for paraffin sections. Fixation lasted 1 hour, and the opened intestines were then rolled onto toothpicks starting from the distal side of the organ and rolling towards the proximal side with the luminal side of the organ facing the roll's inside. The tissue was fixated with minuten pins to prevent it from unrolling and placed in embedding cassettes for further preparation for either cryosectioning as described in 4.3.2 or paraffin embedding and sectioning as described in 4.3.3.

4.3.2 Preparation of cryosections

Fixation and sample storage

For the preparation of cryosections from tissue, the samples were first fixed in a 0.2 % PFA-PBS solution at 4 °C overnight. PFA-PBS was replaced by 30 % w/v sucrose-PBS solution and the samples were incubated at 4 °C overnight. In a polystyrene box half filled with dry ice, a sheet of aluminum foil was placed. To freeze the samples, they were taken from the sucrose-PBS solution and placed on the aluminum foil until they were frozen solid. With a pair of tweezers, the tissue was carefully loosened from the foil and wrapped in Parafilm followed by a layer of aluminum foil for storage at -80 °C.

Cryosectioning

For the sectioning of the fixed and frozen tissue, the samples were placed in the cryotome for equilibration to the temperature at which the tissue was to be sectioned. Using O.C.T. embedding medium, the tissue was frozen to the specimen

disc in the desired orientation. After the embedding medium was cured, 25 µm sections were cut from the sample and collected on a Superfrost Ultra Plus glass slide. The slides were dried at room temperature for 30 minutes and finally stored at -80 °C.

4.3.3 Preparation of paraffin sections

Fixation and embedding

For paraffin embedding, the sample's fixation was continued in 4 % PFA solution overnight at 4 °C followed by dehydration in alcohol solutions of ascending concentrations:

- 70 % ethanol, 2 hours
- 80 % ethanol, 2 hours
- 95 % ethanol, 2 changes of 2 hours each
- 100 % ethanol, 2 hours
- 100 % ethanol, overnight
- Ethanol-xylene 1:1, 1 hour
- Xylene, 2 changes of 30 minutes each
- Paraffin at 56 °C, 2 changes of 2 hours each

Finally, the tissue was embedded in paraffin blocks following standard histological procedure.

Paraffin sectioning

Prior to sectioning paraffin-embedded tissue, the blocks were placed at -20 °C for one hour. In the meantime, the microtome was prepared and a water bath at 40 °C was preheated. Generally, 5 µm sections were cut and placed in the water bath to stretch before being transferred to Superfrost Ultra Plus glass slides and dried on the water bath's rim until the remaining water was evaporated. Samples prepared in this manner were either used for further experiments immediately or stored at room temperature in the dark.

4.3.4 *lacZ* reporter staining

To perform *lacZ* reporter stainings, cryosections of the tissue were prepared as described in 4.3.2. The samples were equilibrated to room temperature and any remaining condensation dried at room temperature. Subsequently, the slides were incubated in fixation buffer for 5 minutes. Three wash steps in wash buffer were performed, followed by staining buffer at 37 °C overnight in the dark. The following day, the samples were washed twice in PBS for 5 minutes per step. The slides were then counterstained with eosin for 5-10 seconds and differentiated in a 1 % v/v acetic acid solution. Next, they were dehydrated in alcohol solutions of ascending concentrations (70 %, 80 %, 95 %, 99 %; 2 minutes each) and two changes of xylene for 5 minutes each. Lastly, they were mounted using Pertex mounting medium. After curing of the mounting medium, the samples were analyzed using the Leica DM750 light microscope.

4.3.5 Immunofluorescence staining

Immunofluorescence (IF) stainings were done on previously prepared cryosections of tissue. To equilibrate the sections, the required number was taken out of the freezer and placed at room temperature until all condensation disappeared, usually for 20-30 minutes. The sections were then post-fixed for 10 minutes in 4 % PFA at 4 °C. To quench the PFA, the samples were treated twice with 50 mM glycine in PBS for 5 minutes each and then washed with PBS for 5 minutes. Permeabilization and blocking were done for 30 minutes in PBS supplemented with 0.1 % Triton X 100 and 5 % horse serum. For incubation with the primary antibody, the slides were placed in a wet chamber and the primary antibodies diluted in blocking solution were pipetted on top of the tissue sections. The samples were incubated overnight at 4 °C in the wet chamber. The following day, all sections were washed three times for 5 minutes with PBS, before the secondary antibodies were added, diluted in blocking solution with added DAPI (1:5,000). The slides were incubated for 2 hours at room temperature in the dark before three final PBS washes for 5 minutes each. Lastly, the sections were mounted with DAKO fluorescence mounting medium and allowed to cure before being stored at 4 °C or being analyzed immediately.

4.3.6 Single-molecule RNA fluorescence *in situ* hybridization

Single-molecule RNA fluorescence *in situ* hybridization (smRNA FISH) is used to detect mRNA molecules on tissue sections by utilizing a mix of targeting probes, that bind to the transcript in a sequence-specific manner. Two of the probes need to bind adjacently on the transcript to increase specificity. Only then, the probes provide binding sites for a series of amplification reagents that serve to enhance signal intensity, making this method extremely sensitive. In the last step, chromogenic reactions produce either a Fast Red or 3,3'-Diaminobenzidine (DAB) precipitate. In addition, IF was used to stain the tissue for Lgr5, identifying stem cells in the intestinal crypt and allowing the quantification of a possible cell-type specific expression of mRNA transcripts. smRNA FISH was done using the RNAscope 2.5 HD assay BROWN or RED kits from ACD Bio. Generally, great care was taken to avoid the contamination of samples or reagents with RNases. Surfaces were regularly and thoroughly cleaned using 70 % v/v ethanol solution. All steps until finalization of the *in situ* hybridization were done using glass ware baked at 180 °C for 2 hours before use. Solutions were prepared using DEPC-treated water. Prior to the preparation of 5 µm paraffin sections as described in 4.3.3, the microtome and water bath were thoroughly cleaned using 70 % v/v ethanol. To remove excess paraffin, the slides were first baked for 1 hour at 60 °C and then treated with 2 changes of xylene for 5 minutes each, followed by 2 changes of 100 % ethanol. Specimens were then air-dried for 5 minutes. Sample pretreatment was done as follows: Samples were incubated with Pretreat solution 1 (H₂O₂) for 10 minutes at room temperature. After washing the slides in DEPC-treated H₂O twice, they were placed in a metal slide rack and boiled at 98-100 °C in Pretreat buffer 2 for 15 minutes. The slide rack was immediately transferred to DEPC-treated H₂O, followed by 2 wash steps in DEPC-treated H₂O and 1 step in 100 % ethanol. The Slides were then air-dried for 5 minutes at room temperature. Using an Immedge hydrophobic barrier pen, the tissue on each slide was framed 2-3 times and stored overnight in the dark at room temperature to let the frame dry. The following day, samples were treated with 50 µl protease for 30 minutes in a humidified rack at 40 °C using the HybEZ II oven. Protease was diluted 1:15 in H₂O if subsequent IF was planned. The slides were briefly washed twice in DEPC-treated water. Without letting the slides dry out, the samples were then

treated with the probe and amplification reagents. All incubation steps were performed at 40 °C in a humidified atmosphere using the HybEZ II oven, followed by 2 wash steps in 1x wash buffer for 2 minutes each. Generally, 1 drop of each reagent was used. Incubation times were as follows:

- Probe: 2 hours 10 minutes
- AMP1: 30 minutes
- AMP2: 15 minutes
- AMP3: 30 minutes
- AMP4: 15 minutes

Following AMP4 incubation and the described wash steps, samples were treated with AMP5 for 40 minutes at room temperature in the dark. After washing as before, 1 drop of AMP6 was applied for 15 minutes at room temperature, followed by another wash step. Signal detection differed between the kits used. When using the RNAscope 2.5 HD BROWN kit, solutions DAB-A and DAB-B were mixed 1:1. After washing the samples in DEPC-treated H₂O, 30 µl of the finalized DAB solution was pipetted onto each slide and the samples were incubated for 10 minutes in the dark. When using the RNAscope 2.5 HD RED kit, the RED-B reagent was diluted 1:60 in the RED-A reagent, pipetted onto the tissue sections and incubated for 10 minutes at room temperature in the humidified incubation chamber. In both cases the tissue sections were briefly washed in distilled H₂O twice after signal detection. The additional IF staining was done using the Alexa Fluor 488 Tyramide Superboost kit, as well as the Avidin/Biotin Blocking kit. All steps were performed at room temperature, unless stated otherwise. The slides were placed in a wet chamber and the tissue was covered with Tris-buffered saline with Tween (TBST) to prevent samples from drying. Peroxidase activity was then blocked by incubation with 3 %H₂O₂ for 10 minutes in the dark, followed by two TBST wash steps. Using the Avidin/Biotin Blocking Kit reagents, samples were first incubated with 1 drop of avidin solution for 10 minutes in the dark, washed twice with TBST and then treated with 1 drop of biotin solution for 10 minutes in the dark and again washed twice with TBST. For blocking, samples were treated with 10 %v/v goat serum for 30 minutes. After that, primary antibodies were applied at the appropriate dilution in 10 % v/v goat serum and incubated overnight at 4 °C in a wet chamber. The next day the wet chamber was placed at room

temperature for 30 minutes prior to washing the tissue sections 4 times with TBST. The biotinylated secondary antibody was diluted in 10 % goat serum and added to each sample, followed by a 30-minute incubation in the wet chamber and 4 wash steps with TBST. The samples were then treated with Streptavidin-HRP for 30 minutes and washed with TBST 4 times. Next, the Tyramide working solution was applied to the tissue, prepared from 100 μ l of 1x Reaction buffer, 1 μ l H₂O₂, and 1 μ l Tyramide Alexa Fluor 488 and incubated for 10 minutes in the dark. An equal volume of reaction stop reagent was then pipetted on each section and incubated for 1 minute, followed by 4 TBST washes. Lastly, the samples were stained with a 1:2,000 dilution of DAPI for 2 minutes in the dark, washed 4 times with TBST and placed in distilled H₂O for 5 minutes, before being mounted using DAKO fluorescence mounting medium. The mounting medium was cured for 10 minutes before analysis or storage at 4 °C.

4.4 Imaging techniques

4.4.1 Imaging and quantification of IF stainings and smRNA-FISH

Immunostaining and single-molecule RNA *in situ* hybridizations were imaged using the Zeiss LSM 700 confocal microscope. Low magnification images were taken using a 20x objective, high magnification images using a 63x objective. The images were further processed in the Fiji distribution of ImageJ (Rueden et al., 2017; Schindelin et al., 2012). In smRNA FISH experiments, cells positive for the mRNA species of interest were identified by either the red fluorescent precipitate or brown precipitate. To display the brown staining in a composite image with the fluorescence colors, T-PMT images of the section were taken to detect DAB precipitate, the brightness inverted, and assigned a false color. In both cases cell type-specificity for ISCs and Paneth cells was determined by IF co-staining for OLFM4. Starting at the crypt bottom, cells were identified as ISCs when they were OLFM4+ and as Paneth cells when they were OLFM4-. Based on the presence of precipitate, they were then counted as either FISH+ when precipitate was present or FISH- if no precipitate was detectable.

4.4.2 Live cell imaging of intestinal organoids

For live cell imaging of intestinal organoids, the Leica Thunder Imaging Microscope was used. Organoids were prepared following the protocol for passaging (4.1.3). 25 μ l of the cell-Matrigel suspension were seeded into ibidi 8-well μ -Slides and covered with the appropriate medium. The slide was placed in the microscope's incubation chamber at 37 °C and 5 % CO₂ for the duration of the imaging experiment. For morphological analysis, imaging was done using a 5x objective, recording a tile scan consisting of 3 by 3 z-stacks for each well covering the entire matrix drop. Z-stacks were transformed into 2D images using the Leica Application Suite X (LAS X) software package's extended depth of field (EDOF) functionality.

4.4.3 Computational analysis of organoid images

The images were further processed in the Fiji distribution of ImageJ (Rueden et al., 2017; Schindelin et al., 2012). The 3x3 EDOF projections of each well were merged into a single image, using the Grid/Collection stitching plugin, and saved in the JPEG format (Preibisch et al., 2009). They were then imported into OrganoSeg (Borten et al., 2018), and organoid separation was generally done using the following slider settings:

Threshold: 0.75

Window size: 250

Size threshold: 750

Organoid metrics were exported and analyzed structures were visually inspected in OrganoSeg to confirm proper recognition of organoids and exclusion of e.g. cell debris. The data of any structure that was not an organoid, was removed from the exported data set prior to statistical analysis.

4.4.4 Statistical analysis of imaging data

4.4.4.1 Quantification of cell type-specific ligand expression in smRNA-FISH images

To quantify cell type-specific mRNA expression in Paneth and stem cells, high magnification images of small intestinal smRNA-FISH samples were analyzed. Starting from the crypt bottom, OLFM4 positive stem cells and OLFM4 negative

Paneth cells were identified and classified into FISH-positive and FISH-negative cells. From the obtained values, the percentage of cells positive and negative for the respective mRNA was calculated for both cell types.

4.4.4.2 Statistical analysis of morphological organoid metrics obtained with OrganoSeg

Morphological data obtained from organoid imaging experiments was analyzed by 2-way ANOVA using GraphPad Prism.

4.5 Single cell RNA sequencing data and analysis

Single cell RNA (scRNA) sequencing data published by Parikh et al. was accessed under the GEO accession number GSE116222 (Parikh et al., 2019). The data of healthy human colon cells from this data set was analyzed by Mario Looso (Max-Planck Institute for Heart and Lung Research, Bad Nauheim).

5 Results

5.1 Expression analysis of semaphorins and plexins in the intestinal epithelium

To investigate the role of semaphorin-plexin signaling in the intestinal epithelium, first a systematic analysis of ligand expression was conducted. To that end, *lacZ* reporter stainings were used to analyze the expression of *Sema4A*, *Sema4B*, *Sema4C* and *Ang*. IF stainings were utilized to characterize expression of *Sema4B* and *Sema4D*. The expression patterns of *Sema4A*, *Sema4G*, *Ang*, and *PlexnB1* transcripts, as well as potential cell type-specificity in the intestinal crypt were investigated by smRNA FISH paired with IF for the stem cell marker OLFM4-. Finally, scRNA sequencing data of healthy human colonic epithelium, previously published by Parikh et al., was analyzed for the expression of class 4 semaphorins and plexins B1 and B2 (Parikh et al., 2019).

5.1.1 *Sema4A*, *4B*, *4C* and angiogenin are expressed in the intestinal epithelium

The expression of *Sema4A*, *Sema4B*, *Sema4C* and *Ang* in the small and large intestine was analyzed in *lacZ* reporter mice (Figure 8 and Figure 9 respectively). In these mice, a *lacZ* cassette was integrated into the genome under the control of the gene of interest's promoter (Schmidt et al., 1998). The cassette contains the *E. coli* gene *lacZ*, encoding beta-galactosidase which is expressed once the promoter becomes active. Thus, beta-galactosidase activity marks cells, in which the promoter is active. Tissue sections were then stained by *lacZ* staining, during which beta-galactosidase enzymatically cleaves X-gal, ultimately producing 5,5'-dibromo-4,4'-dichloro-indigo, an insoluble blue dye, highlighting promoter activity. *Sema4D* and *Sema4G* could not be characterized in this manner, since mice with a *Sema4D* or *Sema4G lacZ* reporter allele were not available.

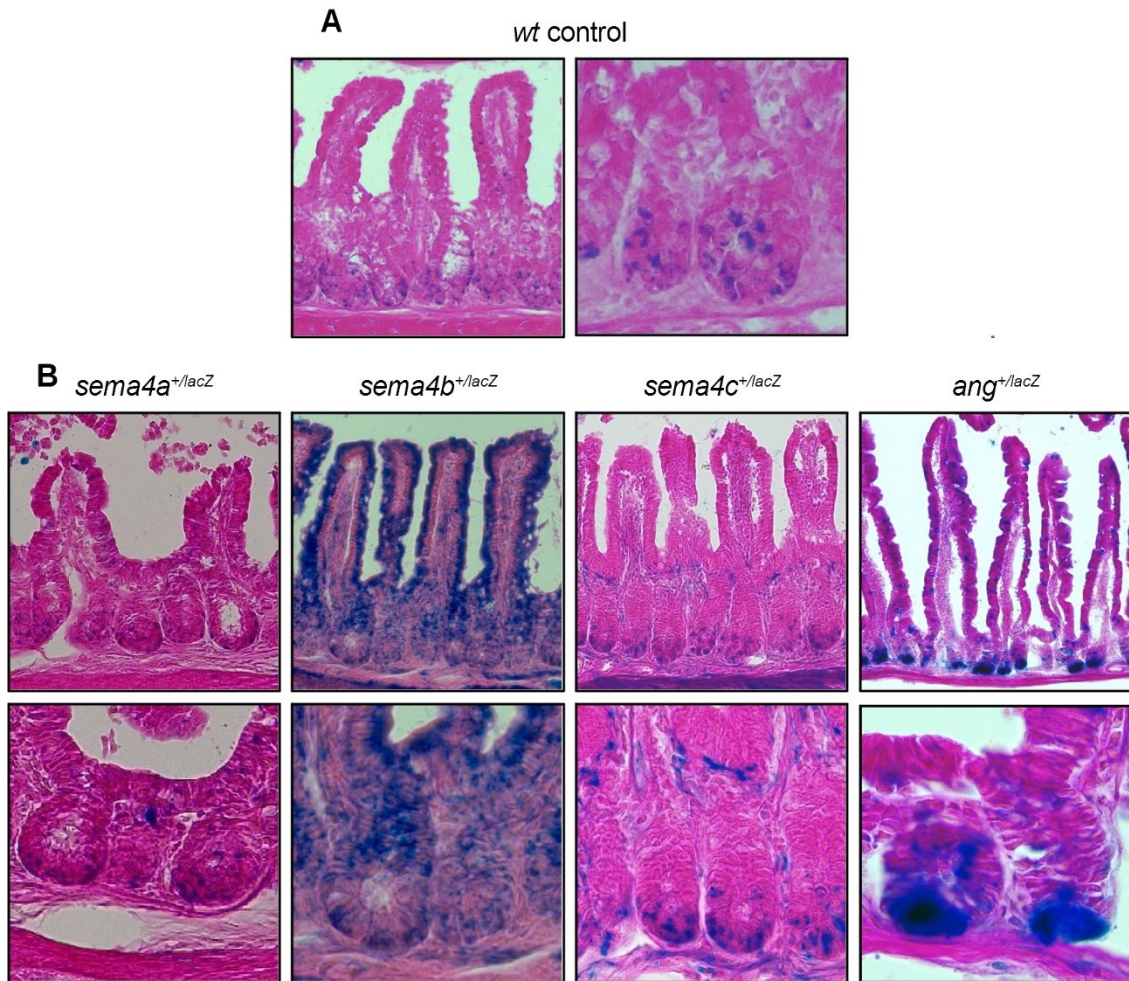


Figure 8 lacZ reporter stainings reveal ligand expression patterns in the small intestine. lacZ reporter stainings of small intestinal cryosections (A) from wt control mice and (B) *sema4a^{+/lacZ}*, *sema4b^{+/lacZ}*, *sema4c^{+/lacZ}* and *ang^{+/lacZ}* transgenic mice reporter mice expressing beta-galactosidase. wt: wild type.

In the small intestine, the wild type (wt) control stainings revealed single spots of lacZ staining in the crypt bottom (Figure 8 A), representing background staining. The *Sema4A* reporter mice displayed a similar pattern in the crypt, but in addition, single epithelial cells in the lower part of the villi also showed weak staining. Expression in the *Sema4B* reporters was prominent in most of the epithelium but was weakest in the crypts. In the *Sema4C* reporter animals, lacZ staining in the crypts was roughly equivalent to the wt controls. Additionally, some stromal cells between crypts and villi were stained. In the *Ang lacZ* reporter stainings, some cells in the crypts were strongly stained, while others showed little or no staining. Along the villi, single cells expressed the reporter as well.

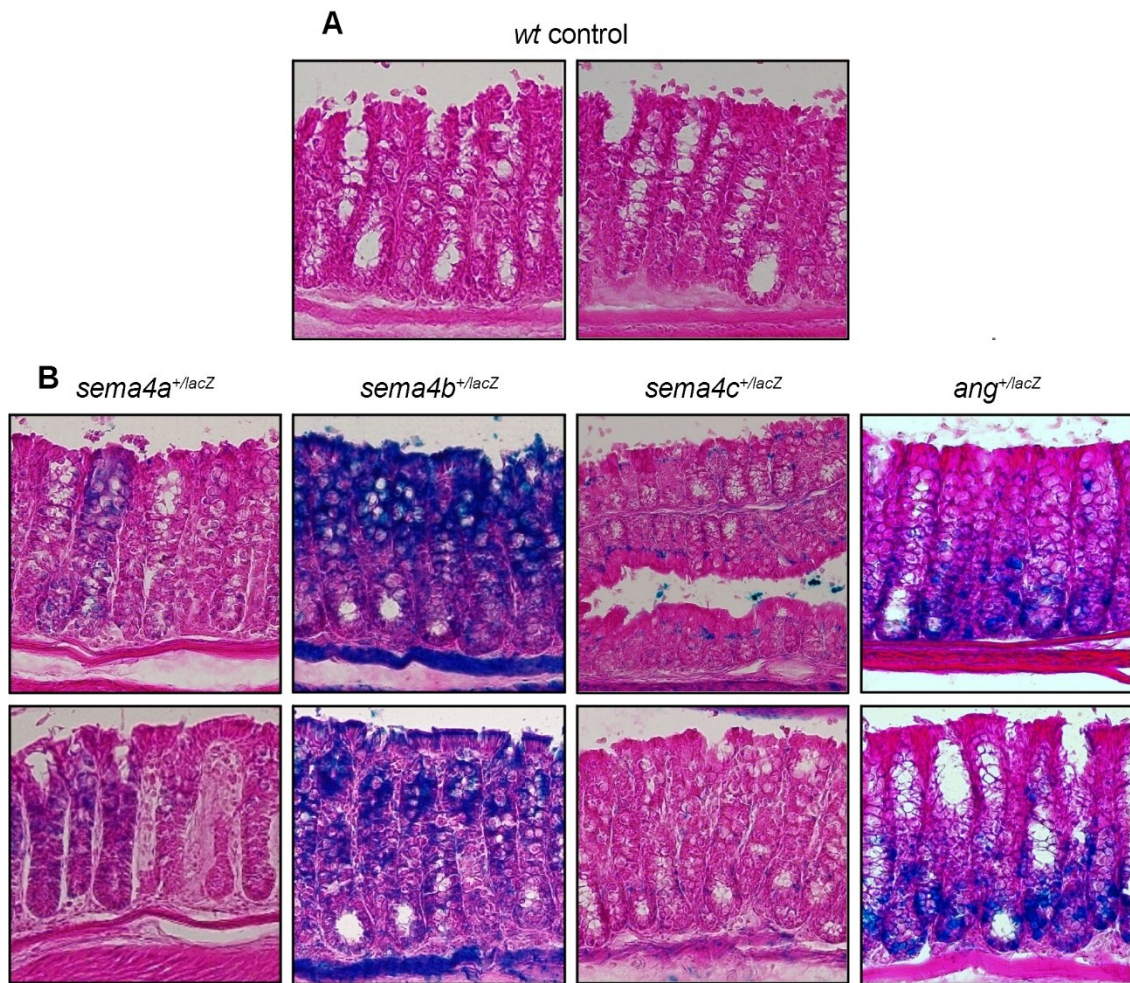


Figure 9 lacZ reporter stainings reveal ligand expression patterns in the large intestine. lacZ reporter stainings of colonic cryosections (A) from wt control mice and (B) *sema4a*^{+/lacZ}, *sema4b*^{+/lacZ}, *sema4c*^{+/lacZ} and *ang*^{+/lacZ} transgenic mice reporter mice expressing beta-galactosidase. wt: wild type.

In the colon, no lacZ staining was detected in wt control samples (Figure 9 A). In the proximal colon of *Sema4A* reporter mice, few crypts were stained (Figure 9 B, top panel), but became more frequent in the distal large intestine. Generally, reporter expression was strongest in the middle of the crypts. Expression of the *Sema4B* reporter was high in the apical epithelium, while staining intensity decreased towards the crypt base. *Sema4C* reporter expression was low in the proximal colon and appeared mostly in luminal subepithelial cells. Towards the distal colon, this luminal staining diminished and only single stromal cells near the crypt were lacZ positive. Like in the small intestine, *Ang* reporter mice showed high expression in the crypt base and intensity decreased towards the luminal epithelium, where only single cells were stained.

5.1.2 Sema4B and 4D display distinct expression patterns

Next, the expression of Sema4B and Sema4D was analyzed by immunofluorescence (IF) staining (Figure 10). For the remaining ligands, no specific antibodies suitable for IF staining were available.

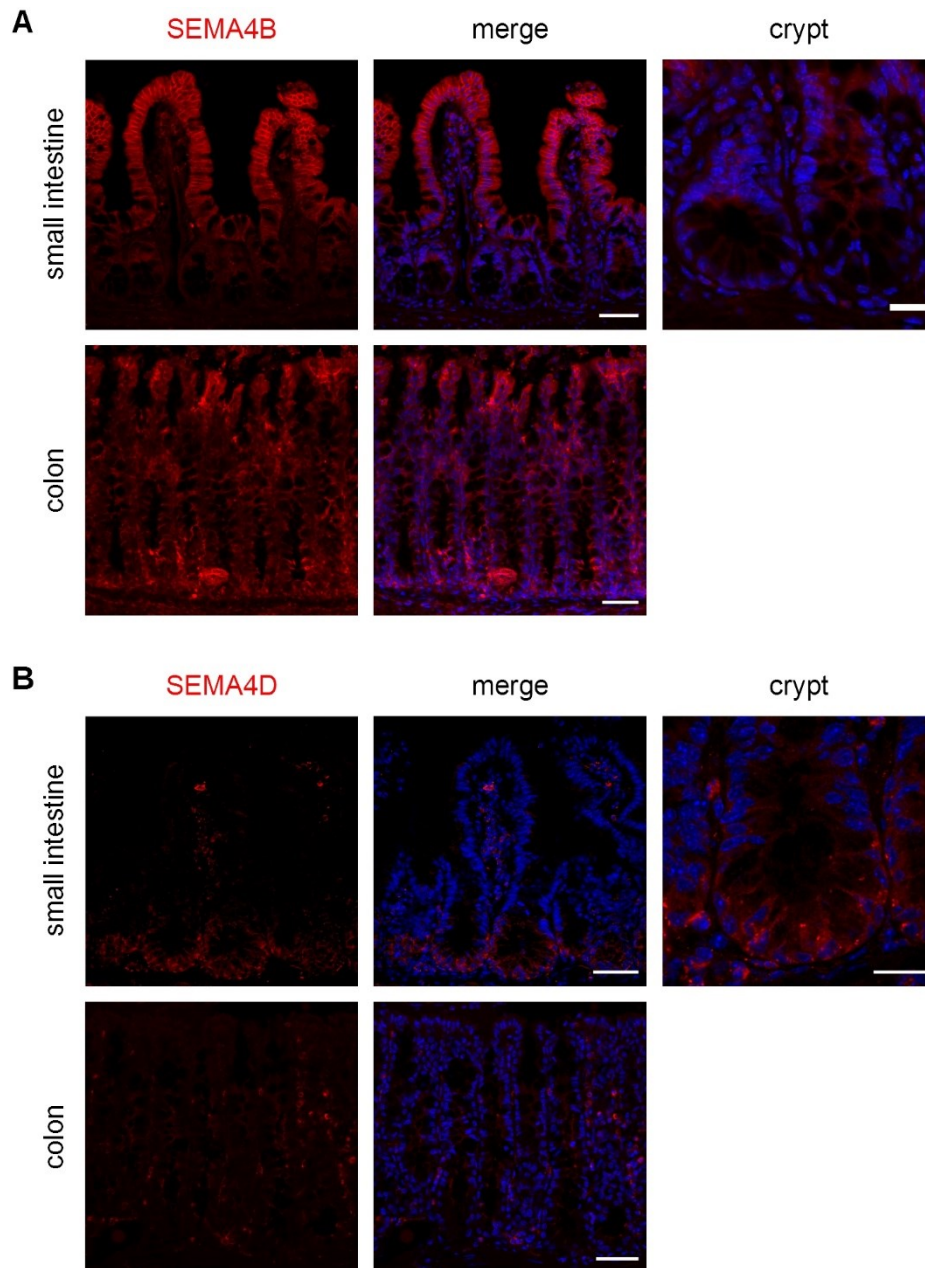


Figure 10 Immunofluorescence stainings of Sema4B and Sema4D. Cryosections of small and large intestine were immunostained for (A) Sema4B and (B) Sema4D. Nuclear counterstaining: DAPI. Scale bar: Low magnification 50 μm , high magnification 20 μm . Sema4B: Semaphorin 4B, Sema4D: Semaphorin 4D.

Sema4B in the small intestine was most strongly detectable in the epithelium of the villi (Figure 10 A, top panels). High magnification of the crypt domain revealed

no expression in the crypt bottom and only very weak expression in the TA zone. In the murine colon, *Sema4B* was expressed in the entire epithelium with no discernible difference in intensity. *Sema4D* on the other hand showed overall weak expression but was detectable in the crypt bottom of the small intestine. No cell type-specificity for either stem or Paneth cells was observed based on cellular morphology. In the colon, *Sema4D* expression was restricted to singular stromal cells.

5.1.3 *Sema4A*, *4G* and angiogenin expression partially overlaps in the intestine

Expression of *Sema4A*, *Sema4G* and *Ang* mRNA was analyzed by single-molecule mRNA fluorescence *in situ* hybridization (smRNA FISH) paired with IF staining for the stem cell marker OLFM4. The RNAscope 2.5 HD kit (ACD Bio) was used. This method detects single mRNA molecules on tissue sections by utilizing a mix of targeting probes, that hybridize to the transcript in a sequence-specific manner. Two probes need to bind adjacently on the transcript to increase specificity. Only then, the probes provide binding sites for a series of amplification reagents that serve to enhance signal intensity, making this method extremely sensitive. In the last step, chromogenic reactions produce either a Fast Red or 3,3'-Diaminobenzidine (DAB) precipitate that indicates the presence of the transcript. In addition, IF was used to stain the same tissue for OLFM4, identifying intestinal stem cells in the crypt and thus enabling the quantification of cell-type specific expression of mRNA transcripts in the crypt base.

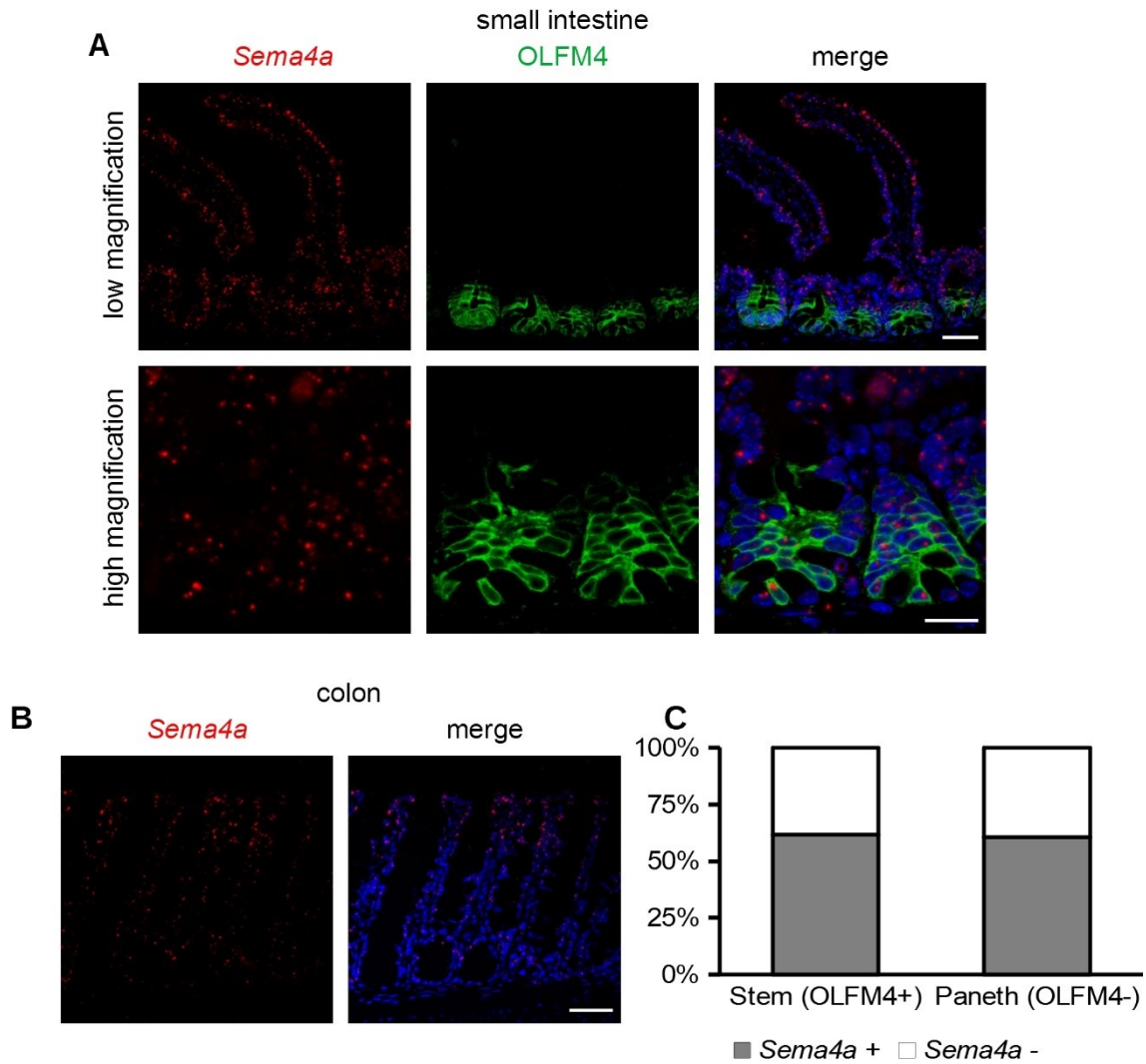


Figure 11 Semaphorin 4A is widely expressed in both small and large intestine. smRNA FISH of *Sema4A* with nuclear counterstaining (DAPI) on (A) SI sections with additional IF of OLFM4 (stem cells) and (B) colon sections. (C) Quantification of *Sema4a*+ stem and Paneth cells of the SI crypt. Scale bar: Low magnification 50 μ m, high magnification 20 μ m.

In the small intestine, *Sema4A* expression was detectable in the entire crypts and villi (Figure 11 A and B). Using a higher magnification, the crypt bottom was analyzed for potential cell type-specific expression of *Sema4A* in the crypt base. Both OLFM4+ stem cells and the interspersed Paneth cells were frequently positive for *Sema4A*. Quantification revealed a rate of ca. 60 % *Sema4A*-positive cells without a discernible difference between the two cell types (Figure 11 C). In the colon, expression was similarly widespread, but the signal was strongest in the luminal epithelium.

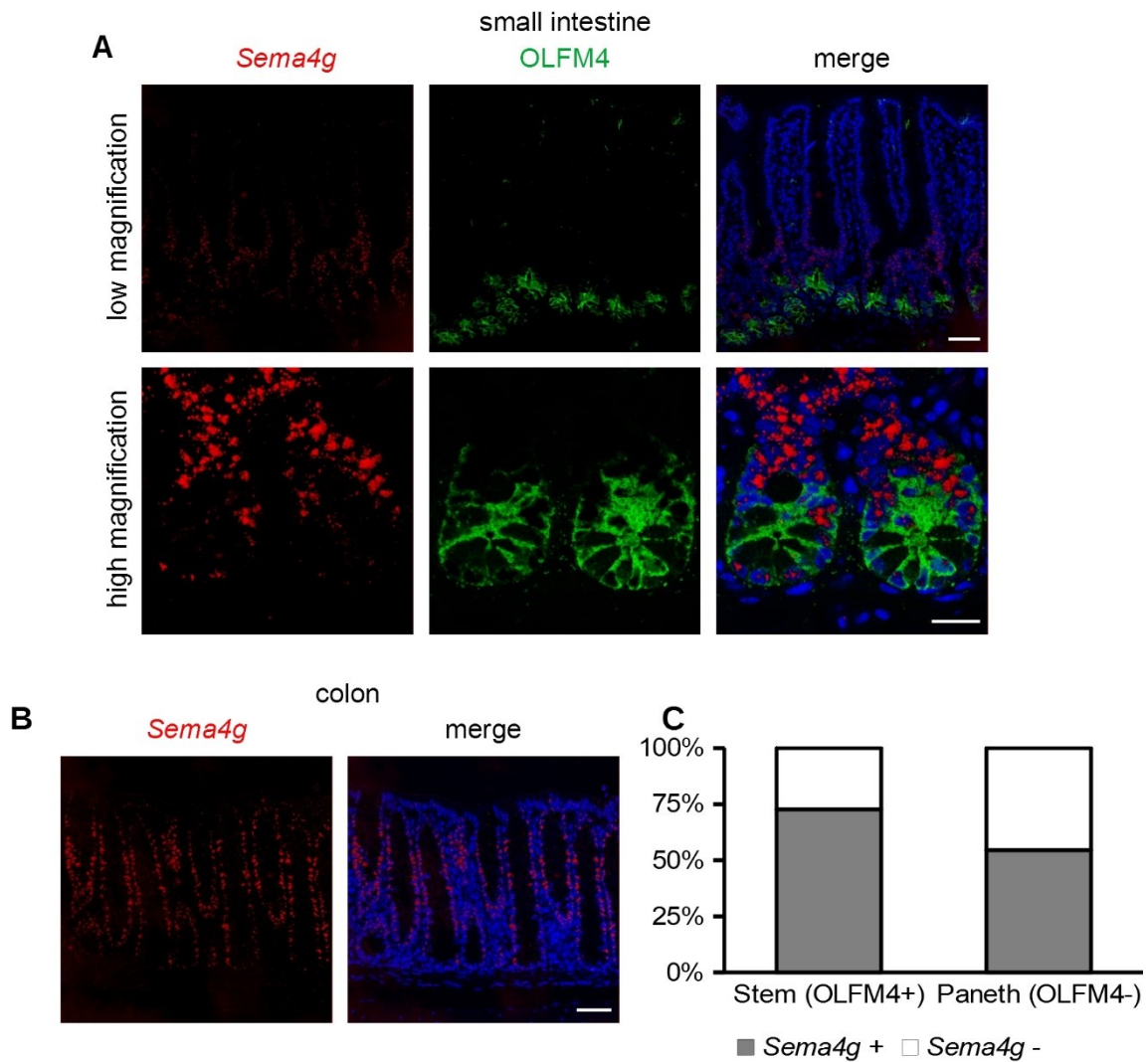


Figure 12 *Semaphorin 4G* is expressed in the TA zone. smRNA FISH of *Sema4G* with nuclear counterstaining (DAPI) on **(A)** SI sections with additional IF of OLFM4 (stem cells) and **(B)** colon sections. **(C)** Quantification of *Sema4g*⁺ stem and Paneth cells of the SI crypt. Scale bar: Low magnification 50 μ m, high magnification 20 μ m. Brown precipitate was used for smRNA FISH and false colors were assigned as described in section 4.4.1.

Sema4G was expressed in both small and large intestinal epithelium (Figure 12 A and B). In the small intestine, the TA zone expressed *Sema4G* most strongly while the crypt bottoms and villi showed low expression and no expression, respectively. Quantification of cell type-specificity showed ca. 75 % of stem cells to be positive for *Sema4G*, although expression in these cells was relatively low. Paneth cells were less frequently positive for *Sema4G*. The large intestine's expression pattern was similar with precipitate being located mostly in the middle of the crypts and comparatively low expression in the crypt bottoms and luminal epithelium.

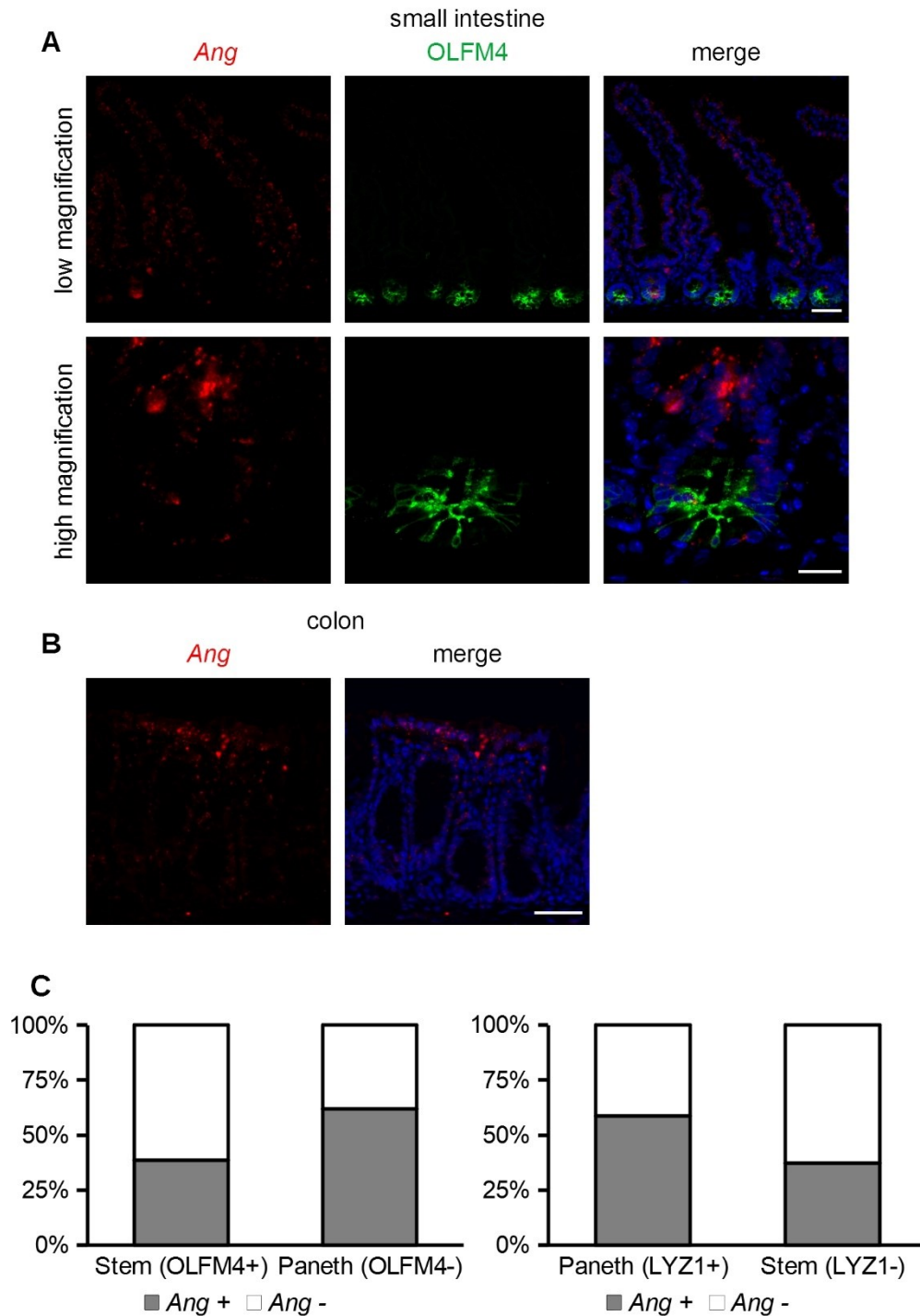


Figure 13 Angiogenin is expressed weakly, but widespread. smRNA FISH of *Ang* with nuclear counterstaining (DAPI) on **(A)** SI sections with additional IF of OLFM4 (stem cells) and **(B)** colon sections. **(C)** Quantification of *Ang*⁺ stem and Paneth cells of the SI crypt. Scale bar: Low magnification 50 μ m, high magnification 20 μ m.

Ang expression was relatively low in the small intestine, although single *Ang*-positive cells were observable along the entire villus. Expression was strongest in the TA zone and crypt bottom (Figure 13 A). Quantification of potential cell

type-specificity in the crypt base showed ca. 40 % of OLFM4+ ISCs and ca. 60 % of OLFM4- cells to be positive for angiogenin. smRNA FISH with a staining for the Paneth cell marker LYZ1 was performed and subjected to the same quantification, which confirmed the initial finding, with 60 % of LYZ1+ Paneth cells and ca. 40 % of LYZ1- cells positive for angiogenin. In the colon the expression pattern was strikingly different with most *Ang*-expressing cells being located at the luminal side of the epithelium and only few *Ang*-positive cells towards the crypt bottom.

5.1.4 Plexin B1 is expressed in the entire intestinal epithelium

Plexin B1 is a known receptor to class 4 semaphorins. Thus, smRNA FISH was used to characterize *Plxnb1* mRNA expression patterns in the intestinal epithelium, as well as possible cell-type specificity in the intestinal crypt. In the small intestine, *Plxnb1* was expressed in the entire epithelium at comparable levels, without apparent specificity for any cell type (Figure 14 A). When focusing on the stem cell niche, both OLFM4+ and OLFM4- cells expressed *Plxnb1* at similar rates, ca. 55 % of cells were positive for *PlxnB1* (Figure 14 C). Like in the small intestine, *Plxnb1* was expressed with no apparent differences between epithelial regions.

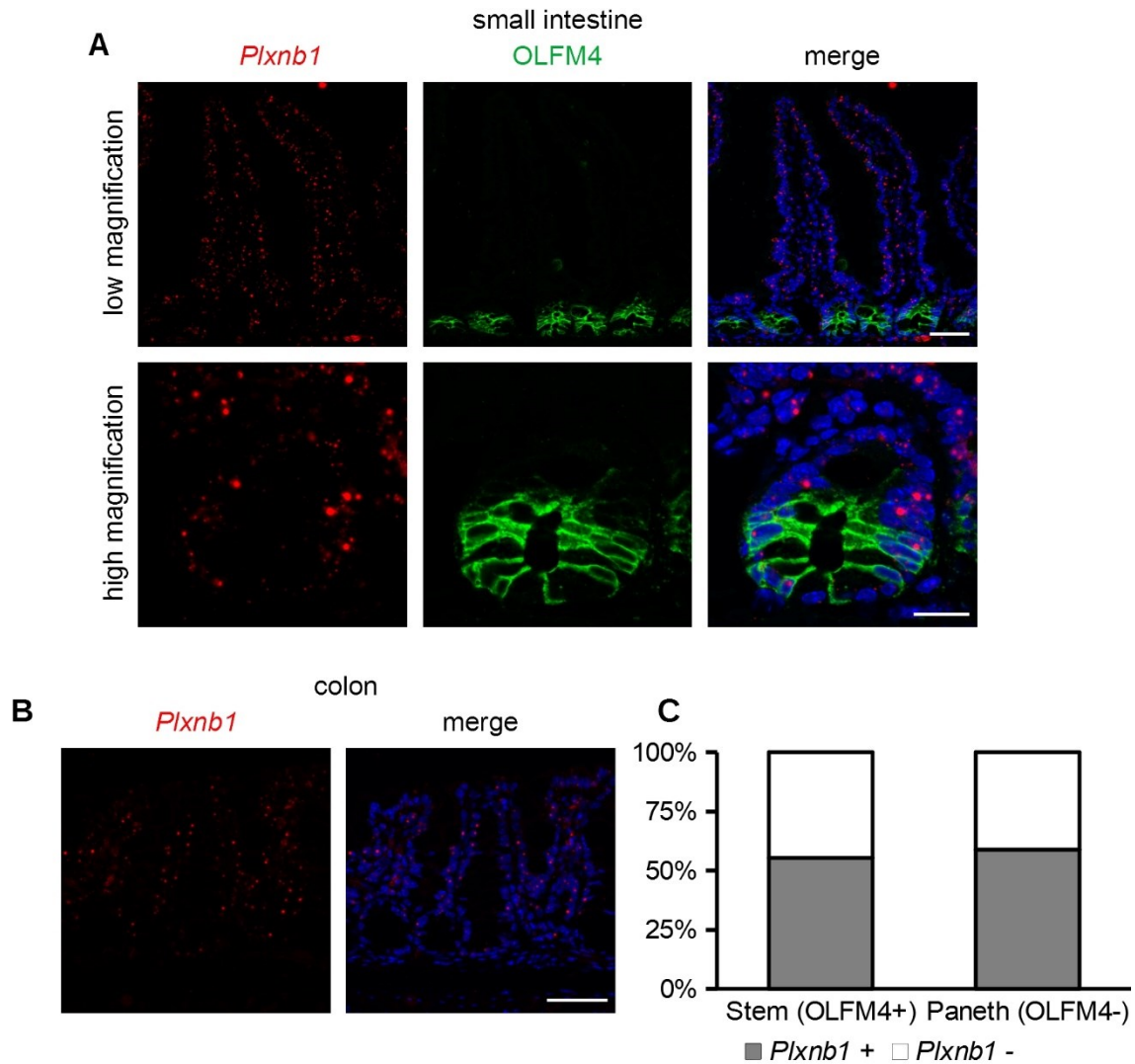


Figure 14 Plexin B1 is widely expressed in both small and large intestine. smRNA FISH of *Plxnb1* with nuclear counterstaining (DAPI) of (A) SI sections with additional IF of OLFM4 (stem cells) and (B) colon sections. (C) Quantification of *Plxnb1*+ stem and Paneth cells of the SI crypt. Scale bar: Low magnification 50 μ m, high magnification 20 μ m.

5.1.5 scRNA sequencing of human intestinal epithelial cells confirms expression analysis in mouse tissues

To transfer the findings from the mouse intestine to human cells, a single cell sequencing data set of healthy human colonic epithelial cells published by Parikh et al. (GEO accession number GSE116222) was analyzed by Mario Looso (Max-Planck Institute, Bad Nauheim) (Parikh et al., 2019). Single cell data was clustered by similarity in gene expression. To identify which cluster represents which intestinal cell type, the expression of a set of marker genes was examined.

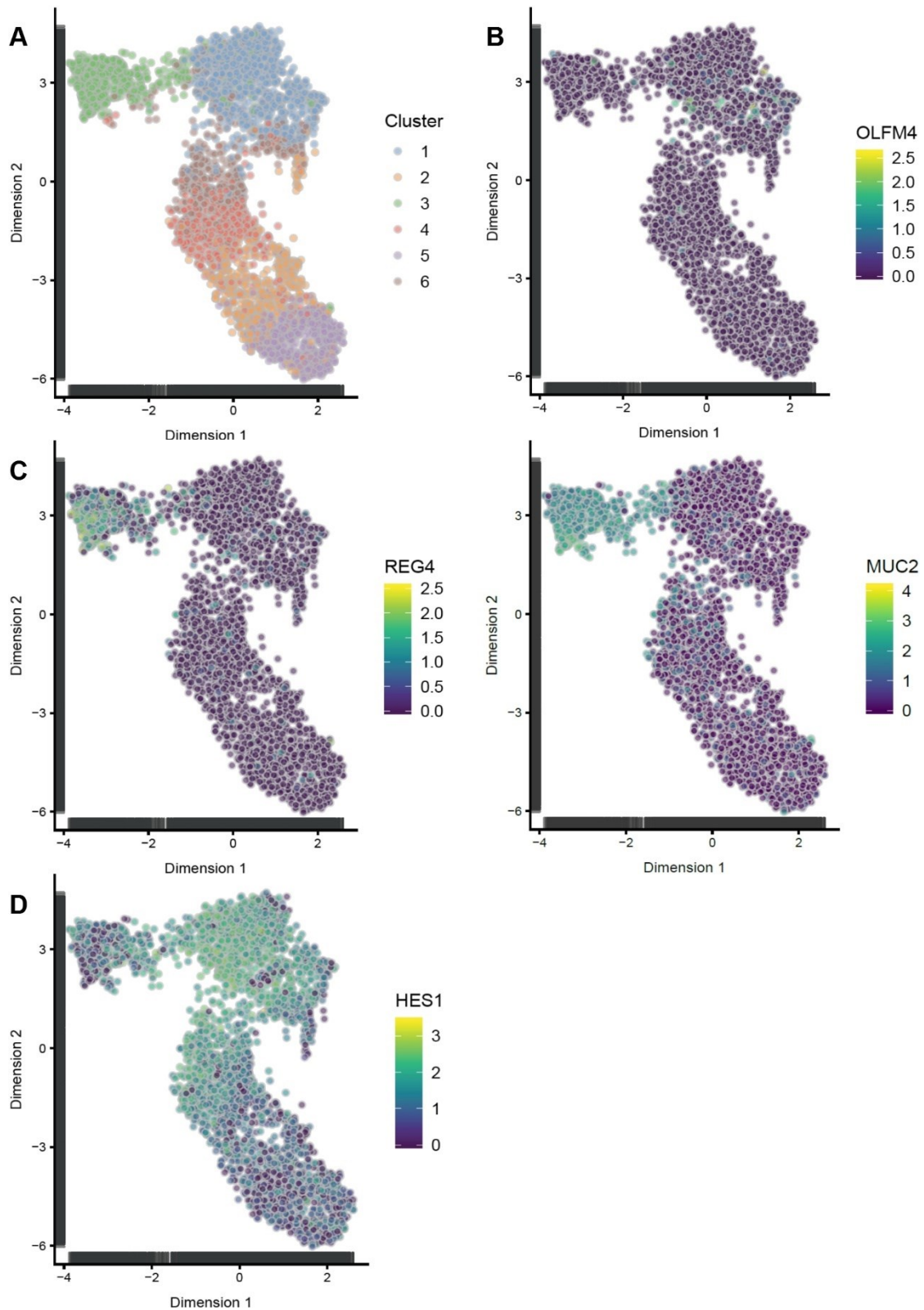


Figure 15 scRNA sequencing of human colonic epithelial cells reveal lineage-specific clusters. Clustering analysis of single-cell RNA sequencing data from human colonic epithelial cells. (A) Color-coded clusters grouped by similar expression patterns. Cell type markers identify lineage clusters: (B) stem cells (*OLFM4*), (C) EEC (*REG4*) and goblet cells (*MUC2*) of the secretory

lineage, (D) enterocytes (*HES1*). Visualization of data by Mario Looso (MPI, Bad Nauheim). Original sequencing data (GSE116222) from (Parikh et al., 2019)

Using the expression of *OLFM4*, cluster 1 was identified to most likely represent stem or early progenitor cells (Figure 15 B). *REG4* and *MUC2* are expressed in enteroendocrine and goblet cells respectively and thus mark cells of the secretory lineage. They were most strongly expressed in cluster 3 (Figure 15 C). Enterocytes are the most abundant epithelial cell type and marked by the expression of *HES1*, which was present in most clusters, but predominantly in clusters 1, 2 and 4 through 6. (Figure 15 D). In summary, the top right cluster 2 likely represents stem cells, cluster 3 towards the top left represents the secretory lineage, and clusters 2 and 4 through 6 the absorptive lineage.

After identifying lineage clusters, the mRNA expression of Semaphorins 4A, 4B, 4D and 4G, as well as their respective receptors Plexins B1 and B2 was analyzed (Figure 16). Only few cells expressed *SEMA4A* and were mostly localized within or adjacent to the stem cell cluster. *SEMA4B* was expressed more frequently and across all clusters but was most prominent in the clusters associated with the absorptive lineage. *SEMA4D* positive cells were the rarest and mostly restricted to the stem cell cluster, as well as the secretory cluster. Cells expressing *SEMA4G* were present in all clusters and relatively evenly distributed, showing the highest frequency of the analyzed ligands. Furthermore, the expression of two receptors, *PLXNB1* and *PLXNB2*, was investigated. Both were expressed across all clusters, but *PLXNB2* with a substantially higher frequency.

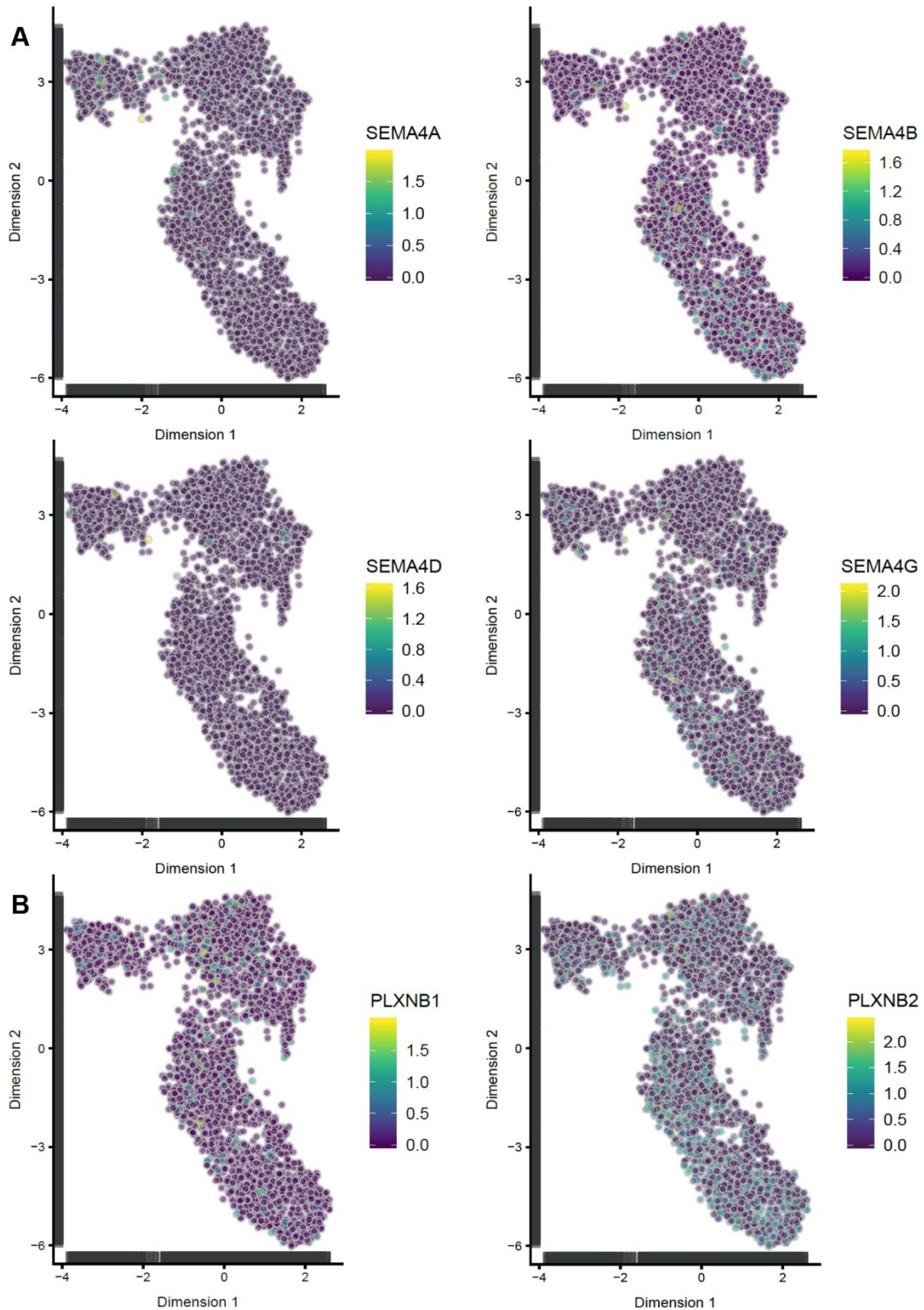


Figure 16 Class 4 semaphorins and B-plexins are expressed in the human colonic epithelium. Clustering analysis of single-cell RNA sequencing data from human colonic epithelial cells. **(A)** Analysis of *SEMA4A*, *SEMA4B*, *SEMA4D*, *SEMA4G* expression. **(B)** Analysis of *PLXNB1* and *PLXNB2* expression. Visualization of data by Mario Looso (MPI, Bad Nauheim). Original sequencing data (GSE116222) from (Parikh et al., 2019)

5.2 Generation of a novel *Alpi-Cre2* BAC through homologous BAC recombination

The expression analysis of class 4 semaphorins and angiogenin revealed some ligands to be restricted to different epithelial compartments e.g., semaphorin 4B to the epithelium of the villi and semaphorin 4D to the crypt base. To enable the dissection of ligand functions in enterocytes compared to other cell types, a BAC was generated by homologous recombination, enabling the enterocyte-specific expression of Cre2 recombinase under the control of the *Alpi* promoter. The BAC was then prepared for oocyte injection. The injection, as well as the subsequent animal husbandry was performed by collaborators of the Max-Planck Institute for Heart and Lung Research (Bad Nauheim). The *Alpi-Cre2* expression analysis in *mT/mG* reporter mice was done in collaboration with Josina Großmann as part of her bachelor's thesis.

5.2.1 A Cre2 cassette was recombined into the *Alpi* gene of a BAC

A Cre2 donor plasmid was constructed, containing the Cre2 insert flanked by homology arms. The full insert was PCR-amplified and integrated into a BAC (RP23-49O20), replacing exon 1 of the *Alpi* gene (Figure 17 A) by homologous Red/ET recombination. Correct modification, as well as structural integrity of the BAC was controlled by restriction digest.

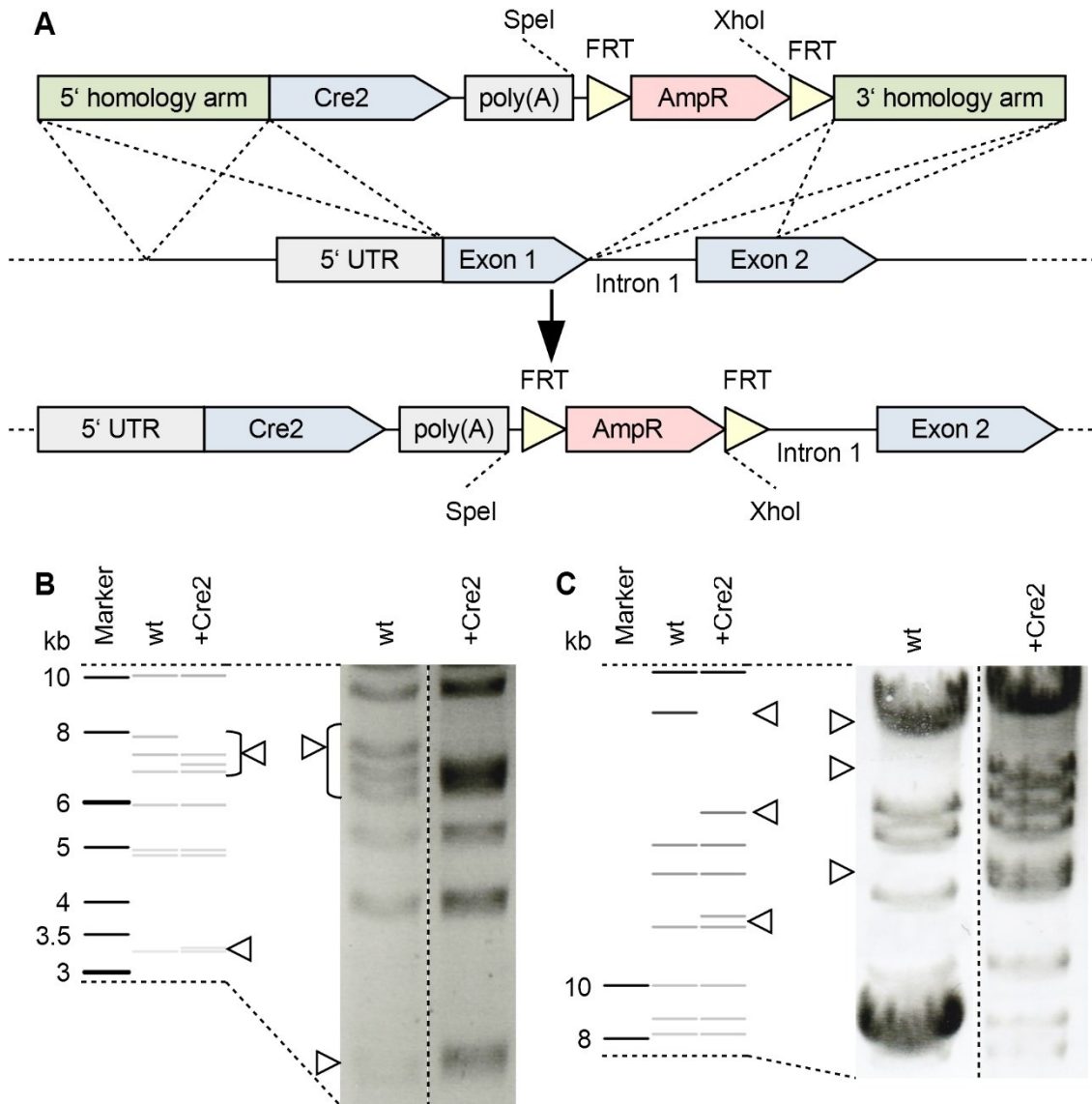


Figure 17 Successful integration of the Cre2 insert by homologous recombination. (A) Schematic of homology-directed BAC recombination; the PCR-amplified Cre2 insert (top) replaced exon 1 of the *Alpi* gene in the BAC RP23-49O20 (middle). The resulting construct is displayed below. (B and C) Spel and XhoI restriction digests respectively of the unmodified BAC (wt) and the recombinant BAC (+Cre2); predicted bands from *in silico* digests are displayed on the left, corresponding digest results on the right.

Both the Spel and XhoI the recombinant BAC (+Cre2) showed the band changes predicted *in silico*, confirming integration of the Cre2 insert (Figure 17 B and C). The next step was to remove the bacterial ampicillin resistance used to select for the insert. Site-directed FLPase recombination of the BAC was used, and recombination was controlled by restriction digest, comparing an unmodified control BAC (wt) and the FLPase-modified BAC (FLPed).

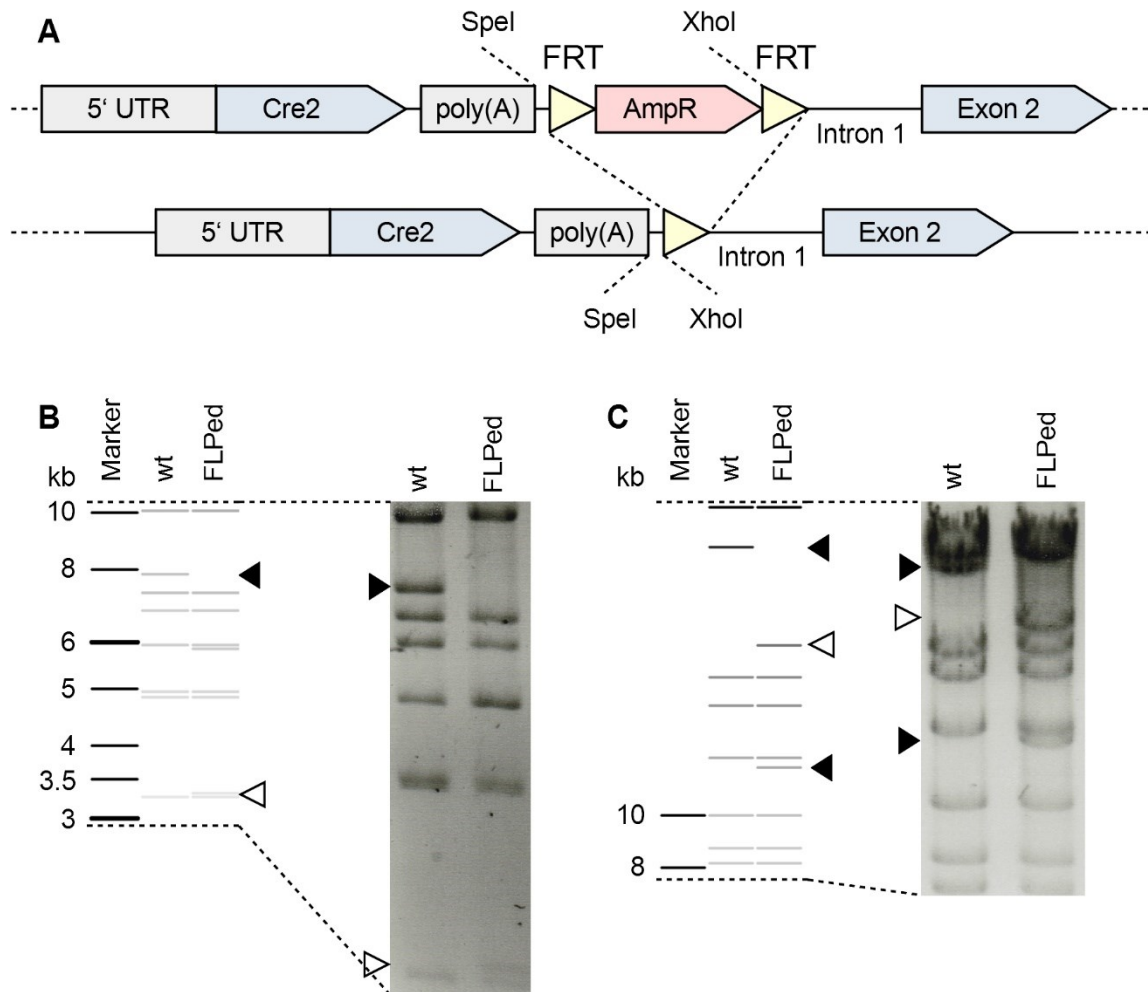


Figure 18 Successful removal of AmpR by FLPase recombination. (A) Schematic of site-directed FLPase BAC recombination; The RP23-49O20-Cre2 BAC (top) was modified by FLPase to remove the ampicillin resistance (*AmpR*), resulting in the final BAC (bottom). **(B and C)** Spel and XhoI restriction digests respectively of the unmodified BAC (*wt*) and the FLPase-modified BAC (FLPed); predicted bands from *in silico* digests are displayed on the left, corresponding digest results on the right.

In both the Spel and XhoI restriction digests, the changes in fragment size corresponded to the changes predicted *in silico* (Figure 18 B and C respectively). This confirmed successful removal of the ampicillin resistance (*AmpR*) that was initially part of the insert. This result, as well as the insert sequence were further verified by sequencing (data not shown).

5.2.2 Preparation of the *Alpi-Cre2* BAC for oocyte injection

Next, the *Alpi-Cre2* BAC was prepared for oocyte injection by linearization and gel permeation chromatography as described in section 4.2.2.3.

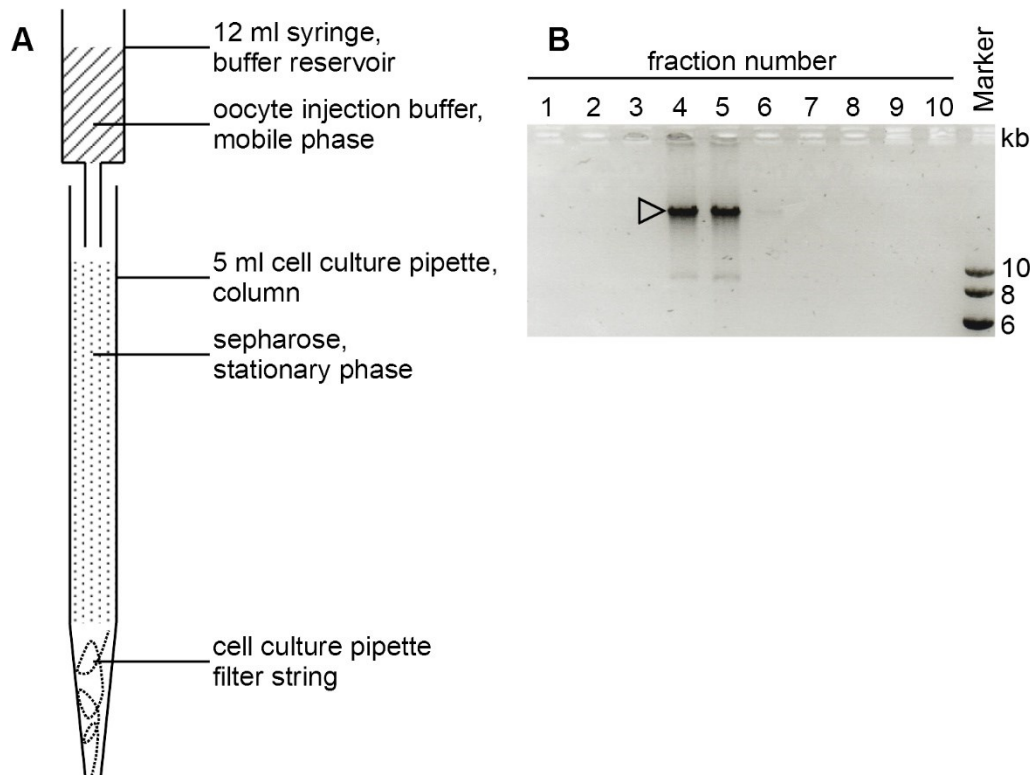


Figure 19 Preparation of the *Alpi-Cre2* BAC for oocyte injection. **(A)** The *Alpi-Cre2* BAC was digested with *NotI* and separated by gel permeation chromatography using a column assembled according to the schematic. **(B)** The resulting Fractions were separated by agarose gel electrophoresis and those enriched with the BAC (▷) were selected for oocyte injection.

All fractions were characterized by agarose gel electrophoresis to identify the fractions containing the highest concentration of the linearized BAC (Figure 19 B, empty arrow head). Fractions 4 and 5 were selected for oocyte injection and passed on to collaborators at the Max-Planck-Institute for Heart and Lung Research (Bad Nauheim), who performed the oocyte injections and animal husbandry.

5.2.3 Cre recombinase is expressed and functional in transgenic *Alpi-Cre2⁺ mT/mG⁺* reporter mice

The functionality of the *Alpi-Cre2* BAC in the intestinal epithelium was validated by integration into the genome of *mT/mG* reporter mice (Muzumdar et al., 2007).

In these mice, *mT* codes for dTomato followed by a stop codon and is flanked by *loxP* sites. Downstream lies *mG*, coding for green fluorescent protein (GFP) (Figure 20). Under basal conditions, cells only express dTomato. Once Cre recombinase is present, the *mT* element of the reporter is excised, including its stop codon, subsequently leading to the replacement of dTomato expression by the expression of GFP.

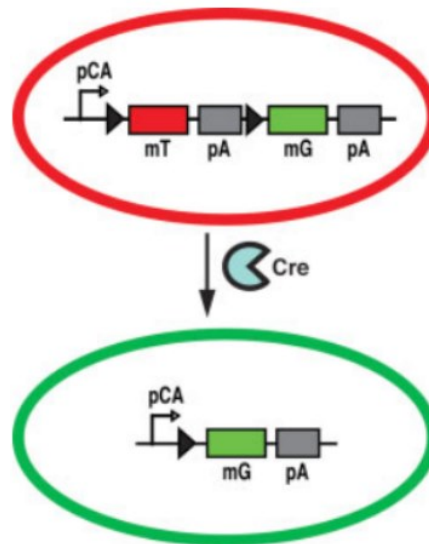


Figure 20 Basic principle of the *mT/mG* reporter locus. Adapted from (Muzumdar et al., 2007).

Since the *Cre2* construct is integrated into the *Alpi* gene, its expression is controlled by the gene's regulatory elements and is only produced, once the gene is actively transcribed. The recombinase then mediates the excision of dTomato and expression of GFP marks the cells in which Cre is expressed and active. This allows (a) the identification of cells, where the *Alpi* gene is expressed and (b) cell type-specific modification of these cells in mice that carry additional *loxP* sites, enabling e.g., the generation of cell type-specific gene knockouts.

Expression and functionality of the *Cre2* recombinase was characterized in the small and large intestines of *mT/mG* reporter mice in collaboration with Josina Großmann, who performed the analysis as part of her bachelor's thesis (Figure 21). In the small intestine, only single crypts or small clusters of crypts showed *Cre2* activity as indicated by GFP expression, while the majority of crypts did not (Figure 21 A, top panels). In the GFP-positive crypts, most cells were strongly expressing GFP except for cells in the crypt base, where GFP intensity was lower. Control animals analyzed in the same manner displayed no GFP expression and

thus no Cre2 activity (Figure 21 A, bottom panels). In the large intestine, expression was distributed similarly with GFP-positive crypts forming small clusters, while no GFP was visible in the colons of *AlpiCre2*- control mice. No difference in GFP intensity was observable between multiple cells within a single positive crypt (Figure 21 B).

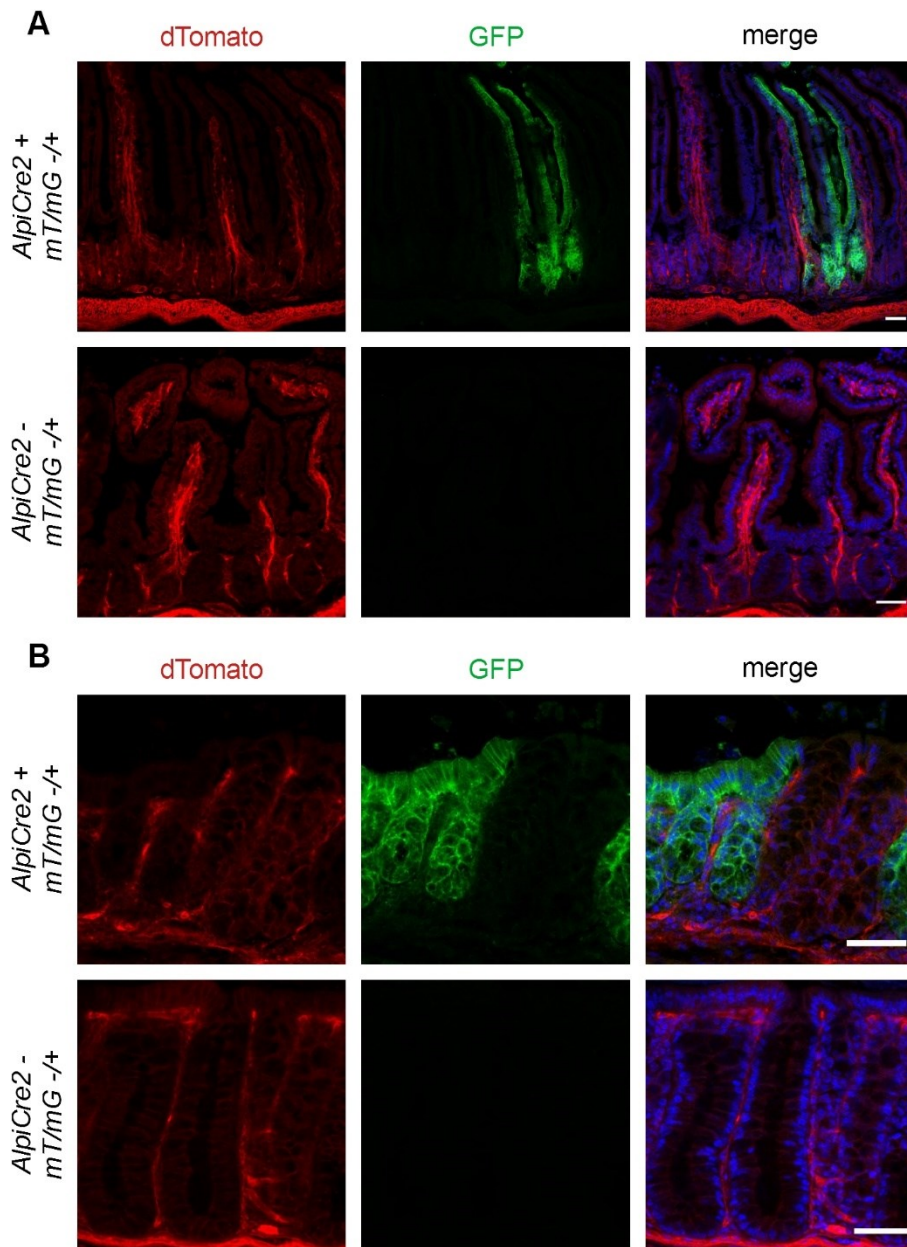


Figure 21 Analysis of intestinal Alpi-Cre2 expression in mT/mG reporter mice. AlpiCre2⁺ and *AlpiCre2*⁻ control mice were analyzed for Cre2 expression. (A) Cryosections of the small intestine and (B) large intestine. DAPI counterstaining. Scale bar: 50 μ m.

Analysis performed in collaboration with Josina Großmann as part of her bachelor's thesis.

5.3 Function of class 4 semaphorins and B-plexins in the intestinal epithelium

To assess a potential regulatory role semaphorin-plexin signaling in intestinal epithelial homeostasis, stem cell function was tested in ligand and receptor knock-out organoids.

5.3.1 *Sema4B* single knockout and *plexin B1/B2* double knockout organoids display intestinal stem cell defects

A functional analysis of organoids derived from semaphorin 4A, 4B, 4D and 4G knockout mice, as well as of plexin B1/B2 double knockout mice and their respective control mice was carried out. Crypts were isolated, seeded and after 5 days of culture, the number of organoids, as well as their size and morphology was assessed using brightfield imaging and OrganoSeg (Figure 22) (Borten et al., 2018).

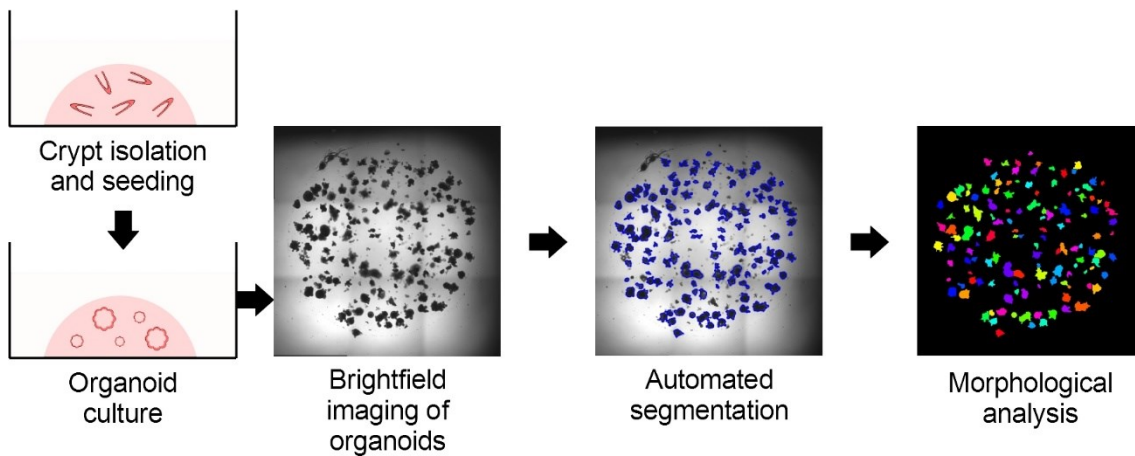


Figure 22 Workflow of functional organoid experiments. Detailed description of the protocol in section 4.1.6.

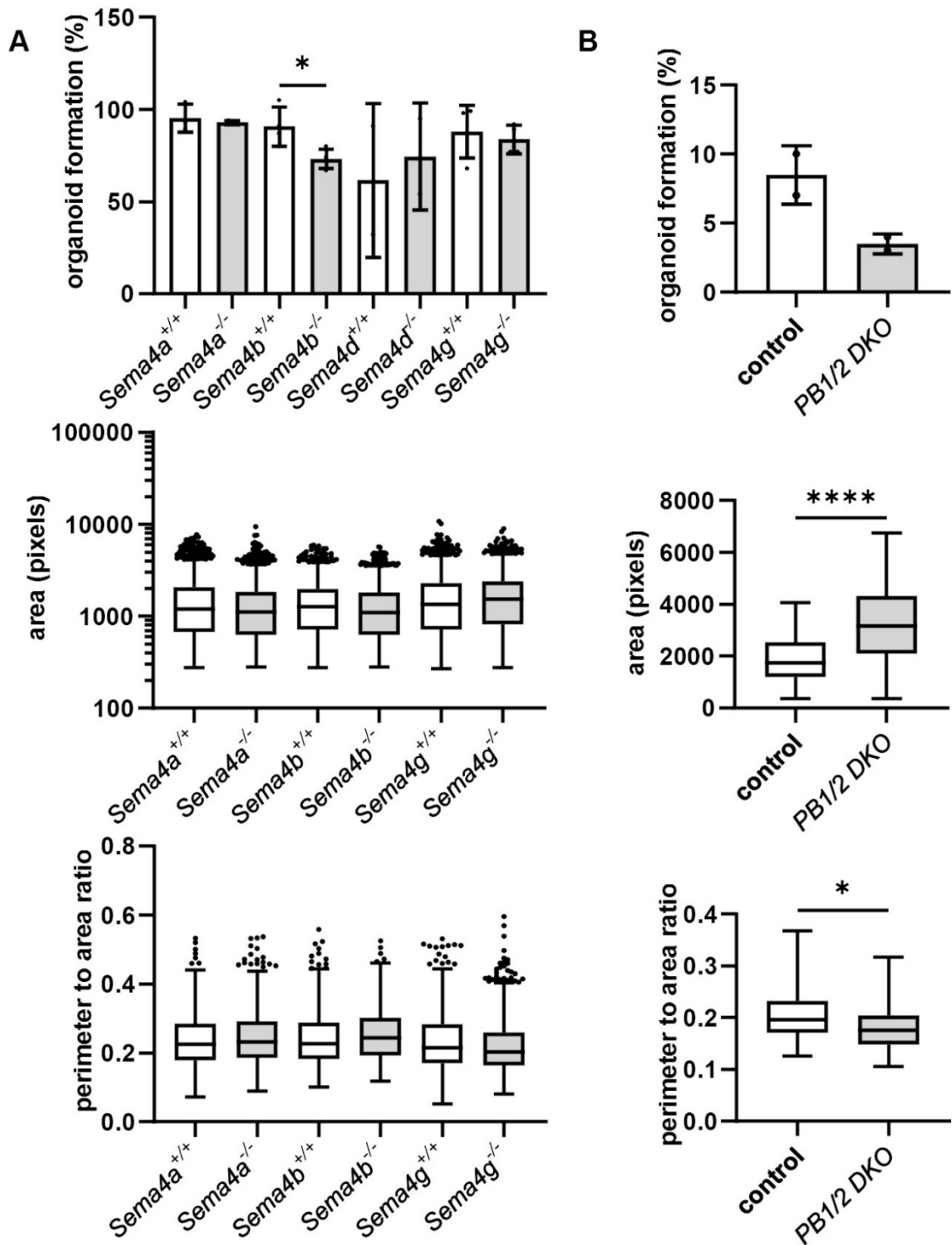


Figure 23 Intestinal stem cell function is reduced in *Sema4B* single knockout and plexin B1/B2 double knockout organoids. Organoid formation (% of crypts growing into organoids), area (2D-area measured in pixels) and perimeter to area ratio analyzed from knockout and control organoids. (A) 3 vs. 3 (*Sema4a*), 4 vs. 4 (*Sema4b*), 2 vs. 2 (*Sema4d*) and 4 vs. 4 (*Sema4g*) control and KO animals, respectively. (B) 2 vs. 2 control and *plexin B1/B2* double knockout animals analyzed. PB1/2: plexin B1/B2; DKO: double knockout. Bar graphs: mean \pm s.d.; Statistical significance: Unpaired t-test, * $p < 0.05$; **** $p < 0.0001$. Box plots after the Tukey method: Whiskers extend to 1.5 times the interquartile range.

Organoid seeding efficiency, i.e., the ratio of growing organoids to initially seeded crypts, was significantly reduced in *Sema4B* knockout organoids but remained unchanged in *Sema4A*, *Sema4D* and *Sema4G* knockout organoids when compared to control cells analyzed in parallel (Figure 23 A). The size of the organoids as measured by their 2-dimensional area was unaffected in the *Sema4A*, *Sema4B* and *Sema4G* knockout organoids. The morphological analysis of the *Sema4D* knockout organoids was hindered by tissue debris left over from the isolation, although visual inspection revealed no observable differences to the control organoids (Figure 23 A). Since class B plexins represent the receptors to the analyzed semaphorin ligands, plexin B1 and B2 double knockout (DKO) organoids were examined as well. Like for the ligand knockout cells, organoid formation was assessed and was substantially lower in the crypts derived from plexin B1/B2 DKO mice when compared to control crypts but did grow into larger organoids. Their morphology was changed as well, as indicated by a lowered perimeter to area ratio, which points to a reduction in structural complexity (Figure 23 C).

5.3.2 Lowered *Lgr5* expression in the intestines of angiogenin knock-out mice points to a possible loss of stem cells

To investigate the functional role of Ang in intestinal epithelial homeostasis, differentiation was analyzed by quantifying the expression of cell type markers in small intestinal tissue from angiogenin knockout mice by RTqPCR. Since live tissue was not available, organoid experiments could not be conducted. RNA isolated from whole intestinal tissue was provided by Michael Mazzola (Center for Regenerative Medicine, Massachusetts General Hospital; Boston, USA), who also confirmed the animal's genotype by PCR and ELISA for angiogenin.

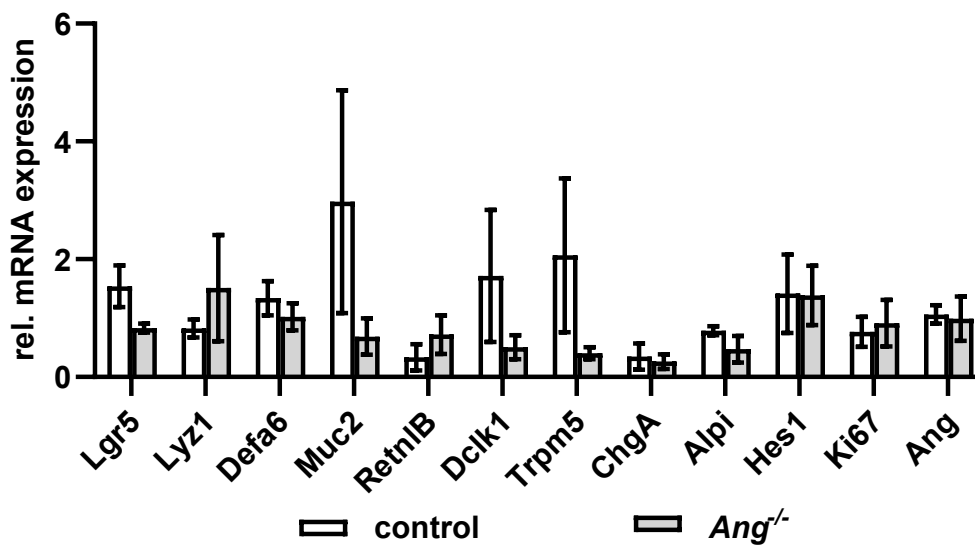


Figure 24 RTqPCR reveals reduction of stem cells in angiogenin knockout tissue. RNA isolated from the whole small intestines of 4 control and 4 angiogenin knockout animals was analyzed for the expression of *Ang* and a panel of intestinal epithelial differentiation markers. Mean \pm S.E.M.; n=2. Stem cells: *Lgr5*; Paneth cells: *Lyz1*, *Defa6*; Goblet cells: *Muc2*, *Retn1B*; Tuft cells: *Dclk1*, *Trpm5*; EECs: *ChgA*; Enterocytes: *Alpi*, *Hes1*; Proliferation: *Ki67*. RNA provided by Michael Mazzola.

qPCR revealed no difference in the expression of angiogenin mRNA and proliferation appeared unchanged between control and knockout tissue as well. The markers *Lgr5* (stem), *Muc2* (goblet), *Dclk1*, *Trpm5* (Tuft) and *Alpi* (enterocytes) were reduced in knockout tissue, while *Lyz1* (Paneth) and *Retn1B* (goblet) were increased. The remaining markers were unchanged.

5.4 Establishment of lentiviral transductions of intestinal organoids

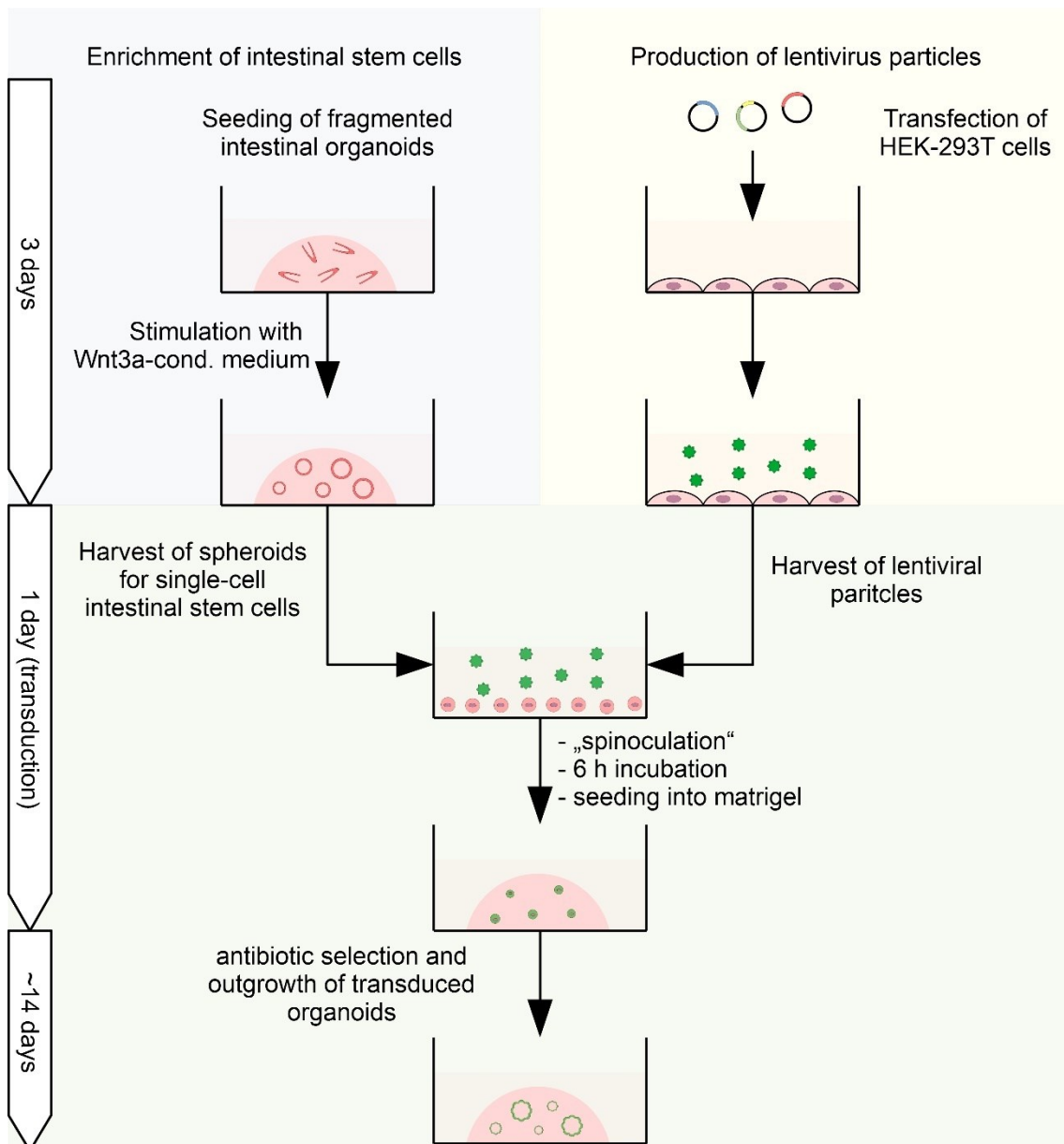


Figure 25 Lentiviral transductions of intestinal organoids.

Given the fact, that knockout mice were not available for all genes of interest, another method was required to investigate ligand function in the intestinal epithelium. Since intestinal organoids proved to be a versatile and powerful tool in modeling ISC function, lentiviral transduction of short hairpin RNAs (shRNAs) into organoids was chosen to modulate gene expression and conduct functional experiments (Koo et al., 2012; van Lidth de Jeude et al., 2015). The plasmid system used to generate the virus particles was based on a doxycycline-inducible Tet on

vector (Gossen et al., 1995). Upon induction, cells express both the shRNA, as well as GFP. Inducibility was critical since a constitutive knockdown carries the risk of making an organoid line non-viable and continued culture might select for cells that successfully compensated for the loss of expression of the target gene. The sequences targeting *Sema4A*, were selected based on screening experiments in CMT-93 cells, that were conducted by Inga Shcheglova as part of her bachelor's thesis: Multiple sequences targeting *Sema4A* were transfected and target gene expression was analyzed by RTqPCR. Whichever sequence reduced target gene expression the most was chosen for cloning into the inducible vector and subsequent organoid transductions.

Generating transgenic organoids by lentiviral transduction is a complex multi-step process (Figure 25). For the culture of murine small intestinal organoids only endogenous Wnt ligand produced by Paneth cells is strictly required. In preparation for the transduction, intestinal organoids were seeded and stimulated with Wnt3a-conditioned medium, which drastically changed organoid morphology. Under Wnt stimulation, organoids appearance was cyst-like, and the epithelium remained flat instead of becoming columnar. The characteristic crypt-like protrusions did not form, possibly because the addition of Wnt ligand prevented the symmetry-breaking events, that precede their formation. The lack of architectural complexity indicated a more homogeneous cellular composition, likely consisting of mostly LGR5+ stem and early progenitor cells. Since stem and progenitor cells are generally most capable to give rise to new organoids, increasing their number was required to receive enough organoids after the transduction. After three days of Wnt3a stimulation, organoids were harvested and processed into a single cell suspension. This enabled a clonal outgrowth of new organoids following transduction. Lentiviral supernatant was generated in parallel and combined with the single cell suspension, followed by a process termed spinoculation, a 60-minute-long centrifugation step at low speed. After this, the cell-virus suspension was incubated for six hours, the cells were collected and seeded into Matrigel. In the initial culture medium Wnt3a stimulation was maintained for another three days to supplement endogenous Wnt ligand production. This was done to promote stemness, which overall improved cell survival and organoid growth. After that time period, organoids had already formed and Wnt3a was removed from the culture medium. Antibiotics were added to the medium to select transduced

organoids until a control well was free of proliferating cells, followed by an out-growth period, during which organoids regained their crypt-villus morphology, usually within 14 days.

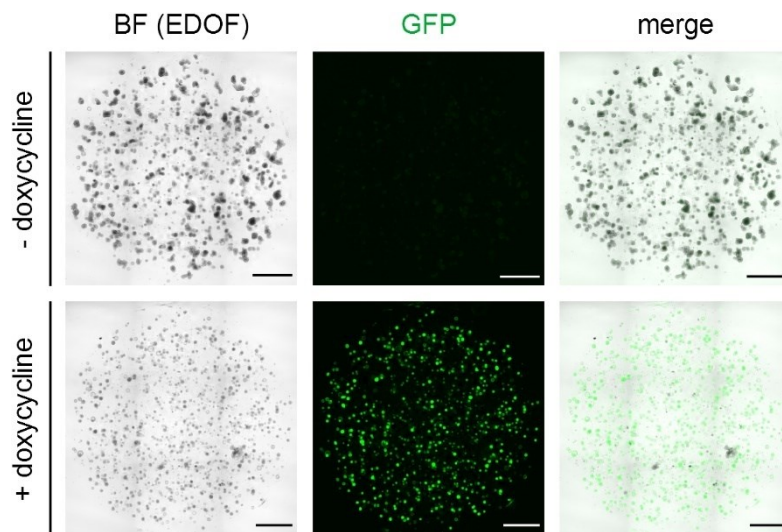


Figure 26 Lentiviral transduction yields a high number of transduced intestinal organoids. Exemplary images of intestinal organoids transduced with a doxycycline-inducible construct containing both an shRNA sequence and GFP. Images taken after 5 days of culture. Scale bar: 0.1 cm. BF: Brightfield, EDOF: Extended depth of field.

An important improvement to the protocol was made based on experiences with cultivating human organoids: Instead of PBS, BSA-PBS was used to resuspend cells, which prevented them from sticking to plastic or glass surfaces, substantially increasing the numbers of recovered cells. This was especially crucial during preparation for the transduction and subcultivation after selection, when only few organoids grew. After transfection and selection, organoids grew well and regained their crypt-villus architecture. In the absence of doxycycline, inspection with a microscope showed very low levels of GFP fluorescence (Figure 26, top panels), indicating low levels of background expression. Upon induction with doxycycline over as little as 24 h GFP fluorescence increased dramatically in a large percentage of organoids, confirming a high rate of infection. GFP reporter expression was monitored for up to seven days and remained stable when doxycycline was supplied with the culture medium, indicating stable integration into the cell's genome. Exemplary images after 5 days of culture are shown in Figure 26 (bottom panels).

5.4.1 shRNA-mediated knockdown in organoids is a powerful tool to study gene function

As part of a collaboration with the group of Ralf Jacob (Institute of Cell Biology and Cell Pathology, Marburg) and as a proof-of-concept, the lentiviral shRNA expression system was used to generate tubulin tyrosine ligase (TTL) knockdown organoids. *TTL* mRNA expression was quantified and functional organoid experiments analyzing growth and morphology were carried out.

5.4.1.1 Induction of shRNA expression reduces *TTL* mRNA-expression in murine intestinal organoids

The relative mRNA expression of murine intestinal *TTL* knockdown organoids was quantified using RTqPCR.

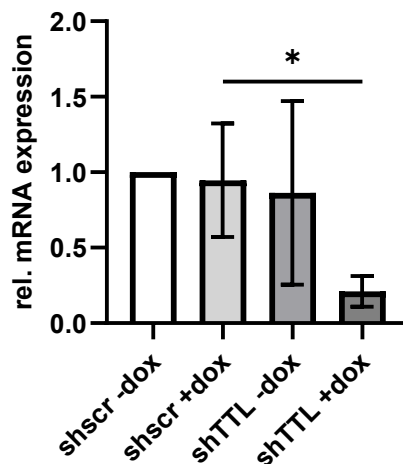


Figure 27 *TTL* expression is reduced in shTTL-expressing intestinal organoids. Relative *TTL* mRNA expression in scrambled (*shscr*) control organoids and *TTL* knockdown organoids (*shTTL*) in the presence (+dox) or absence (-dox) of doxycycline after 96 h of culture. Values were calculated relative to *shscr* -dox control. Measured by RTqPCR. Mean \pm s.d., n=3. Statistical significance: Student's t-test, * p<0.05.

Upon doxycycline induction for 96 h, a significant reduction in *TTL* mRNA expression was observable in the *shTTL* organoids, while expression in the control organoids was unaffected (Figure 27). Protein expression was analyzed by members of the laboratory of Ralf Jacob using western blotting and confirmed a reduction of *TTL*. Furthermore, the product of the reaction catalyzed by *TTL*, tyrosinated tubulin, was reduced as well, confirming a functional knockdown (data not shown).

5.4.1.2 Organoid size and structural complexity are reduced in TTL knock-down organoids

After confirming the ability of the shRNA constructs to reduce TTL expression in intestinal organoids, functional experiments were conducted, culturing organoids for 168 h in total.

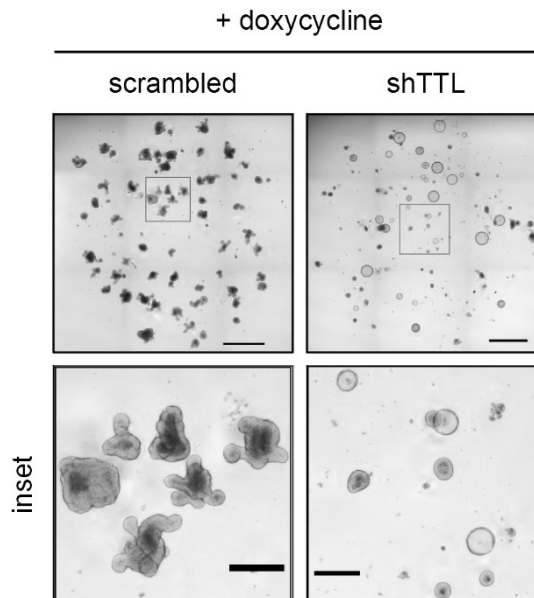


Figure 28 TTL knockdown strikingly changes intestinal organoid morphology. Scrambled control and shTTL knockdown organoids under doxycycline treatment. Representative images after 168 h. A second independent experiment was conducted for 96 h, showing similar morphology. Scale bar low magnification: 1 mm; high magnification: 250 μ m.

Upon induction, organoids remained visibly smaller and displayed a lower level of structural complexity. Crypt-like protrusions failed to form, and the epithelium remained flat in most organoids (Figure 28).

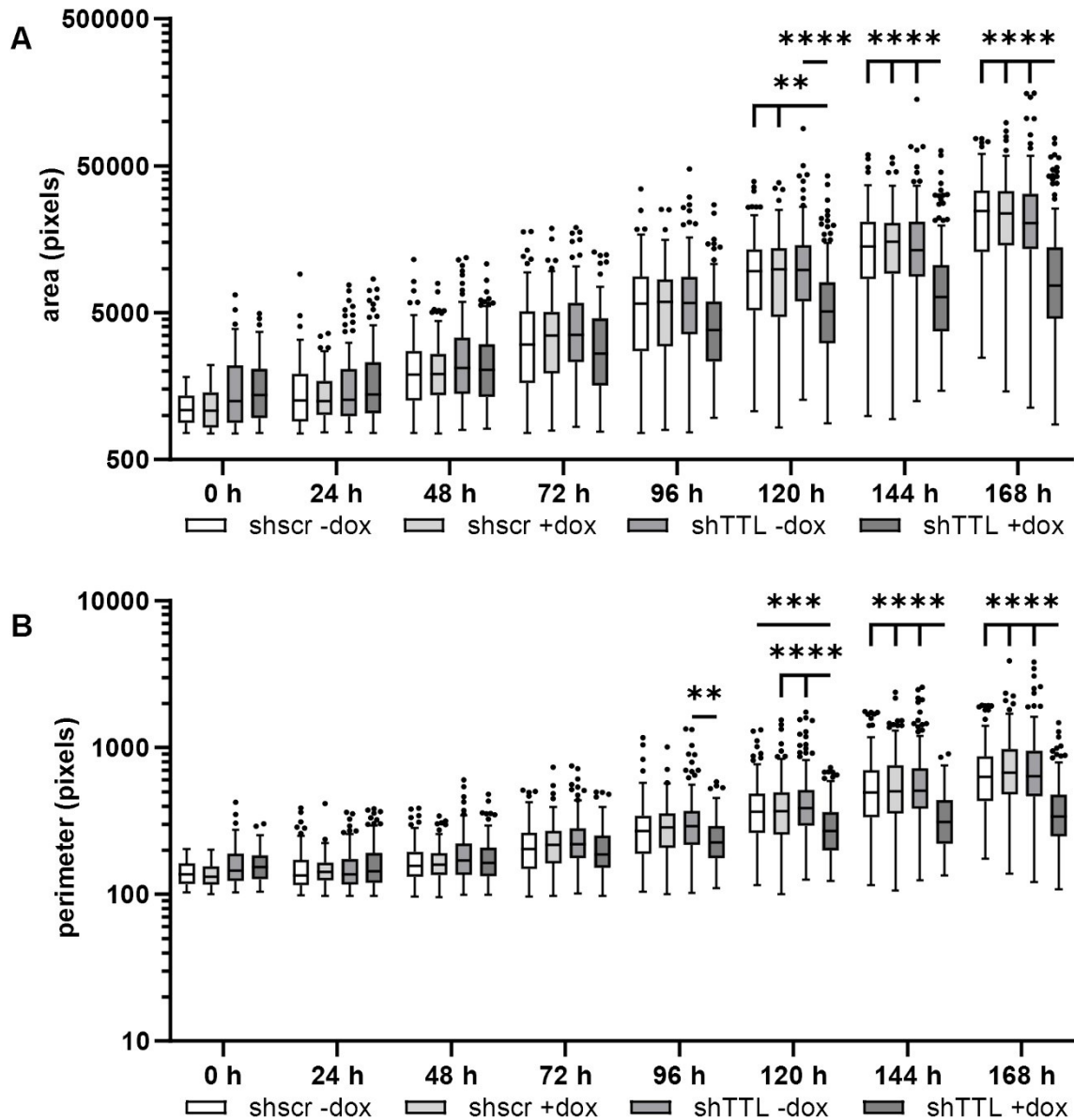
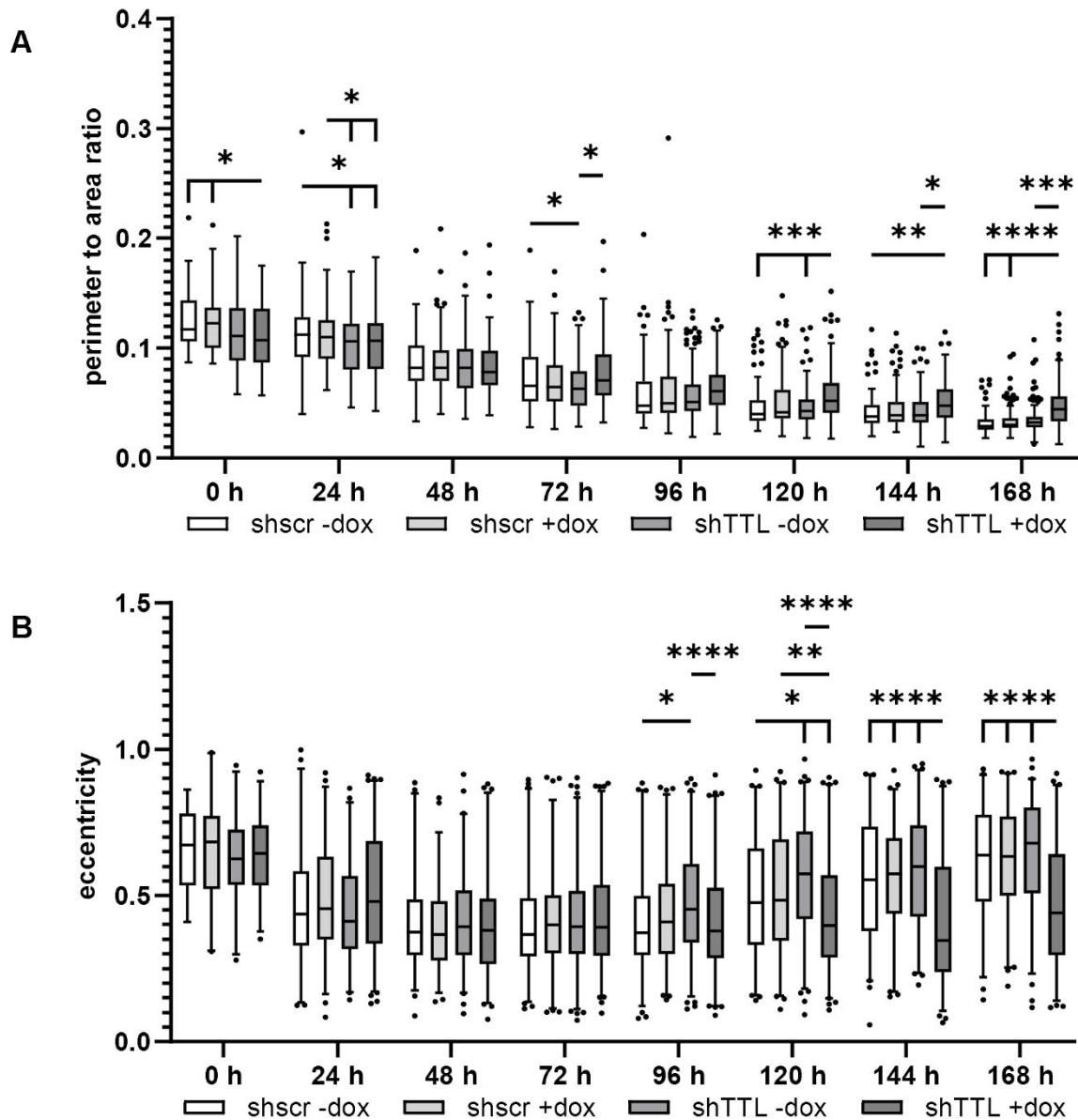


Figure 29 Knockdown of TTL reduces intestinal organoid size. *shTTL* knockdown and scrambled (*shscr*) control organoids were cultivated for 168 h and imaged every 24 h with (+dox) or without (-dox) doxycycline treatment. (A) 2D-area of organoids measured in pixels and (B) 2D-perimeter of organoids measured in pixels. Box plots after the Tukey method: Whiskers extend to 1.5 times the interquartile range; two-way ANOVA, ** $p < 0.0021$, *** $p < 0.0002$, **** $p < 0.0001$.

Organoid size was quantified for all time points by analysis of the 2D area and perimeter (Figure 29). All organoid cultures continued to grow over the course of the entire experiment. While both control organoids (*shscr*) and non-induced *shTTL* organoids grew at similar rates, the knockdown of TTL noticeably slowed organoid growth as early as 72 h after seeding and the difference in area and perimeter was significant after 120 h of culture.



*Figure 30 Morphological complexity of TTL knockdown organoids is reduced. shTTL knockdown and scrambled (shscr) control organoids were cultivated for 168 h and imaged every 24 h with (+dox) or without (-dox) doxycycline treatment. (A) Perimeter to area ratio as calculated for each organoid individually. (B) Eccentricity, i.e., the ratio of the distance between foci of ellipse and major axis length. Box plots after the Tukey method: Whiskers extend to 1.5 times the interquartile range; two-way ANOVA, * $p < 0.0332$, ** $p < 0.0021$, *** $p < 0.0002$, **** $p < 0.0001$.*

To quantify the noticeable reduction in structural complexity, the ratio of perimeter to area, as well as eccentricity were analyzed (Figure 30). As the organoids grew, the perimeter to area ratio decreased under all conditions, but did so more slowly in TTL knockdown organoids. In addition, measured values were distributed more widely, pointing to a morphologically more heterogeneous population of organoids. Eccentricity is the ratio of the distance between the foci and major axis

length of an ellipse laid over an organoid. It is lower, when organoids are approximately circular and increases as their overall shape becomes less so. At seeding, eccentricity was comparable under both control and knockdown conditions and decreased over the first 72 h of culture, as organoids became more spherical and grew. Starting at 96 h of culture, eccentricity started to increase again under control conditions as organoids broke symmetry and crypt-like protrusions started to grow. Under knockdown conditions eccentricity remained low, reflective of the observed lack of crypt-like protrusions. Data from a second independent experiment in which cells were cultured for 96 h revealed similar trends (data not shown).

5.4.1.3 No clear trends emerge in the differentiation of *TTL* knockdown organoids

Epithelial differentiation was analyzed using RTqPCR to quantify marker gene expression. Expression of *TTL* mRNA was reduced reliably under doxycycline induction as shown previously (Figure 27). Three independent experiments were conducted after 96 h of doxycycline induction (Figure 31 A), a second experiment was carried out after 168 h of doxycycline treatment (Figure 31 B).

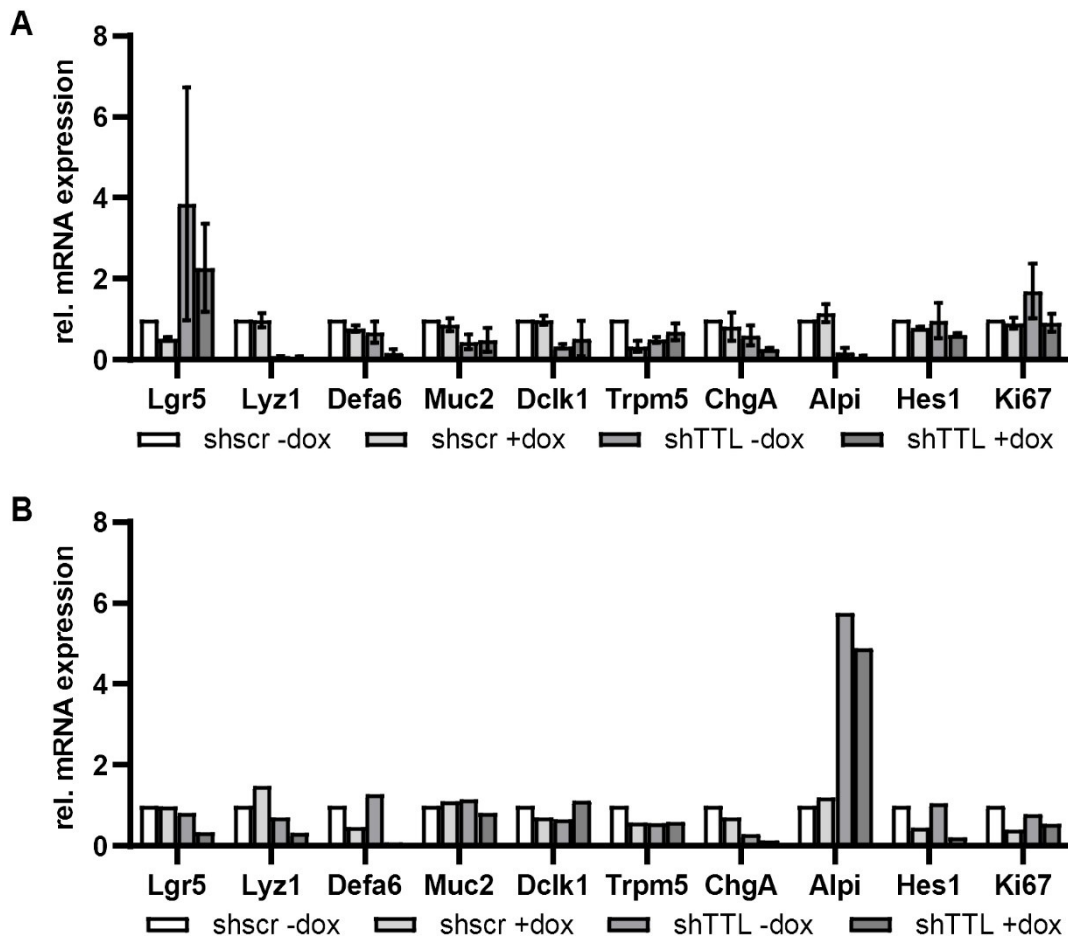


Figure 31 Expression analysis of intestinal epithelial marker genes in *TTL* knockdown organoids. Marker gene mRNA expression levels were measured by RTqPCR in scrambled (*shscr*) control organoids and *TTL* knockdown organoids (*shTTL*) in the presence (+dox) or absence (-dox) of doxycycline. Values were calculated relative to *shscr* -dox control. (A) After 96 h (mean \pm s.d., n=3) or (B) after 168 h of culture (mean, n=1). Stem cells: *Lgr5*; Paneth cells: *Lyz1*, *Defa6*; Goblet cells: *Muc2*; Tuft cells: *Dclk1*, *Trpm5*; EECs: *ChgA*; Enterocytes: *Alpi*, *Hes1*; Proliferation: *Ki67*.

Overall, no clear trends in differentiation could be identified when cell type markers were analyzed by RTqPCR. For some genes, induction of the scrambled control construct already influenced marker expression, e.g., *Lgr5*, *Trpm5* at 96 h.

The same was true for non-induced shTTL organoids, in which expression levels were sometimes drastically different from the scrambled control organoids, e.g., *Lgr5*, *Lyz1*, *Dclk1*, *Alpi* at 96 h. For the 168 h time point, the control conditions provided similarly unpredictable results.

5.4.2 Semaphorin 4A shRNAi reduces expression in CMT-93, but not murine intestinal organoids

To further investigate the functional role of semaphorins in the intestinal epithelium, inducible shRNA constructs targeting *Sema4A* were used to generate murine small intestinal knockdown organoids. Due to their high efficiency in CMT-93 cells, two sequences targeting *Sema4A* (shSema4A_1, shSema4A_4) were chosen and cloned into the inducible LT3GEPIR vector. To test the knockdown efficiency of the new constructs, they were introduced into both CMT-93 cells and murine small intestinal organoids by lentiviral transduction. In parallel, lipofections of CMT-93 were carried out with the same constructs as control experiments. Relative semaphorin 4A mRNA expression was quantified by RTqPCR.

After lipofection of the constructs into CMT-93 cells, the construct shSema4A_1 caused a knockdown upon doxycycline induction. Under control conditions or with the second shSema4A_4 construct, *Sema4A* expression was either marginally decreased or increased, respectively (Figure 32 A). Utilizing lentiviral transduction of CMT-93, expression of *Sema4A* was slightly decreased in scrambled control cells upon induction with doxycycline, but was strongly reduced in shSema4A cells, even when doxycycline was not applied (Figure 32 B). Finally, the constructs were transduced into intestinal organoids. GFP co-expression under doxycycline treatment was used to evaluate transduction efficiency and indicated a high number of transduced organoids (Figure 32 C, left panel). Despite successful selection of the organoids with antibiotics and a high transduction efficiency, no knockdown of *Sema4A* was detectable in any of the constructs (Figure 32 C).

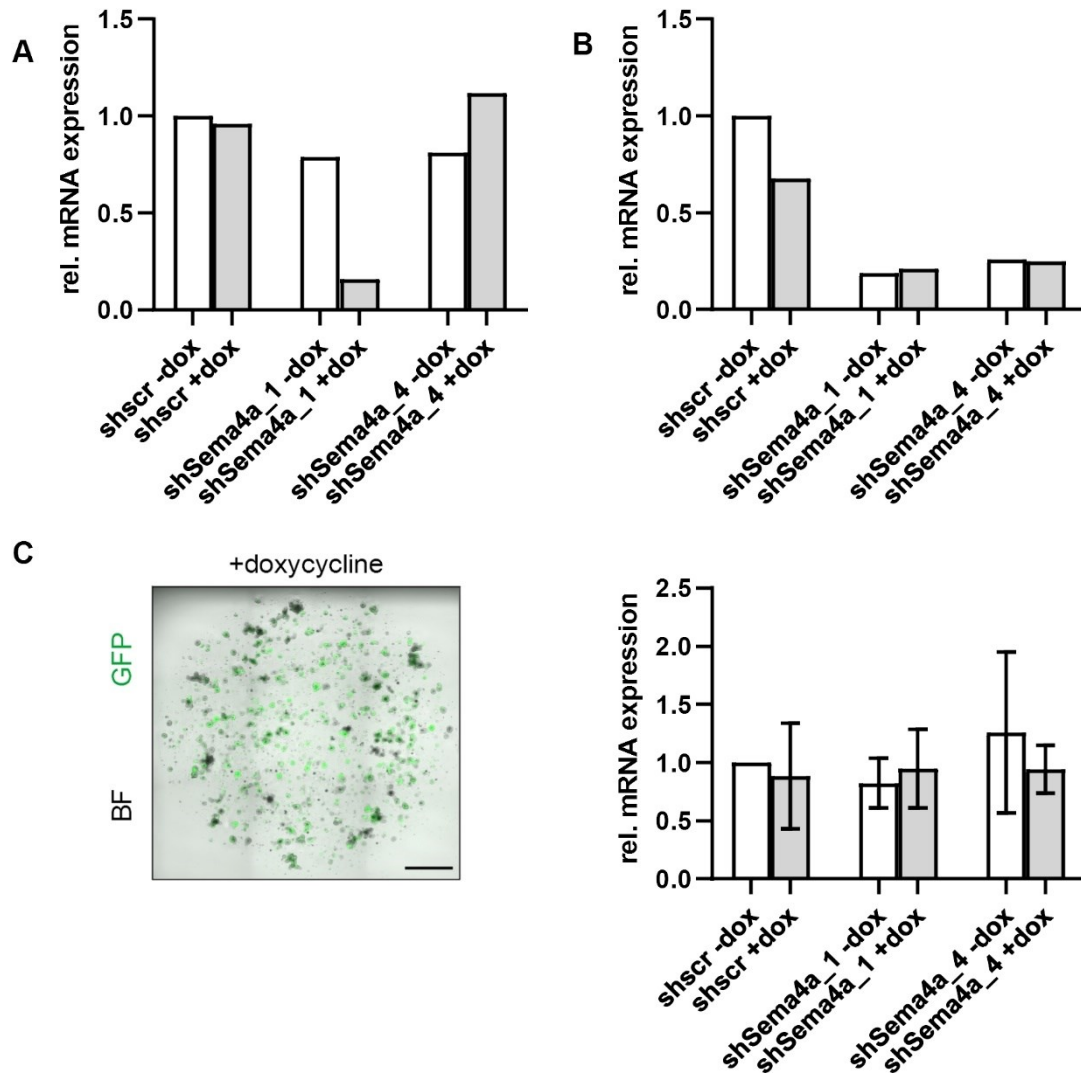


Figure 32 Lentiviral *shSema4A* constructs reduce *Sema4A* mRNA expression in CMT-93, but not intestinal organoids. CMT-93 cells or intestinal organoids were transfected or transduced with a scrambled (shscr) control or an shRNA-construct targeting *Sema4A* (shSema4a). Relative *Sema4A* mRNA expression measured by RTqPCR. **(A)** Transfected CMT-93 cells 48 h post-transfection with (+dox) or without (-dox) doxycycline induction (mean, n=1). **(B)** Transduced CMT-93 cells after 48 h of culture with (+dox) or without (-dox) doxycycline induction (Mean, n=1). **(C)** Transduced intestinal organoids after 96 h with (+dox) or without (-dox) doxycycline induction. Left panel: Co-expression of GFP in *shSema4A*-expressing intestinal organoids after 96 h of culture +dox confirms high rate of transduction. (mean \pm s.d., n=3). Scale bar: 0.1 cm. BF: Brightfield.

5.5 Establishment of human colonic organoid cultures from normal and tumor tissue

Since organoids are a powerful tool to study both physiological and pathological processes under conditions, that closely resemble the situation *in vivo*, human colonic organoids were established from both normal and cancerous tissue as described in section 4.1.2. All samples were acquired in cooperation with the Department of Visceral, Thoracic and Vascular Surgery and the Department of Pathology of the University Clinic Gießen and Marburg from CRC patients undergoing surgery to remove their tumor and with their consent.

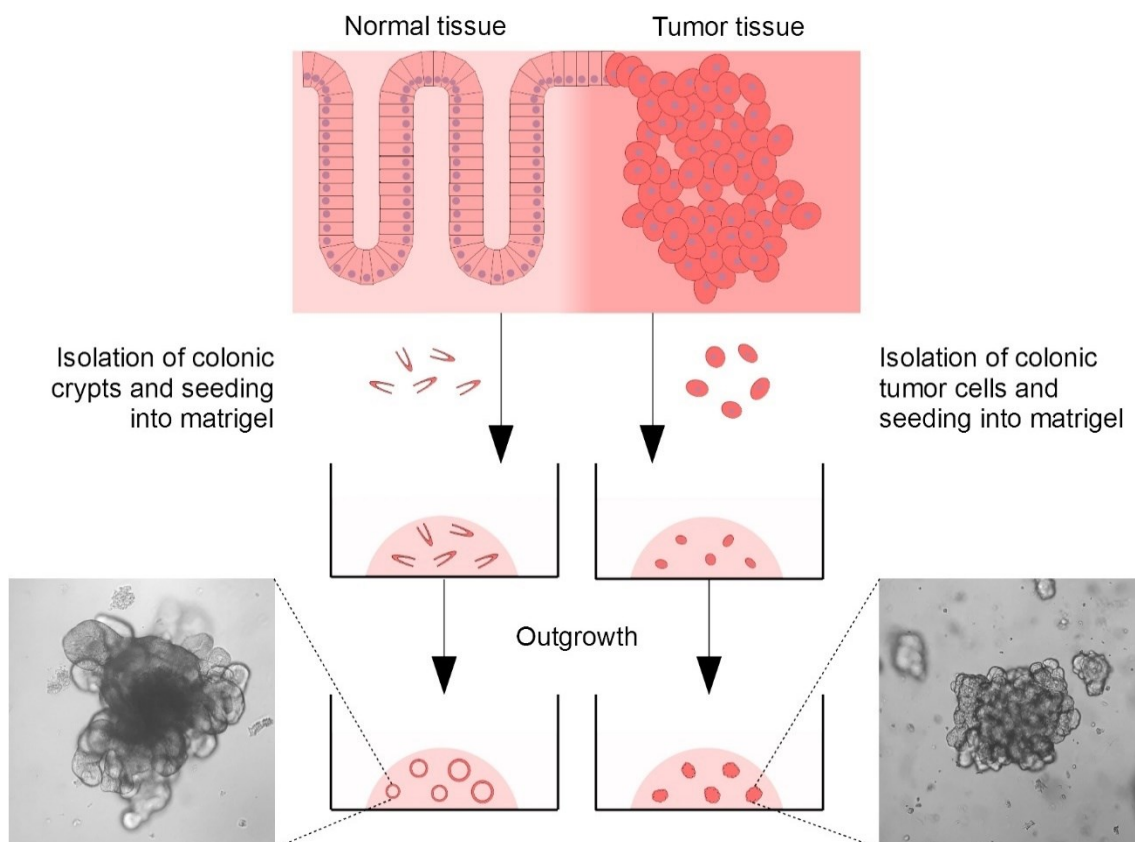


Figure 33 Establishment of human colonic organoid cultures. Schematic of human colonic organoid culture establishment. Part of a surgically removed colon tumor and corresponding normal tissue are used to isolate epithelial tumor cells and crypts, respectively. Both are taken into culture and grown out to form organoids. Representative images of a normal organoid (left) and a tumor organoid (right).

Establishing the culture of human intestinal organoids, especially from healthy tissue samples proved to be more challenging than the culture of murine intestinal organoids, due to several factors: Frequently, the isolation of crypts yielded few

viable cells and instead contained mostly differentiated cells incapable of growing into organoids. Adjustments to the isolation protocol were made based on recommendations from the group of Kim Bak Jensen (BRIC; Copenhagen, Denmark) and led to a considerable increase in the number of stem cells obtained from the procedure, a prerequisite for sustainable organoid cultures. Nonetheless, efficiency varied from sample to sample, and incubation times in the chelation solution often needed to be adjusted, as short incubation times yielded mostly debris, while longer incubation times jeopardized viability of the isolated cells. Due to the changes made to the protocol, the initial number of growing structures increased, but organoids often failed to entirely close and most cells ceased to proliferate after 3 to 4 days. Consequently, subcultivation was at first not successful and cells that seemingly survived the process quickly underwent apoptosis, leading to the disintegration of organoids. In addition, the subcultivation protocol used up to that point was associated with a high loss of cells, because fragmented organoids frequently stuck to glass or plastic surfaces of cell culture materials. A significant improvement to that protocol was achieved using BSA-PBS when resuspending organoids and pipetting cell suspensions, again increasing the number of viable cells obtained from all procedures. This later proved critical for the successful expansion of the cultures as starting material was usually scarce compared to e.g., murine organoids. Finally, culture media requirements for human organoids differed from mouse organoids, as previous publications already demonstrated. Therefore, certain requirements were known, i.e., the addition of exogenous Wnt ligands which were supplemented by adding Wnt3a- and R-Spondin1-conditioned medium. However, using those media compositions proved unsuccessful in maintaining organoid cultures from healthy tissue for more than ca. 4 days. A study by Fujii et al. investigated the use of niche-inspired growth factors to improve organoid self-renewal and cellular diversity (M. Fujii et al., 2018). Based on this publication, the growth factors insulin-like growth factor 1 (IGF-1) and fibroblast growth factor (FGF) were incorporated into the culture medium and substantially improved organoid survival and growth. The changes made to these protocols also improved culture conditions of the tumor organoids, although the medium composition differed in some ways: Tumor organoids were cultured without exogenous Wnt ligands since a constitutive activation of Wnt signaling is often the first step in intestinal tumorigenesis. While this did select for

tumors with gain-of-function mutations in the Wnt pathway, it more importantly ensured that no healthy epithelial cells would start growing, thus preventing contamination.

In summary, these improvements established isolation and culture conditions under which normal organoids grew well. They reached a relatively large size when compared to murine small intestinal organoids but maintained the typical architecture, consisting of a simple columnar epithelium, forming a central lumen and crypt-like protrusions. Organoids derived from cancerous tissue grew drastically less structured. No lumen was observable, and the cells appeared to form a compact mass instead of an epithelial monolayer. While the outside surface of organoids is typically smooth, in tumor organoids it was commonly uneven. The lumen of healthy organoids started to fill with apoptotic cells after several days of culture and became opaque in light microscopy. This was regularly not the case in tumor organoids, which remained translucent, possibly indicating fewer cells becoming apoptotic (Figure 33). Taken together these features morphologically distinguish normal from tumor organoids and recapitulate identifying properties of tumors *in vivo* e.g., dysplasia and a reduction of apoptosis compared to healthy tissue. Ultimately, both normal and tumor organoids could be expanded, subcultivated, frozen in liquid nitrogen and continued to grow after thawing, which indicated the cultures to be sustainable for extended periods of time, making them suitable for further experiments.

6 Discussion

6.1 Potential redundant and non-redundant functions of B-plexins and their ligands in the intestinal epithelium

The semaphorin-plexin signaling system has been shown to play important roles in a variety of tissues, regulating important processes like organ development, angiogenesis, immune responses and epithelial architecture while also being relevant in cancer. It is also an extraordinarily complex family of proteins, in which most members have multiple interaction partners, as summarized previously (Worzfeld & Offermanns, 2014). Its complexity is further increased by the discovery of non-semaphorin ligands like angiogenin (W. Yu et al., 2017). In addition, previous studies frequently demonstrated semaphorins to act in a redundant manner, e.g. Maier et al. and Xia et al. in the brain and kidney, respectively (Maier et al., 2011; Xia et al., 2015). Thus, the methodical dissection of its elements is a prerequisite for experiments that aim to reveal the function of semaphorins and plexins.

The first section of this thesis systematically mapped the expression of B-plexin ligands and plexin B1 in the intestinal epithelium, a summary of these analyses is provided in Figure 34. The smRNA FISH experiments showed plexin B1 to be expressed throughout the entire epithelium of the murine small intestine and colon (Figure 14). In addition, the analysis of a previously published scRNA sequencing data set by Parikh et al. showed *plexin B1* to be expressed in the human colonic epithelium (Figure 16 B) (Parikh et al., 2019). Both methods detect mRNA, allowing no direct conclusions regarding the protein levels. However, previous work by another doctoral candidate, Ivana Matković, as well as several publications demonstrated plexin B2 to be widely expressed in the small and large intestine, providing evidence on both the mRNA and protein level (Meehan et al., 2014). Given that plexin B1 and B2 are closely related homologues and expressed in the intestinal epithelium, a shared and possibly redundant functional role appears plausible.

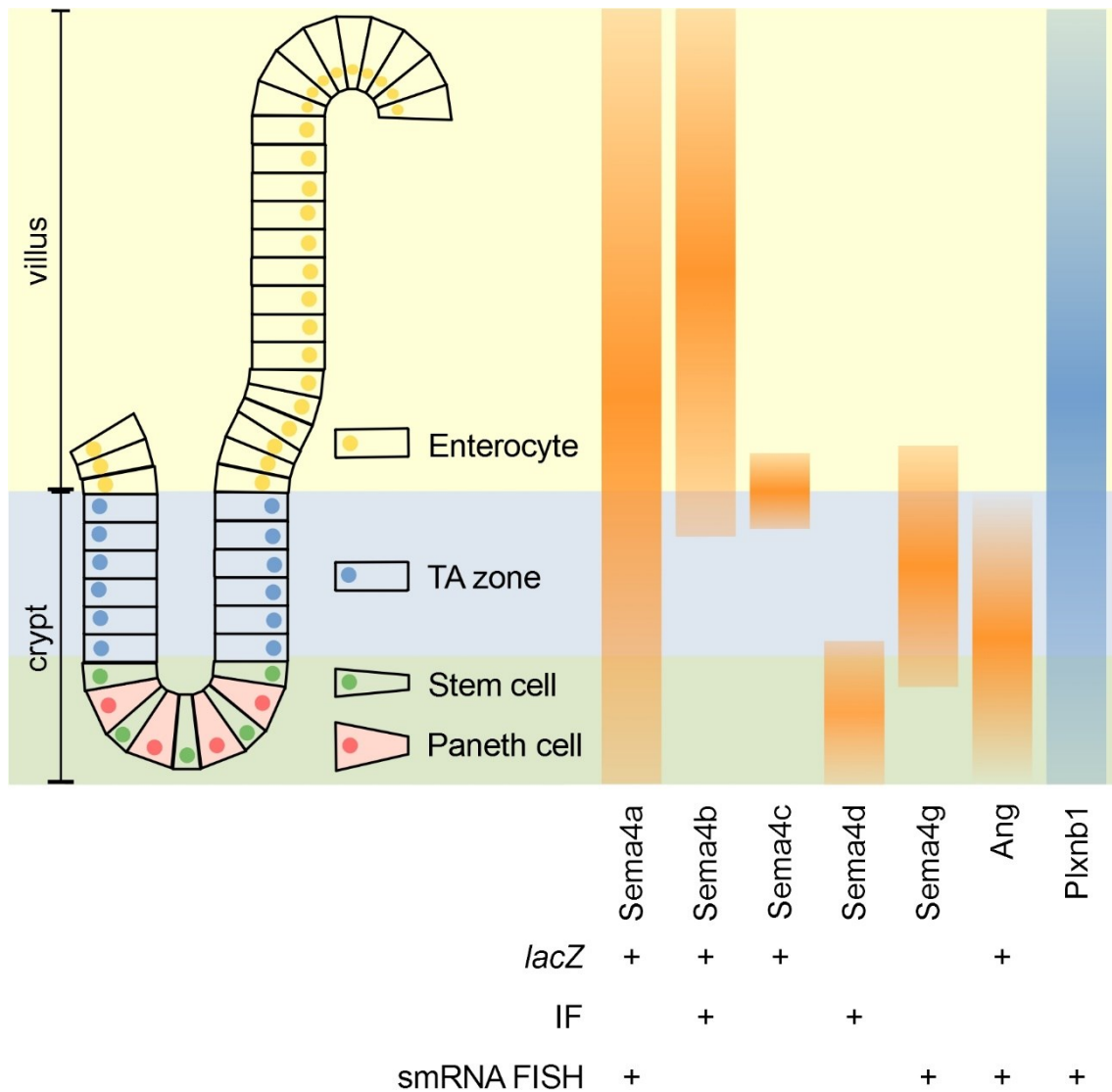


Figure 34 Ligands display distinct expression patterns in the intestinal epithelium. For each ligand (orange) or receptor (blue), the methods used to examine its expression are indicated (+).

In this study, intestinal organoids derived from plexin B1/B2 double knockout mice were analyzed to examine intestinal epithelial dynamics *ex vivo*: They formed with reduced efficiency and morphological complexity, but grew larger when compared to control organoids (Figure 23 B). The reduction in organoid formation likely indicates either a decrease in the number of ISCs or their function, since LGR5+ stem cells are significantly more competent at forming organoids than LGR5- cells (Sato et al., 2009). The reduced perimeter to area ratio could support both explanations: On the one hand, it may be caused by a reduction in the number of crypt-like protrusions and thus in the number of ISCs, on the other hand, shorter crypt-like protrusions might indicate reduced proliferation in the stem cell niche. However, the overall larger plexin B1/B2 double-deficient organoids rather

point to an increase in proliferation. Experiments done by a former colleague linked the loss of plexins B1 and B2 to a reduced number of LGR5+ ISCs, reduced proliferation at the crypt base, but overall hyperproliferation of the epithelium *in vivo*. Consequently, the organoid experiments reflect these previous observations and strongly endorse a role of plexin B1 and B2 in the regulation of epithelial homeostasis, possibly by supporting stemness.

Examinations of the renal epithelium might provide indications, how B-plexins function in epithelial tissues: Plexin B1 is essential for appropriate embryonic kidney development, despite being co-expressed with plexin B2 (Korostylev et al., 2008). Plexin B2 on the other hand is globally expressed in the adult kidney (Zielonka et al., 2010), where it was shown to be indispensable for epithelial repair upon ischemic injury (Xia et al., 2015), pointing to distinct functional roles. However, under physiological conditions Xia et al. found epithelial architecture to be unaffected in plexin B1 and B2 single knockout mice, while it was disrupted when both receptors were knocked out, likely because one ligand was able to compensate the loss of the other, despite their distinct roles (Xia et al., 2015). A similar dynamic between these receptors might exist in the intestine, in which each receptor is essential under certain conditions e.g., one being most relevant during development, while the other is essential in epithelial repair of the adult organ. Since the function of plexins has been linked to proliferation, an important difference between these organs might lie in their rate of proliferation: Tubular epithelial cells are largely quiescent in the adult kidney (Witzgall et al., 1994), while the intestinal epithelium has a high cellular turnover (Stevens & Leblond, 1947). Consequently, the regulation of intestinal epithelial dynamics is crucially important, and compensatory mechanisms are likely at play, given the relatively normal morphology of plexin B1/B2 double knockout organoids. A systematic characterization of the number of ISCs, the rate of proliferation and tissue morphology in receptor single knockout mice and organoids might paint a clearer picture, how plexins B1 and B2 complement each other in the intestinal epithelium.

Further clues regarding the function of semaphorins and plexins in the intestine come from the localization of their ligands: Plexins B1 and B2 are receptors to class 4 semaphorins, as has been summarized previously (Worzfeld & Offermanns, 2014). Furthermore, another study revealed Ang to signal through plexin

B2 (W. Yu et al., 2017). Therefore, this thesis systematically mapped the expression of these B-plexin ligands in the different epithelial compartments of the intestine. All analyzed ligands were found to be expressed and the observed patterns, as well as the methods used are summarized in Figure 34.

Sema4A was analyzed in *lacZ* reporter mice as well as smRNA FISH, characterizing promoter activity and mRNA expression, respectively. Despite the *lacZ* staining revealing only weak promoter activity (Figure 8 and Figure 9), the transcript was detectable throughout the entire intestinal epithelium by smRNA FISH. In the crypt base, no cell type-specificity was discernable (Figure 11). In human colonic epithelium, the analyzed scRNA sequencing data showed relatively low expression of *SEMA4A* (Figure 16). Expression did not appear compartmentalized, offering little evidence concerning a specific functional role. However, none of the methods used give direct evidence regarding *Sema4A* protein levels. Especially the high sensitivity of smRNA FISH might be deceiving, as it detects minute amounts of transcript. To characterize *Sema4A* function, *Sema4A* knockout organoids were studied and organoid formation, size and morphology were unchanged (Figure 23). While these findings do not preclude a role for *Sema4A* in intestinal epithelial dynamics, it is likely not the only ligand to act on plexins B1 and B2, as it failed to reproduce the defects observed in the receptor double knockout organoids. As laid out earlier, ligand redundancy is a phenomenon well documented in semaphorin-plexin signaling, meaning other ligands are likely compensating for the loss of *Sema4A*. Breeding and analyzing e.g., ligand double knockout mice, or generating multiple-knockdown organoids appears to be necessary to fully dissect these redundancies in the intestine.

The expression analysis conducted as part of this thesis demonstrated *Sema4B* to be expressed in both small and large intestine: The initial *lacZ* reporter stainings showed high promoter activity in the upper epithelial compartment of the small intestine with a marked decrease towards the intestinal crypts (Figure 8). This finding was confirmed using IF stainings, where the epithelium of the villi was strongly stained for *Sema4B*, while no staining was detectable in the crypts (Figure 10). Similarly, promoter activity was strongest in the colonic luminal epithelium (Figure 9), however no difference in *Sema4B* protein levels was detectable in IF stainings (Figure 10). In the human colonic epithelium, *SEMA4B*-expressing cells were the most frequent when compared to the other analyzed

ligands, a finding that might indicate expression levels to be similar when compared to the mouse colon. In the small intestine, *Sema4B* is expressed in the highly differentiated epithelium of the villi, making it appealing to speculate, that it might send pro-differentiation and anti-proliferation signals to neighboring cells. However, when analyzing *Sema4B* knockout organoids, their size and morphology was not affected, making a role in the regulation of proliferation unlikely. Instead, *Sema4B* was the only ligand, whose knockout affected organoid formation, a process strongly linked to stem cell function (Sato et al., 2009). How *Sema4B* might influence stem cell niche dynamics remains unclear, as its localization within the epithelium appears ill-suited to fill that role. A possible mechanism might be the proteolytic release of its extracellular domain, that could then reach distant target cells, conceivably within the crypt. Proteolytic cleavage has been documented for class 4 semaphorins: Hemming et al. specifically identified *Sema4B* as a putative β -secretase target but only provided experimental evidence for the cleavage of *Sema4C* (Hemming et al., 2009). Studies of other class 4 semaphorins identified metalloproteases as likely mediators their cleavage (Elhabazi et al., 2001; Nakatsuji et al., 2012). To test whether intestinal *Sema4B* is cleaved, culture supernatants of organoids could be analyzed for the presence of its solubilized extracellular domain e.g., by immunoprecipitation. Whether this process is of physiological relevance could then be examined e.g., by inhibiting putative proteases to prevent *Sema4B* cleavage, or by adding recombinant *Sema4B* to the culture medium of *Sema4B* knockout organoids. Especially the examination of ISC number and proliferation under these conditions might help to understand the observed phenotype. Although the mode of action is unclear, the fact that only the *Sema4B* knockout affected organoid formation makes it an interesting target for the generation of multiple knockouts or knockdowns to investigate ligand redundancies. The expression of *Sema4B* in the epithelium of the villi also makes an enterocyte-specific knockout by e.g., utilizing an *Alpi-Cre* mouse line an appealing approach.

The least evidence for its expression was obtained for *Sema4C*, for which only *lacZ* reporter stainings could be performed. The ligand was only weakly expressed around the crypt-villus border of the SI, most likely in stromal cells (Figure 8). Additional staining was observable in the crypt base but likely represented unspecific background signal since a similar pattern was observable in the *wt*

control. In the proximal colon, expression was localized in a thin ribbon immediately below the luminal epithelium (Figure 9, upper panel), but interestingly decreased in intensity towards the distal parts of the organ (Figure 9, lower panel). While these experiments do not allow direct conclusions on the functions of *Sema4C*, its apparent stromal localization in the intestine is intriguing, as it is similar to the expression in other organs: Two studies analyzed expression of *Sema4C* in the kidney and found it to be primarily expressed in interstitial cells of the medulla, while Xia et al. further observed an upregulation of its expression after ischemic injury of the kidneys (Xia et al., 2015; Zielonka et al., 2010). Perälä et al. further found *Sema4C*-plexin B2 signaling to be essential during kidney development (Perälä et al., 2011). These studies demonstrate a role in tissue morphogenesis and possibly in its repair, both tasks that *Sema4C* might fill in the intestine as well. Based on the data gathered in this study however, no conclusions can be drawn regarding its intestinal function. Any future investigations would certainly need to further characterize its expression. Based on the *lacZ* reporter stainings, it could not be unambiguously concluded, whether the detected *Sema4C* promoter activity is of epithelial or stromal origin. One approach to address this question could be to isolate the intestinal epithelium and compare its *Sema4C* expression against the remaining intestinal tissue by RTqPCR. To characterize its expression gradient along the intestine, tissue from different sections of the organ could be studied in the same fashion. Regarding a functional role, *Sema4C* knockout mice or knockdown organoids could be studied. Another option might be the analysis of organoids treated with recombinant *Sema4C* protein. This approach could be particularly interesting, as the proteolytic cleavage of the extracellular domain of *Sema4C* has been described previously (Hemming et al., 2009), and similar signaling has been described for class 3 semaphorins, that are secreted by fibroblasts in the colonic crypt and support epithelial growth by signaling through Nrp2 (Karpus et al., 2019).

In the SI, the expression of *Sema4D* was restricted to the crypt base, where no obvious cell type-specificity was observable. In the colon, only stromal cells displayed detectable amounts of *Sema4D* (Figure 10). The analyzed scRNA sequencing data showed only few human colonic epithelial cells positive for *SEMA4D*, most of which localized to the stem cell and secretory clusters (Figure 16). While this finding possibly highlights discrepancies in *SEMA4D* expression

patterns between species, it cannot be ruled out that the use of different methods is the cause: In the murine colon, antibody stainings were used, while scRNA sequencing detects mRNA transcripts. To address this open question e.g., IF stainings of murine vs. human colonic organoids could be used to further characterize SEMA4D expression, although other studies also found no epithelial Sema4D expression in the murine colon (Meehan et al., 2014). Studying potential functions of *Sema4D*, knockout organoids were analyzed. Organoid formation as a metric for stem cell function was not negatively affected by the knockout. The analysis of organoid morphology was hindered by tissue debris that was carried over when seeding the isolated crypts. Given its localization within the epithelium, it is attractive to hypothesize that *Sema4D* may contribute to stem cell niche regulation. Since both semaphorins and plexins are not only membrane-bound, but also expressed in the crypt, signals might be passed between adjacent cells within the niche, i.e., ISCs and Paneth cells. However, the knockout of *Sema4D* did not recapitulate the defects observed in the *plexin B1/B2* double knockout organoids, leading to the conclusion, that *Sema4D* is either filling a different functional role, or is part of a redundant group of ligands. In the renal tubular epithelium, Xia et al. observed a similar phenomenon, where only a triple ligand knockout of *Sema4D*, *Sema4B* and *Sema4G* phenocopied a *plexin B2* knockout (Xia et al., 2015). In the colon, the observed stromal Sema4D expression likely indicates the presence of intraepithelial $\gamma\delta$ T lymphocytes, that were previously described to interact with the plexin B2-expressing epithelium and to be essential for epithelial repair in a colitis model (Meehan et al., 2014). While a similar interaction cannot be excluded in the small intestine, a key difference is the expression pattern: Unlike the colonic epithelium, the small intestinal epithelium does express Sema4D in a highly specific compartment, the crypt base. Therefore, further investigation of its function is warranted. Especially potential ligand redundancies be investigated e.g., by generating double knockout mice or double-knockdown organoids.

Sema4G was most strongly expressed in the TA zone of the small intestine, while expression in the crypt base was observable, but substantially weaker (Figure 12). Interestingly, ISCs were more frequently expressing *Sema4G*, than OLFM4-negative Paneth cells. Similarly, the middle section of the colonic crypts showed the strongest expression, while transcript levels in the crypt bottom and luminal

epithelium were lower (Figure 12). In the human colonic epithelium, the scRNA sequencing data showed *SEMA4G* to be expressed at the highest rate of all analyzed ligands, albeit without an observable preference for any particular cluster (Figure 16). Although scRNA sequencing allows only limited conclusions regarding the localization of *SEMA4G*-positive cells within the colonic epithelium, their even spread across all clusters fits well with the expression in the TA zone, a region in which less differentiated progenitor cells of all lineages can be found (Spit et al., 2018). Given the fact that *Sema4G* is predominantly expressed in the TA zone, it stands to reason that it might be associated with either epithelial lineage determination or regulation of proliferation, the two central processes taking place there. However, the analysis of *Sema4G* knockout organoids offered only limited clues regarding its function: Organoid formation, size and morphology were unaffected by its loss. While at first glance, this finding makes a role in stem cell dynamics or regulation of proliferation unlikely, like for most ligands discussed here, redundancies are well documented for *Sema4G*: In the renal tubular epithelium it acts in concert with *Sema4B* and *Sema4D* (Xia et al., 2015), and in cerebellar development plays a joint role with *Sema4C* (Maier et al., 2011). Therefore, it might fulfill its function together with other ligands, or serve an entirely different role. Based on these findings, further investigations might go into two main directions: Firstly, a possible effect of the *Sema4G* knockout on epithelial differentiation might have remained hidden. To address this e.g., the quantification of differentiation markers in knockout vs. wt control tissue might be analyzed. Secondly, it remains unclear, whether other ligands might compensate for the loss of *Sema4G*. Like for the ligands discussed before, generating double-knockdown organoids might be a useful tool in identifying these redundancies. Due to its prominent localization within the epithelium, *Sema4G* would be an attractive target for such an investigation.

The fact that Angiogenin is expressed in the intestine has been known for several decades (Weiner et al., 1987). As part of this thesis, its expression specifically in the intestinal epithelium was explored: Angiogenin was expressed in the small intestine's crypt base and lower TA zone, but expression levels were relatively low. smRNA FISH paired with IF staining for the stem cell marker OLFM4 revealed *Ang* to be expressed more frequently in Paneth cells, than in stem cells. In the colon, *Ang* expression was low in the crypt, but increased towards the

lumen, where epithelial cells showed the strongest expression (Figure 13). While no fresh tissue was available to grow organoids, epithelial differentiation was analyzed by RTqPCR in the intestines of *Ang* knockout mice (Figure 24). Although the *Ang* mRNA levels were unchanged between knockout and control animals, samples were analyzed, as the knockout was previously confirmed by genotyping PCR and ELISA detecting ANG protein by our collaborator, indicating a functional knockout (data not shown). In *Ang* knockout mice the decreased *Lgr5* mRNA expression indicated a reduction in stem cells, while the increase in *Lyz1* expression pointed to a compensatory increase in Paneth cells. Based on these findings, it is appealing to hypothesize, that ANG secreted by Paneth cells supports stemness in the intestinal epithelium: On the one hand, Paneth cells are known to support stemness in the intestine by secreting essential niche factors (Sato, van Es, et al., 2011). Since they express ANG more frequently than ISCs, it is likely secreted and acts on stem cells via plexin B2 in a paracrine manner. On the other hand, ANG is known to support stemness in other cell types, e.g., hematopoietic cells: Yu et al. demonstrated ANG treatment to increase the expression of self-renewal genes e.g., *Bmi1* (W. Yu et al., 2017), a gene that has been identified as an ISC marker (Sangiorgi & Capecchi, 2008). Furthermore, this thesis demonstrated that the loss of *Ang* in knockout mice led to a reduction in the expression of the stem cell marker *Lgr5*. However, Paneth cells are not the only intestinal source of ANG. Bai et al. found stromal myeloid cells of the colon to express ANG, which signals through plexin B2 and has a protective effect against colitis (Bai et al., 2020). Despite that, ANG is usually not added to organoid culture media, raising the question how stromal ANG affects epithelial homeostasis, as it is non-essential to culture primary intestinal epithelial cells (Sato et al., 2013).

Treating wildtype organoids with recombinant ANG might provide clues regarding its function although the effects may be subtle, given its expendability in organoid culture. In the same way that endogenous Wnt ligand produced by Paneth cells is sufficient to culture murine small intestinal organoids, endogenous expression of ANG by Paneth cells may be sufficient to maintain the epithelium.

A second approach to characterize Angiogenin's function might be a knockdown of *Ang* in intestinal organoids, as tissue from knockout animals was not available. Like for the ligand knockout studies, organoid formation and morphology, as well as epithelial differentiation could be studied with these approaches. Overall, the

findings discussed here provide evidence for a pro-stemness and pro-survival function of ANG in the intestinal epithelium, mediated by plexin B2 as its receptor. In summary, these results precisely map the expression of B-plexin ligands in the intestinal epithelium and highlight some of their potential roles, as well as their likely redundancies, which lays the foundation for further functional studies. Especially the expression in distinct sections of the intestinal epithelium makes the concept of specialized ligand functions in epithelial homeostasis appealing. The strongest evidence for a functional role of the semaphorin-plexin system in the intestinal epithelium comes from the organoid knockout experiments, which link semaphorin-plexin signaling to ISC function. However, redundant semaphorin roles must be considered as most single knockouts did not cause obvious phenotypes. Such redundancies have been well documented in other organs, e.g., the nervous system and the kidney (Basile et al., 2006; Xia et al., 2015). This possibility is further supported by the fact that no epithelial compartment expressed only a single ligand. Beyond that, Sema4A, Sema4C, and Sema4D are known to act as receptors as well, a characteristic that will need to be explored further (Gurrapu et al., 2019; Sun et al., 2017; Zhou et al., 2017). Additional experiments are needed to fully elucidate the functions of B-plexin ligands in the intestinal epithelium, for which obtaining multiple knockout or knockdown organoids may prove crucial. Moreover, treating organoids with recombinant ligands might be a viable option to identify their effects on the intestinal epithelium. The analysis of organoid culture supernatants for proteolytically cleaved extracellular domains of semaphorins might help to elucidate, whether paracrine semaphorin signaling might contribute to intestinal epithelial maintenance.

6.2 Generating mouse lines through BAC recombination

Genetically modified mouse models are a useful tool in investigating the functional role of genes. In knockout animals, potential defects allow conclusions about the functional role of the missing genes. Mouse lines that are modified in a specific cell type can be especially helpful to identify gene functions within a certain epithelial compartment. A mouse line expressing an enterocyte-specific, inducible *Alpi-CreERT* construct has been described previously (Tetteh et al., 2016). Given the high cellular turnover of the intestinal epithelium (Stevens &

Leblond, 1947), an inducible Cre recombinase is not necessarily suitable for all experimental setups. Modified cells might be lost from the epithelium before any effects can be observed.

However, a constitutive *Alpi*-Cre2 mouse line would alleviate this problem. As part of this thesis, an *Alpi*-Cre2 BAC was created by homologous Red/ET and FLP-FRT recombination (Figure 17 and Figure 18). Using this BAC, our collaborators successfully established a mouse line, that constitutively expressed Cre2 under the control of the *Alpi* promoter. Expression and functionality of the *Alpi*-Cre2 construct was then analyzed in *Alpi*-Cre2⁺ *mT/mG*⁺ reporter mice in collaboration with Josina Großmann as part of her bachelor thesis. While the BAC recombination and the generation of the mouse line were successful, the analysis of reporter mice revealed unexpected results: Based on the switch from dTom to GFP expression that indicated Cre activity, only a small fraction of crypt-villus axes expressed the *Alpi*-Cre2 construct (Figure 21). Given that most epithelial cells covering the villi are *Alpi*⁺ enterocytes, a more widespread expression of Cre2 and subsequent switch to GFP would have been expected. Furthermore, in GFP⁺ crypt-villus-axes, GFP was also expressed in the lower crypts, even though *Alpi* expression and *Lgr5* expression had previously been found to be mutually exclusive (Tetteh et al., 2016). This indicated Cre-mediated recombination in early progenitor cells, possibly even *Lgr5*⁺ ISCs. Consequently, their differentiated offspring would also carry the modification independently of their lineage. Since ISCs give rise to all epithelial cell types (Barker et al., 2007), this would essentially eliminate cell type specificity.

Another possible explanation is provided by the study of Tetteh et al.: They found *Alpi*-positive progenitor cells to be capable of replacing niche cells upon damage to the epithelium (Tetteh et al., 2016). However, it does appear unlikely, that under basal conditions, epithelial damage caused progenitor cells to dedifferentiate and repopulate lower parts of the crypt. Finally, it remains unclear why only a small fraction of crypt-villus axes showed recombination events. Utilizing inducible *Alpi*CreERT mice, Tetteh et al. observed a gradient of *Alpi* expression along the small intestine: While it was most expressed in the proximal and least expressed in the distal small intestine, the *Alpi* transcript was detectable in both sections by *in situ* hybridization (Tetteh et al., 2016). Based on this observation, one might hypothesize that the *Alpi*-Cre2 construct is most strongly expressed in

the proximal small intestine and less so in the distal small intestine. However, given the previous observation of even early progenitors undergoing Cre-mediated modification, a high Cre efficiency must be assumed, meaning even low expression should be sufficient to cause recombination. Furthermore, Cre activation in the *Alpi-Cre2⁺ mT/mG⁺* reporter mice was characterized in tissue sections from swiss rolls, providing a longitudinal overview over most of the organ and no obvious GFP gradient was observed. A genetic mosaic of the *Alpi-Cre2* construct might be the cause for the observed expression pattern, although thorough genotyping of the analyzed mice likely excludes that possibility.

Despite these findings, generation of the *Alpi-Cre2* BAC and mouse line was successful, qualifying this approach for the creation of further transgenic animals. However, the suitability of the *Alpi-Cre2* construct for enterocyte-specific expression is drawn into question, as recombination occurred in only few crypts and in early progenitor cells. An approach targeting a different part of the *Alpi* gene might alleviate these problems: While the *Alpi-Cre2* construct generated as part of this thesis replaced the first exon of the *Alpi* gene, the study by Tetteh et al. introduced an IRES-CreERT2 cassette at the STOP codon of the last exon (Tetteh et al., 2016). This might be a determining factor, although difficult to judge given the complexity of gene regulation. Furthermore, the use of alternative enterocyte-specific genes for a similar approach might be explored: *Hes1* for example is a central regulator in absorptive lineage determination and could be targeted with a comparable strategy. However, in the adult mouse it has been found to be expressed in proliferating crypt cells, possibly disqualifying it (Jensen et al., 2000). Finally, BACs have been used to generate transgenic organoids (Schwank, Andersson-Rolf, et al., 2013). This method could potentially be used to verify the functionality and specificity of newly recombined BACs before animal experiments are conducted.

6.3 Intestinal organoids in the study of intestinal epithelial function

Organoids derived from semaphorin single knockout mice were analyzed as part of this thesis and proved insufficient to reproduce a plexin B1/B2 knockout phenotype (Figure 23). Since this was likely due to ligand redundancy as discussed above, a major goal of this thesis was to establish knockdown organoids utilizing a lentiviral, inducible shRNA approach. As a proof of concept, the gene *TTL* was targeted in intestinal organoids and the resulting cultures were characterized. Transduced organoids were obtained with high efficiency and grew normally when expression of the shRNA construct was not induced (Figure 26). Upon induction, *TTL* mRNA levels were reduced significantly, demonstrating the validity of the chosen approach (Figure 27).

Next, experiments were conducted to investigate ISC function and epithelial differentiation by measuring organoid growth and morphology, as well as the expression of differentiation markers, respectively. Using these approaches, several changes could be observed in *TTL* knockdown organoids: Based on the measurement of both their 2D area and perimeter, *TTL* knockdown organoids grew slower than control organoids (Figure 29). This trend was first observable 72 h after seeding, indicating that organoid development was affected early on. Serra et al. found the cellular composition of intestinal organoids to be homogeneous during the first 48 h of culture, before Paneth cells emerge and initiate symmetry breaking events by establishing the intestinal stem cell niche (Serra et al., 2019). From these early niches, the typical crypt-like structures grow out. This was reflected by the measurement of organoid eccentricity, which was lowest after 48 h of culture i.e., organoids were most spherical. After that, eccentricity increased, reflecting their rise in structural complexity (Figure 30). Interestingly, the structural complexity of *TTL* knockdown organoids did not appreciably increase, as crypt-like protrusions failed to form. Thus, one could hypothesize that the loss of *TTL* hinders the formation of the stem cell niche, rather than interfering with proliferation directly. As a result, the TA zone, where most mitoses take place, cannot develop and organoid growth is substantially hindered.

Next, the quantification of intestinal differentiation markers by RTqPCR revealed no consistent trends (Figure 31), although the structural alterations made

changes in cellular composition appear plausible. A possible explanation could be a loss of epithelial properties resulting from epithelial-to-mesenchymal transition (EMT), as Whipple et al. observed a reduction of TTL in cells undergoing EMT (Whipple et al., 2010). Therefore, epithelial marker expression may be affected in unpredictable ways. Interestingly, EMT is a process linked to tissue regeneration (Kalluri & Weinberg, 2009), and Serra et al. found intestinal organoids to express regeneration gene signatures during growth (Serra et al., 2019), possibly linking TTL to these processes. However, evidence for a role of TTL in regeneration has previously only been provided in injured neurons, where it was linked to axonal transport (Song et al., 2015). Furthermore, two technical factors might contribute to the challenging detection of differentiation markers: First, the amount of sample RNA can be restrictive, as organoid cultures are usually kept small due to the cost and time required to maintain them. Second, the expression of some epithelial marker genes can be low, making the detection of biologically relevant differences between samples more difficult. To address this, future experiments might additionally utilize e.g., histological or immunofluorescence stainings of organoids to identify effects on epithelial lineage determination, as protocols for these methods are readily available (E. Fujii et al., 2018; O'Rourke et al., 2016).

An interesting strategy for further experiments might also be to characterize growth and stem cell niche formation in knockdown organoids during the first 72 h after seeding. Utilizing IF stainings, the composition of cell types in knockdown organoids could be analyzed to elucidate e.g., whether organoids contain sufficient Paneth cells to initiate niche formation. Since the shRNA expression is inducible, TTL expression could furthermore be restored, answering the question whether the observed effects are reversible and organoid growth could be resumed. This could be particularly interesting, as organoids that failed to generate stem cells mostly differentiate into enterocytes (Serra et al., 2019).

To further apply this approach to the study of semaphorin-plexin signaling in the intestine, *Sema4A* was targeted with an shRNA construct in intestinal organoids. *Sema4A* was selected as it is widely expressed in the intestinal epithelium as discussed above, and experiments screening for effective shRNA sequences in multiple cell lines indicated a high knockdown efficiency. The initial validation of the construct in CMT-93 cells was successful and RTqPCR revealed a reduction

in *Sema4A* mRNA levels when the plasmid was transfected (Figure 32 A). Using transduction however, the knockdown took effect even when doxycycline was not applied to the cells (Figure 32 B). Mutations in the lentiviral plasmids were ruled out by sequencing (data not shown). Strikingly, the same did not happen when intestinal organoids were transduced (Figure 32 D). Instead no knockdown of *Sema4A* was detectable after doxycycline induction, raising the question how the target cell may decisively influence construct efficiency. Although CMT-93 cells are of intestinal epithelial origin, these results draw their use as a screening cell line into question since the findings from previous experiments did not translate well into the organoid model. Instead, it may be necessary to e.g., include other intestinal cell lines in the screening experiments, test additional targeting sequences, or to screen shRNA sequences in organoids. Despite that, the fact that *TTL* was successfully targeted with the same method demonstrates, that the approach is in principal suitable.

Lastly, patient-derived colonic human organoids from both normal and tumor tissue were established with the goal of studying the role of semaphorin-plexin signaling in intestinal cancer. The initial problems establishing working culture conditions highlight the challenges in maintaining these cells: Human organoids are generally sensitive to suboptimal culture conditions and handling. A crucial factor is the preparation of conditioned media that are used to supply the essential growth factors Wnt3a and R-Spondin1 (Sato, Stange, et al., 2011). In the protocol used here, conditioned media make up 70 % of the complete culture medium of healthy human organoids, underlining the importance of their composition. Eventually, normal colonic organoids convincingly resembled the intestinal epithelium, forming crypt-like protrusions, while tumor organoids recapitulated known morphological characteristics of tumors *ex vivo* (Figure 33). Although no functional experiments could be conducted with these cells so far, the methods established in murine organoids as part of this thesis have proven useful in organoid studies and should be transferrable to human organoids.

Especially the establishment of paired tumor and normal organoids from the same patient opens a new avenue of investigation: Examining the expression of semaphorins and plexins could be a first approach to identify differences between healthy and tumor cells. In this thesis, several candidates have been found to be expressed in the colonic epithelium and were previously linked to cancer:

SEMA4A germline mutations were identified in hereditary CRCs (Schulz et al., 2014), a fact that warrants the characterization of its role in non-hereditary tumors as well. In breast cancer, *Sema4A* also increased tumor growth (Gurrapu et al., 2018). Acting as a receptor to plexin B1, *Sema4A* furthermore increased migratory behavior in cancer cells (Sun et al., 2017), raising the question if the plexin B1-*SEMA4A* signaling axis might contribute to metastasis in CRC. *ANG* would be another interesting subject of study, as it is known to be highly expressed in human CRCs and negatively influence prognosis (Etoh et al., 2000). Although little evidence links *Sema4B* and *Sema4G* to CRC, both are also expressed in the colonic epithelium and may be subject to further investigation.

Applying the methods established in this thesis, these genes could be targeted by shRNA to investigate e.g., whether they influence tumor organoid growth or differentiation. In an opposite approach they could also be overexpressed in organoids, or recombinant protein could be added to the culture medium. Furthermore, organoids generated with these methods could be xenografted into mice, a common model to study metastasis (Bleijs et al., 2019).

In summary, the proof-of-concept experiments characterizing TTL knockdown organoids demonstrated lentiviral shRNA transductions to effectively modulate target gene expression. Combined with imaging techniques and expression analyses they enabled monitoring of ISC function, proliferation and differentiation, important metrics in the study of epithelial homeostasis. Given the high transduction efficiency, this method will enable the generation of multi-deficient organoid lines, a requirement to investigate the redundancies of B-plexin ligands. When applied to human organoids, this model will furthermore enable studies of the semaphorin-plexin system in colorectal cancer. Especially the comparison between primary CRC organoids and normal organoids from the same patient will yield highly relevant data regarding semaphorins in CRC.

References

- Adams, R. H., Betz, H., & Püschel, A. W. (1996). A novel class of murine semaphorins with homology to thrombospondin is differentially expressed during early embryogenesis. *Mechanisms of Development*, 57(1), 33–45. [https://doi.org/10.1016/0925-4773\(96\)00525-4](https://doi.org/10.1016/0925-4773(96)00525-4)
- Bai, R., Sun, D., Chen, M., Shi, X., Luo, L., Yao, Z., Liu, Y., Ge, X., Gao, X., Hu, G., Zhou, W., Sheng, J., & Xu, Z. (2020). Myeloid cells protect intestinal epithelial barrier integrity through the angiogenin/plexin-B2 axis. *The EMBO Journal*, 39(13). <https://doi.org/10.15252/emj.2019103325>
- Bamberg, J. A., Baumgartner, S., Betz, H., Bolz, J., Chedotal, A., Christensen, C. R. L., Comoglio, P. M., Culotti, J. G., Doherty, P., Drabkin, H., Ensser, A., Fishman, M. C., Fleckenstein, B., Freeman, G. J., Fujisawa, H., Ghosh, A., Ginty, D. D., Goodman, C. S., Guthrie, S., ... Yagi, T. (1999). Unified nomenclature for the semaphorins/collapsins [1]. In *Cell* (Vol. 97, Issue 5, pp. 551–552). Cell Press. [https://doi.org/10.1016/S0092-8674\(00\)80766-7](https://doi.org/10.1016/S0092-8674(00)80766-7)
- Bankaitis, E. D., Ha, A., Kuo, C. J., & Magness, S. T. (2018). Reserve Stem Cells in Intestinal Homeostasis and Injury. In *Gastroenterology* (Vol. 155, Issue 5, pp. 1348–1361). W.B. Saunders. <https://doi.org/10.1053/j.gastro.2018.08.016>
- Barker, N., van Es, J. H., Kuipers, J., Kujala, P., van den Born, M., Cozijnsen, M., Haegerbarth, A., Korving, J., Begthel, H., Peters, P. J., & Clevers, H. (2007). Identification of stem cells in small intestine and colon by marker gene Lgr5. *Nature*, 449(7165), 1003–1007. <https://doi.org/10.1038/nature06196>
- Basile, J. R., Castilho, R. M., Williams, V. P., & Gutkind, J. S. (2006). Semaphorin 4D provides a link between axon guidance processes and tumor-induced angiogenesis. *Proceedings of the National Academy of Sciences of the United States of America*, 103(24), 9017–9022. <https://doi.org/10.1073/pnas.0508825103>
- Bastide, P., Darido, C., Pannequin, J., Kist, R., Robine, S., Marty-Double, C., Bibeau, F., Scherer, G., Joubert, D., Hollande, F., Blache, P., & Jay, P. (2007). Sox9 regulates cell proliferation and is required for Paneth cell differentiation in the intestinal epithelium. *Journal of Cell Biology*, 178(4), 635–648. <https://doi.org/10.1083/jcb.200704152>
- Bjerknes, M., & Cheng, H. (1981). The stem-cell zone of the small intestinal epithelium. I. Evidence from paneth cells in the adult mouse. *American Journal of Anatomy*, 160(1), 51–63. <https://doi.org/10.1002/aja.1001600105>
- Bleijis, M., Wetering, M., Clevers, H., & Drost, J. (2019). Xenograft and organoid model systems in cancer research. *The EMBO Journal*, 38(15). <https://doi.org/10.15252/emj.2019101654>
- Bohórquez, D. v., Shahid, R. A., Erdmann, A., Kreger, A. M., Wang, Y., Calakos, N., Wang, F., & Liddle, R. A. (2015). Neuroepithelial circuit formed by

- innervation of sensory enteroendocrine cells. *Journal of Clinical Investigation*, 125(2), 782–786. <https://doi.org/10.1172/JCI78361>
- Borten, M. A., Bajikar, S. S., Sasaki, N., Clevers, H., & Janes, K. A. (2018). Automated brightfield morphometry of 3D organoid populations by OrganoSeg. *Scientific Reports*, 8(1), 1–10. <https://doi.org/10.1038/s41598-017-18815-8>
- Bray, F., Ferlay, J., Soerjomataram, I., Siegel, R. L., Torre, L. A., & Jemal, A. (2018). Global cancer statistics 2018: GLOBOCAN estimates of incidence and mortality worldwide for 36 cancers in 185 countries. *CA: A Cancer Journal for Clinicians*, 68(6), 394–424. <https://doi.org/10.3322/caac.21492>
- Buchholz, F. (1996). A simple assay to determine the functionality of Cre or FLP recombination targets in genomic manipulation constructs. *Nucleic Acids Research*, 24(15), 3118–3119. <https://doi.org/10.1093/nar/24.15.3118>
- Carulli, A. J., Samuelson, L. C., & Schnell, S. (2014). Unraveling intestinal stem cell behavior with models of crypt dynamics. In *Integrative Biology (United Kingdom)* (Vol. 6, Issue 3, pp. 243–257). Royal Society of Chemistry. <https://doi.org/10.1039/c3ib40163d>
- Chen, Y., Chou, K., Fuchs, E., Havran, W. L., & Boismenu, R. (2002). Protection of the intestinal mucosa by intraepithelial $\gamma\delta$ T cells. *Proceedings of the National Academy of Sciences of the United States of America*, 99(22), 14338–14343. <https://doi.org/10.1073/pnas.212290499>
- Cheng, H., & Leblond, C. P. (1974). Origin, differentiation and renewal of the four main epithelial cell types in the mouse small intestine V. Unitarian theory of the origin of the four epithelial cell types. *American Journal of Anatomy*, 141(4), 537–561. <https://doi.org/10.1002/aja.1001410407>
- Clevers, H. (2013). The intestinal crypt, a prototype stem cell compartment. In *Cell* (Vol. 154, Issue 2, p. 274). Cell Press. <https://doi.org/10.1016/j.cell.2013.07.004>
- Davis, M. W. (2020). *ApE (A plasmid Editor)* (2.0.61). <https://jorgensen.biology.utah.edu/wayned/ape/>
- Deng, S., Hirschberg, A., Worzfeld, T., Penachioni, J. Y., Korostylev, A., Swiercz, J. M., Vodrazka, P., Mauti, O., Stoeckli, E. T., Tamagnone, L., Offermanns, S., & Kuner, R. (2007). Plexin-B2, but not plexin-B1, critically modulates neuronal migration and patterning of the developing nervous system in vivo. *Journal of Neuroscience*, 27(23), 6333–6347. <https://doi.org/10.1523/JNEUROSCI.5381-06.2007>
- Dutta, D., & Clevers, H. (2017). Organoid culture systems to study host–pathogen interactions. In *Current Opinion in Immunology* (Vol. 48, pp. 15–22). Elsevier Ltd. <https://doi.org/10.1016/j.coi.2017.07.012>
- Elhabazi, A., Delaire, S., Bensussan, A., Boumsell, L., & Bismuth, G. (2001). Biological Activity of Soluble CD100. I. The Extracellular Region of CD100 Is

Released from the Surface of T Lymphocytes by Regulated Proteolysis. *The Journal of Immunology*, 166(7), 4341–4347. <https://doi.org/10.4049/jimmunol.166.7.4341>

- Etoh, T., Shibuta, K., Barnard, G. F., Kitano, S., & Mori, M. (2000). Angiogenin Expression in Human Colorectal Cancer: The Role of Focal Macrophage Infiltration. *Clinical Cancer Research*, 6(9).
- Fearon, E. R., & Vogelstein, B. (1990). A genetic model for colorectal tumorigenesis. In *Cell* (Vol. 61, Issue 5, pp. 759–767). Cell. [https://doi.org/10.1016/0092-8674\(90\)90186-l](https://doi.org/10.1016/0092-8674(90)90186-l)
- Fellmann, C., Hoffmann, T., Sridhar, V., Hopfgartner, B., Muhar, M., Roth, M., Lai, D. Y., Barbosa, I. A. M., Kwon, J. S., Guan, Y., Sinha, N., & Zuber, J. (2013). An optimized microRNA backbone for effective single-copy RNAi. *Cell Reports*, 5(6), 1704–1713. <https://doi.org/10.1016/j.celrep.2013.11.020>
- Fett, J. W., Strydom, D. J., Lobb, R. R., Alderman, E. M., Bethune, J. L., Riordan, J. F., & Vallee, B. L. (1985). Isolation and Characterization of Angiogenin, an Angiogenic Protein from Human Carcinoma Cells. *Biochemistry*, 24(20), 5480–5486. <https://doi.org/10.1021/bi00341a030>
- Fre, S., Huyghe, M., Mourikis, P., Robine, S., Louvard, D., & Artavanis-Tsakonas, S. (2005). Notch signals control the fate of immature progenitor cells in the intestine. *Nature*, 435(7044), 964–968. <https://doi.org/10.1038/nature03589>
- Friedel, R. H., Kerjan, G., Rayburn, H., Schüller, U., Sotelo, C., Tessier-Lavigne, M., & Chédotal, A. (2007). Plexin-B2 controls the development of cerebellar granule cells. *The Journal of Neuroscience: The Official Journal of the Society for Neuroscience*, 27(14), 3921–3932. <https://doi.org/10.1523/JNEUROSCI.4710-06.2007>
- Fujii, E., Yamazaki, M., Kawai, S., Ohtani, Y., Watanabe, T., Kato, A., & Suzuki, M. (2018). A simple method for histopathological evaluation of organoids. *J Toxicol Pathol*. <https://doi.org/10.1293/tox.2017-0060>
- Fujii, M., Matano, M., Nanki, K., & Sato, T. (2015). Efficient genetic engineering of human intestinal organoids using electroporation. *Nature Protocols*, 10(10), 1474–1485. <https://doi.org/10.1038/nprot.2015.088>
- Fujii, M., Matano, M., Toshimitsu, K., Takano, A., Mikami, Y., Nishikori, S., Sugimoto, S., & Sato, T. (2018). Human Intestinal Organoids Maintain Self-Renewal Capacity and Cellular Diversity in Niche-Inspired Culture Condition. *Cell Stem Cell*, 23(6), 787-793.e6. <https://doi.org/10.1016/j.stem.2018.11.016>
- Gerbe, F., Brulin, B., Makrini, L., Legraverend, C., & Jay, P. (2009). DCAMKL-1 Expression Identifies Tuft Cells Rather Than Stem Cells in the Adult Mouse Intestinal Epithelium. In *Gastroenterology* (Vol. 137, Issue 6, pp. 2179–2180). W.B. Saunders. <https://doi.org/10.1053/j.gastro.2009.06.072>

- Gerbe, F., Sidot, E., Smyth, D. J., Ohmoto, M., Matsumoto, I., Dardalhon, V., Cesses, P., Garnier, L., Pouzolles, M., Brulin, B., Bruschi, M., Harcus, Y., Zimmermann, V. S., Taylor, N., Maizels, R. M., & Jay, P. (2016). Intestinal epithelial tuft cells initiate type 2 mucosal immunity to helminth parasites. *Nature*, *529*(7585), 226–230. <https://doi.org/10.1038/nature16527>
- Giordano, S., Corso, S., Conrotto, P., Artigiani, S., Gilestro, G., Barberis, D., Tamagnone, L., & Comoglio, P. M. (2002). The semaphorin 4D receptor controls invasive growth by coupling with Met. *Nature Cell Biology*, *4*(9), 720–724. <https://doi.org/10.1038/ncb843>
- Gloerich, M., & Bos, J. L. (2011). Regulating Rap small G-proteins in time and space. In *Trends in Cell Biology* (Vol. 21, Issue 10, pp. 615–623). Trends Cell Biol. <https://doi.org/10.1016/j.tcb.2011.07.001>
- Goncalves, K. A., Silberstein, L., Li, S., Severe, N., Hu, M. G., Yang, H., Scadden, D. T., & Hu, G. fu. (2016). Angiogenin Promotes Hematopoietic Regeneration by Dichotomously Regulating Quiescence of Stem and Progenitor Cells. *Cell*, *166*(4), 894–906. <https://doi.org/10.1016/j.cell.2016.06.042>
- Gossen, M., Freundlieb, S., Bender, G., Müller, G., Hillen, W., & Bujard, H. (1995). Transcriptional activation by tetracyclines in mammalian cells. *Science*, *268*(5218), 1766–1769. <https://doi.org/10.1126/science.7792603>
- Greenway, M. J., Andersen, P. M., Russ, G., Ennis, S., Cashman, S., Donaghy, C., Patterson, V., Swingler, R., Kieran, D., Prehn, J., Morrison, K. E., Green, A., Acharya, K. R., Brown, R. H., & Hardiman, O. (2006). ANG mutations segregate with familial and “sporadic” amyotrophic lateral sclerosis. *Nature Genetics*, *38*(4), 411–413. <https://doi.org/10.1038/ng1742>
- Gribble, F. M., & Reimann, F. (2016). Enteroendocrine Cells: Chemosensors in the Intestinal Epithelium. *Annual Review of Physiology*, *78*(1), 277–299. <https://doi.org/10.1146/annurev-physiol-021115-105439>
- Grün, D., Lyubimova, A., Kester, L., Wiebrands, K., Basak, O., Sasaki, N., Clevers, H., & van Oudenaarden, A. (2015). Single-cell messenger RNA sequencing reveals rare intestinal cell types. *Nature*, *525*(7568), 251–255. <https://doi.org/10.1038/nature14966>
- Gu, C., & Giraudo, E. (2013). The role of semaphorins and their receptors in vascular development and cancer. In *Experimental Cell Research* (Vol. 319, Issue 9, pp. 1306–1316). Academic Press Inc. <https://doi.org/10.1016/j.yexcr.2013.02.003>
- Gu, H., Marth, J. D., Orban, P. C., Mossmann, H., & Rajewsky, K. (1994). Deletion of a DNA polymerase β gene segment in T cells using cell type-specific gene targeting. *Science*, *265*(5168), 103–106. <https://doi.org/10.1126/science.8016642>

- Gurrapu, S., Franzolin, G., Fard, D., Accardo, M., Medico, E., Sarotto, I., Sapino, A., Isella, C., & Tamagnone, L. (2019). Reverse signaling by semaphorin 4C elicits SMAD1/5- And ID1/3-dependent invasive reprogramming in cancer cells. *Science Signaling*, *12*(595). <https://doi.org/10.1126/scisignal.aav2041>
- Gurrapu, S., Pupo, E., Giulia Franzolin, •, Lanzetti, L., & Luca Tamagnone, •. (2018). Sema4C/PlexinB2 signaling controls breast cancer cell growth, hormonal dependence and tumorigenic potential. *Cell Death & Differentiation*, *25*, 1259–1275. <https://doi.org/10.1038/s41418-018-0097-4>
- Guzman, L. M., Belin, D., Carson, M. J., & Beckwith, J. (1995). Tight regulation, modulation, and high-level expression by vectors containing the arabinose P(BAD) promoter. *Journal of Bacteriology*, *177*(14), 4121–4130. <https://doi.org/10.1128/jb.177.14.4121-4130.1995>
- H. Karasov, W., & Douglas, A. E. (2013). Comparative Digestive Physiology. In *Comprehensive Physiology* (Vol. 3, Issue 2, pp. 741–783). John Wiley & Sons, Inc. <https://doi.org/10.1002/cphy.c110054>
- Hall, P. A., Coates, P. J., Ansari, B., & Hopwood, D. (1994). Regulation of cell number in the mammalian gastrointestinal tract: The importance of apoptosis. *Journal of Cell Science*, *107*(12), 3569–3577. <https://europepmc.org/article/med/7706406>
- Haramis, A. P. G., Begthel, H., van den Born, M., van Es, J., Jonkheer, S., Offerhaus, G. J. A., & Clevers, H. (2004). De Novo Crypt Formation and Juvenile Polyposis on BMP Inhibition in Mouse Intestine. *Science*, *303*(5664), 1684–1686. <https://doi.org/10.1126/science.1093587>
- Hayashi, S., & McMahon, A. P. (2002). Efficient recombination in diverse tissues by a tamoxifen-inducible form of Cre: A tool for temporally regulated gene activation/inactivation in the mouse. *Developmental Biology*, *244*(2), 305–318. <https://doi.org/10.1006/dbio.2002.0597>
- He, H., Yang, T., Terman, J. R., & Zhang, X. (2009). Crystal structure of the plexin A3 intracellular region reveals an autoinhibited conformation through active site sequestration. *Proceedings of the National Academy of Sciences of the United States of America*, *106*(37), 15610–15615. <https://doi.org/10.1073/pnas.0906923106>
- Hemming, M. L., Elias, J. E., Gygi, S. P., & Selkoe, D. J. (2009). Identification of b-Secretase (BACE1) Substrates Using Quantitative Proteomics. *PLoS ONE*, *4*(12), 8477. <https://doi.org/10.1371/journal.pone.0008477>
- Hill, M. J. (1997). Intestinal flora and endogenous vitamin synthesis. *European Journal of Cancer Prevention*, *6*(SUPPL. 1), S43–S45. <https://doi.org/10.1097/00008469-199703001-00009>
- Hooper, L. v., Stappenbeck, T. S., Hong, C. v., & Gordon, J. I. (2003). Angiogenins: a new class of microbicidal proteins involved in innate immunity. *Nature Immunology*, *4*(3), 269–273. <https://doi.org/10.1038/ni888>

- Howitt, M. R., Lavoie, S., Michaud, M., Blum, A. M., Tran, S. v., Weinstock, J. v., Gallini, C. A., Redding, K., Margolskee, R. F., Osborne, L. C., Artis, D., & Garrett, W. S. (2016). Tuft cells, taste-chemosensory cells, orchestrate parasite type 2 immunity in the gut. *Science*, *351*(6279), 1329–1333. <https://doi.org/10.1126/science.aaf1648>
- Ikeya, T., Maeda, K., Nagahara, H., Shibutani, M., Iseki, Y., & Hirakawa, K. (2016). *The combined expression of Semaphorin4D and PlexinB1 predicts disease recurrence in colorectal cancer*. <https://doi.org/10.1186/s12885-016-2577-6>
- Ireland, H., Houghton, C., Howard, L., & Winton, D. J. (2005). Cellular inheritance of a Cre-activated reporter gene to determine paneth cell longevity in the murine small intestine. *Developmental Dynamics*, *233*(4), 1332–1336. <https://doi.org/10.1002/dvdy.20446>
- Ito, D., & Kumanogoh, A. (2016). *Cell Adhesion & Migration The role of Sema4A in angiogenesis, immune responses, carcinogenesis, and retinal systems*. <https://doi.org/10.1080/19336918.2016.1215785>
- Ito, D., Nojima, S., Nishide, M., Okuno, T., Takamatsu, H., Kang, S., Kimura, T., Yoshida, Y., Morimoto, K., Maeda, Y., Hosokawa, T., Toyofuku, T., Ohshima, J., Kamimura, D., Yamamoto, M., Murakami, M., Morii, E., Rakugi, H., Isaka, Y., & Kumanogoh, A. (2015). mTOR Complex Signaling through the SEMA4A–Plexin B2 Axis Is Required for Optimal Activation and Differentiation of CD8 + T Cells . *The Journal of Immunology*, *195*(3), 934–943. <https://doi.org/10.4049/jimmunol.1403038>
- Ivanov, P., Emara, M. M., Villen, J., Gygi, S. P., & Anderson, P. (2011). Angiogenin-Induced tRNA Fragments Inhibit Translation Initiation. *Molecular Cell*, *43*(4), 613–623. <https://doi.org/10.1016/j.molcel.2011.06.022>
- Janssen, B. J. C., Malinauskas, T., Weir, G. A., Cader, M. Z., Siebold, C., & Jones, E. Y. (2012). Neuropilins lock secreted semaphorins onto plexins in a ternary signaling complex. *Nature Structural and Molecular Biology*, *19*(12), 1293–1299. <https://doi.org/10.1038/nsmb.2416>
- Janssen, B. J. C., Robinson, R. A., Pérez-Brangulý, F., Bell, C. H., Mitchell, K. J., Siebold, C., & Jones, E. Y. (2010). Structural basis of semaphoring-plexin signalling. *Nature*, *467*(7319), 1118–1122. <https://doi.org/10.1038/nature09468>
- Jenny, M., Uhl, C., Roche, C., Duluc, I., Guillermin, V., Guillemot, F., Jensen, J., Keding, M., & Gradwohl, G. (2002). Neurogenin3 is differentially required for endocrine cell fate specification in the intestinal and gastric epithelium. *The EMBO Journal*, *21*(23), 6338–6347. <https://doi.org/10.1093/emboj/cdf649>
- Jensen, J., Pedersen, E. E., Galante, P., Hald, J., Heller, R. S., Ishibashi, M., Kageyama, R., Guillemot, F., Serup, P., & Madsen, O. D. (2000). Control of

- endodermal endocrine development by Hes-1. *Nature Genetics*, 24(1), 36–44. <https://doi.org/10.1038/71657>
- Jian, H., Zhao, Y., Liu, B., & Lu, S. (2014). SEMA4b inhibits MMP9 to prevent metastasis of non-small cell lung cancer. *Tumour Biology: The Journal of the International Society for Oncodevelopmental Biology and Medicine*, 35(11), 11051–11056. <https://doi.org/10.1007/s13277-014-2409-8>
- Jian, H., Zhao, Y., Liu, B., & Lu, S. (2015). SEMA4B inhibits growth of non-small cell lung cancer in vitro and in vivo. *Cellular Signalling*, 27(6), 1208–1213. <https://doi.org/10.1016/j.cellsig.2015.02.027>
- Jiang, C., Javed, A., Kaiser, L., Nava, M. M., Zhao, D., Brandt, D. T., Fernández-Baldovinos, J., Zhou, L., Höß, C., Sawmynaden, K., Oleksy, A., Matthews, D., Weinstein, L. S., Gröne, H.-J., Niessen, C. M., Offermanns, S., Wickström, S. A., & Worzfeld, T. (2020). Mechanochemical control of epidermal stem cell divisions by B-plexins. *BioRxiv*.
- Kalluri, R., & Weinberg, R. A. (2009). The basics of epithelial-mesenchymal transition. In *Journal of Clinical Investigation* (Vol. 119, Issue 6, pp. 1420–1428). American Society for Clinical Investigation. <https://doi.org/10.1172/JCI39104>
- Karpus, O. N., Westendorp, B. F., Vermeulen, J. L. M., Meisner, S., Koster, J., Muncan, V., Wildenberg, M. E., & van den Brink, G. R. (2019). Colonic CD90+ Crypt Fibroblasts Secrete Semaphorins to Support Epithelial Growth. *Cell Reports*, 26(13), 3698-3708.e5. <https://doi.org/10.1016/J.CELREP.2019.02.101>
- Kleinman, H. K., & Martin, G. R. (2005). Matrigel: Basement membrane matrix with biological activity. In *Seminars in Cancer Biology* (Vol. 15, Issue 5 SPEC. ISS., pp. 378–386). Academic Press. <https://doi.org/10.1016/j.semcan.2005.05.004>
- Klostermann, A., Lohrum, M., Adams, R. H., & Püschel, A. W. (1998). The chemorepulsive activity of the axonal guidance signal semaphorin D requires dimerization. *Journal of Biological Chemistry*, 273(13), 7326–7331. <https://doi.org/10.1074/jbc.273.13.7326>
- Kolodkin, A. L., Matthes, D. J., & Goodman, C. S. (1993). The semaphorin genes encode a family of transmembrane and secreted growth cone guidance molecules. *Cell*, 75(7), 1389–1399. [https://doi.org/10.1016/0092-8674\(93\)90625-Z](https://doi.org/10.1016/0092-8674(93)90625-Z)
- Koo, B.-K., Stange, D. E., Sato, T., Karthaus, W., Farin, H. F., Huch, M., van Es, J. H., & Clevers, H. (2012). Controlled gene expression in primary Lgr5 organoid cultures. *Nature Methods*, 9(1), 81–83. <https://doi.org/10.1038/nmeth.1802>
- Korostylev, A., Worzfeld, T., Deng, S., Friedel, R. H., Swiercz, J. M., Vodrazka, P., Maier, V., Hirschberg, A., Ohoka, Y., Inagaki, S., Offermanns, S., &

- Kuner, R. (2008). A functional role for semaphorin 4D/plexin B1 interaction in epithelial branching morphogenesis during organogenesis. *Development*, 135(20), 3333–3343. <https://doi.org/10.1242/dev.019760>
- Kuipers, E. J., Grady, W. M., Lieberman, D., Seufferlein, T., Sung, J. J., Boelens, P. G., van de Velde, C. J. H., & Watanabe, T. (2015). Colorectal cancer. *Nature Reviews Disease Primers*, 1. <https://doi.org/10.1038/nrdp.2015.65>
- Kumanogoh, A., & Kikutani, H. (2013). Immunological functions of the neuropilins and plexins as receptors for semaphorins. In *Nature Reviews Immunology* (Vol. 13, Issue 11, pp. 802–814). <https://doi.org/10.1038/nri3545>
- Kumanogoh, A., Shikina, T., Suzuki, K., Uematsu, S., Yukawa, K., Kashiwamura, S. I., Tsutsui, H., Yamamoto, M., Takamatsu, H., Ko-Mitamura, E. P., Takegahara, N., Marukawa, S., Ishida, I., Morishita, H., Prasad, D. V. R., Tamura, M., Mizui, M., Toyofuku, T., Akira, S., ... Kikutani, H. (2005). Nonredundant roles of Sema4A in the immune system: Defective T cell priming and Th1/Th2 regulation in Sema4A-deficient mice. *Immunity*, 22(3), 305–316. <https://doi.org/10.1016/j.immuni.2005.01.014>
- Le, A. P., Huang, Y., Pingle, S. C., Kesari, S., Wang, H., Yong, R. L., Zou, H., & Friedel, R. H. (2015). Plexin-B2 promotes invasive growth of malignant glioma. *Oncotarget*, 6(9), 7293–7304. <https://doi.org/10.18632/oncotarget.3421>
- LeBlanc, J. G., Milani, C., de Giori, G. S., Sesma, F., van Sinderen, D., & Ventura, M. (2013). Bacteria as vitamin suppliers to their host: A gut microbiota perspective. In *Current Opinion in Biotechnology* (Vol. 24, Issue 2, pp. 160–168). *Curr Opin Biotechnol*. <https://doi.org/10.1016/j.copbio.2012.08.005>
- Li, D., Bell, J., Brown, A., & Berry, C. L. (1994). The observation of angiogenin and basic fibroblast growth factor gene expression in human colonic adenocarcinomas, gastric adenocarcinomas, and hepatocellular carcinomas. *The Journal of Pathology*, 172(2), 171–175. <https://doi.org/10.1002/path.1711720203>
- Li, H., Wu, D. K., & Sullivan, S. L. (1999). Characterization and expression of sema4g, a novel member of the semaphorin gene family. *Mechanisms of Development*, 87(1–2), 169–173. [https://doi.org/10.1016/S0925-4773\(99\)00125-2](https://doi.org/10.1016/S0925-4773(99)00125-2)
- Li, S., Goncalves, K. A., Lyu, B., Yuan, L., & Hu, G. fu. (2020). Chemosensitization of prostate cancer stem cells in mice by angiogenin and plexin-B2 inhibitors. *Communications Biology*, 3(1). <https://doi.org/10.1038/s42003-020-0750-6>
- Li, S., & Hu, G. F. (2012). Emerging role of angiogenin in stress response and cell survival under adverse conditions. In *Journal of Cellular Physiology* (Vol. 227, Issue 7, pp. 2822–2826). <https://doi.org/10.1002/jcp.23051>

- Li, X., Nadauld, L., Ootani, A., Corney, D. C., Pai, R. K., Gevaert, O., Cantrell, M. A., Rack, P. G., Neal, J. T., Chan, C. W. M., Yeung, T., Gong, X., Yuan, J., Wilhelmy, J., Robine, S., Attardi, L. D., Plevritis, S. K., Hung, K. E., Chen, C. Z., ... Kuo, C. J. (2014). Oncogenic transformation of diverse gastrointestinal tissues in primary organoid culture. *Nature Medicine*, *20*(7), 769–777. <https://doi.org/10.1038/nm.3585>
- Lieberkühn, J. N. (1745). *Dissertatio anatomico-physiologica de fabrica et actione villorum intestinorum tenuium hominis. Lugduni Batavorum: Apud Conrad et. Georg. Jac. Wishof, 1745.*
- Lopez-Garcia, C., Klein, A. M., Simons, B. D., & Winton, D. J. (2010). Intestinal stem cell replacement follows a pattern of neutral drift. *Science*, *330*(6005), 822–825. <https://doi.org/10.1126/science.1196236>
- Love, C. A., Harlos, K., Mavaddat, N., Davis, S. J., Stuart, D. I., Jones, E. Y., & Esnouf, R. M. (2003). The ligand-binding face of the semaphorins revealed by the high-resolution crystal structure of SEMA4D. *Nature Structural Biology*, *10*(10), 843–848. <https://doi.org/10.1038/nsb977>
- Lynch, H. T., & de la Chapelle, A. (2003). Hereditary Colorectal Cancer. *New England Journal of Medicine*, *348*(10), 919–932. <https://doi.org/10.1056/NEJMra012242>
- Maier, V., Jolicoeur, C., Rayburn, H., Takegahara, N., Kumanogoh, A., Kikutani, H., Tessier-Lavigne, M., Wurst, W., & Friedel, R. H. (2011). Semaphorin 4C and 4G are ligands of Plexin-B2 required in cerebellar development. *Molecular and Cellular Neuroscience*, *46*(2), 419–431. <https://doi.org/10.1016/j.mcn.2010.11.005>
- Matano, M., Date, S., Shimokawa, M., Takano, A., Fujii, M., Ohta, Y., Watanabe, T., Kanai, T., & Sato, T. (2015). Modeling colorectal cancer using CRISPR-Cas9-mediated engineering of human intestinal organoids. *Nature Medicine*, *21*(3), 256–262. <https://doi.org/10.1038/nm.3802>
- McKinley, E. T., Sui, Y., Al-Kofahi, Y., Millis, B. A., Tyska, M. J., Roland, J. T., Santamaria-Pang, A., Ohland, C. L., Jobin, C., Franklin, J. L., Lau, K. S., Gerdes, M. J., & Coffey, R. J. (2017). Optimized multiplex immunofluorescence single-cell analysis reveals tuft cell heterogeneity. *JCI Insight*, *2*(11). <https://doi.org/10.1172/jci.insight.93487>
- McLellan, M. A., Rosenthal, N. A., & Pinto, A. R. (2017). Cre-loxP-Mediated Recombination: General Principles and Experimental Considerations. *Current Protocols in Mouse Biology*, *7*(1), 1–12. <https://doi.org/10.1002/cpmo.22>
- Meehan, T. F., Witherden, D. A., Kim, C. H., Sendaydiego, K., Ye, I., Garijo, O., Komori, H. K., Kumanogoh, A., Kikutani, H., Eckmann, L., & Havran, W. L. (2014). Protection against colitis by CD100-dependent modulation of intraepithelial $\gamma\delta$ T lymphocyte function. *Mucosal Immunology*, *7*(1), 134–142. <https://doi.org/10.1038/mi.2013.32>

- Milano, J., McKay, J., Dagenais, C., Foster-Brown, L., Pognan, F., Gadiant, R., Jacobs, R. T., Zacco, A., Greenberg, B., & Ciaccio, P. J. (2004). Modulation of Notch Processing by γ -Secretase Inhibitors Causes Intestinal Goblet Cell Metaplasia and Induction of Genes Known to Specify Gut Secretory Lineage Differentiation. *Toxicological Sciences*, 82(1), 341–358. <https://doi.org/10.1093/toxsci/kfh254>
- Miron, N., & Cristea, V. (2012). Enterocytes: active cells in tolerance to food and microbial antigens in the gut. *Clinical & Experimental Immunology*, 167(3), 405–412. <https://doi.org/10.1111/j.1365-2249.2011.04523.x>
- Morgan, K. M., Riedlinger, G. M., Rosenfeld, J., Ganesan, S., & Pine, S. R. (2017). Patient-derived xenograft models of non-small cell lung cancer and their potential utility in personalized medicine. *Frontiers in Oncology*, 7(JAN). <https://doi.org/10.3389/fonc.2017.00002>
- Moroianu, J., & Riordan, J. F. (1994). Nuclear translocation of angiogenin in proliferating endothelial cells is essential to its angiogenic activity. *Proceedings of the National Academy of Sciences of the United States of America*, 91(5), 1677–1681. <https://doi.org/10.1073/pnas.91.5.1677>
- Muyrers, J. P. P., Zhang, Y., Testa, G., & Stewart, A. F. (1999). Rapid modification of bacterial artificial chromosomes by ET-recombination. *Nucleic Acids Research*, 27(6), 1555–1557. <https://doi.org/10.1093/nar/27.6.1555>
- Muzumdar, M. D., Tasic, B., Miyamichi, K., Li, L., & Luo, L. (2007). A global double-fluorescent Cre reporter mouse. *Genesis*, 45(9), 593–605. <https://doi.org/10.1002/dvg.20335>
- Nagai, H., Sugito, N., Matsubara, H., Tatematsu, Y., Hida, T., Sekido, Y., Nagino, M., Nimura, Y., Takahashi, T., & Osada, H. (2007). CLCP1 interacts with semaphorin 4B and regulates motility of lung cancer cells. *Oncogene*, 26(27), 4025–4031. <https://doi.org/10.1038/sj.onc.1210183>
- Nakagawa, Y., Takamatsu, H., Okuno, T., Kang, S., Nojima, S., Kimura, T., Kataoka, T. R., Ikawa, M., Toyofuku, T., Katayama, I., & Kumanogoh, A. (2011). Identification of Semaphorin 4B as a Negative Regulator of Basophil-Mediated Immune Responses. *The Journal of Immunology*, 186(5), 2881–2888. <https://doi.org/10.4049/jimmunol.1003485>
- Nakatsuji, Y., Okuno, T., Moriya, M., Sugimoto, T., Kinoshita, M., Takamatsu, H., Nojima, S., Kimura, T., Kang, S., Ito, D., Nakagawa, Y., Toyofuku, T., Takata, K., Nakano, M., Kubo, M., Suzuki, S., Matsui-Hasumi, A., Uto-Konomi, A., Ogata, A., ... Kumanogoh, A. (2012). Elevation of Sema4A Implicates Th Cell Skewing and the Efficacy of IFN- β Therapy in Multiple Sclerosis. *The Journal of Immunology*, 188(10), 4858–4865. <https://doi.org/10.4049/jimmunol.1102023>
- Neufeld, G., Mumblat, Y., Smolkin, T., Toledano, S., Nir-Zvi, I., Ziv, K., & Kessler, O. (2016). The role of the semaphorins in cancer. In *Cell Adhesion and*

- Migration* (Vol. 10, Issue 6, pp. 652–674). Taylor and Francis Inc. <https://doi.org/10.1080/19336918.2016.1197478>
- Neufeld, G., Sabag, A. D., Rabinovicz, N., & Kessler, O. (2012). Semaphorins in angiogenesis and tumor progression. *Cold Spring Harbor Perspectives in Medicine*, 2(1), a006718. <https://doi.org/10.1101/cshperspect.a006718>
- Nogi, T., Yasui, N., Mihara, E., Matsunaga, Y., Noda, M., Yamashita, N., Toyofuku, T., Uchiyama, S., Goshima, Y., Kumanogoh, A., & Takagi, J. (2010). Structural basis for semaphorin signalling through the plexin receptor. *Nature*, 467(7319), 1123–1127. <https://doi.org/10.1038/nature09473>
- O'Rourke, K., Dow, L., & Lowe, S. (2016). Immunofluorescent Staining of Mouse Intestinal Stem Cells. *BIO-PROTOCOL*, 6(4). <https://doi.org/10.21769/bioprotoc.1732>
- Paldy, E., Simonetti, M., Worzfeld, T., Bali, K. K., Vicuña, L., Offermanns, S., & Kuner, R. (2017). Semaphorin 4C Plexin-B2 signaling in peripheral sensory neurons is pronociceptive in a model of inflammatory pain. *Nature Communications*, 8(1). <https://doi.org/10.1038/s41467-017-00341-w>
- Parikh, K., Antanaviciute, A., Fawcner-Corbett, D., Jagielowicz, M., Aulicino, A., Lagerholm, C., Davis, S., Kinchen, J., Chen, H. H., Alham, N. K., Ashley, N., Johnson, E., Hublitz, P., Bao, L., Lukomska, J., Andev, R. S., Björklund, E., Kessler, B. M., Fischer, R., ... Simmons, A. (2019). Colonic epithelial cell diversity in health and inflammatory bowel disease. *Nature*, 567(7746), 49–55. <https://doi.org/10.1038/s41586-019-0992-y>
- Pascoe, H. G., Wang, Y., & Zhang, X. (2015). Structural mechanisms of plexin signaling. In *Progress in Biophysics and Molecular Biology* (Vol. 118, Issue 3, pp. 161–168). Elsevier Ltd. <https://doi.org/10.1016/j.pbiomolbio.2015.03.006>
- Pasterkamp, R. J. (2012). Getting neural circuits into shape with semaphorins. In *Nature Reviews Neuroscience* (Vol. 13, Issue 9, pp. 605–618). <https://doi.org/10.1038/nrn3302>
- Pastuła, A., Middelhoff, M., Brandtner, A., Tobiasch, M., Höhl, B., Nuber, A. H., Demir, I. E., Neupert, S., Kollmann, P., Mazzuoli-Weber, G., & Quante, M. (2016). Three-Dimensional Gastrointestinal Organoid Culture in Combination with Nerves or Fibroblasts: A Method to Characterize the Gastrointestinal Stem Cell Niche. *Stem Cells International*, 2016. <https://doi.org/10.1155/2016/3710836>
- Pelaseyed, T., Bergström, J. H., Gustafsson, J. K., Ermund, A., Birchenough, G. M. H., Schütte, A., van der Post, S., Svensson, F., Rodríguez-Piñeiro, A. M., Nyström, E. E. L., Wising, C., Johansson, M. E. V., & Hansson, G. C. (2014). The mucus and mucins of the goblet cells and enterocytes provide the first defense line of the gastrointestinal tract and interact with the immune system.

In *Immunological Reviews* (Vol. 260, Issue 1, pp. 8–20). Blackwell Publishing Ltd. <https://doi.org/10.1111/imr.12182>

- Perälä, N., Jakobson, M., Ola, R., Fazzari, P., Penachioni, J. Y., Nymark, M., Tanninen, T., Immonen, T., Tamagnone, L., & Sariola, H. (2011). Sema4C-Plexin B2 signalling modulates ureteric branching in developing kidney. *Differentiation*, *81*(2), 81–91. <https://doi.org/10.1016/j.diff.2010.10.001>
- Porter, E. M., Bevins, C. L., Ghosh, D., & Ganz, T. (2002). The multifaceted Paneth cell. In *Cellular and Molecular Life Sciences* (Vol. 59, Issue 1, pp. 156–170). Springer. <https://doi.org/10.1007/s00018-002-8412-z>
- Potiron, V., Nasarre, P., Roche, J., Healy, C., & Boumsell, L. (2007). Semaphorin signaling in the immune system. In *Advances in Experimental Medicine and Biology* (Vol. 600, pp. 132–144). Springer New York. https://doi.org/10.1007/978-0-387-70956-7_11
- Preibisch, S., Saalfeld, S., & Tomancak, P. (2009). Globally optimal stitching of tiled 3D microscopic image acquisitions. *Bioinformatics*, *25*(11), 1463–1465. <https://doi.org/10.1093/bioinformatics/btp184>
- Püschel, A. W., Adams, R. H., & Betz, H. (1995). Murine semaphorin D/collapsin is a member of a diverse gene family and creates domains inhibitory for axonal extension. *Neuron*, *14*(5), 941–948. [https://doi.org/10.1016/0896-6273\(95\)90332-1](https://doi.org/10.1016/0896-6273(95)90332-1)
- Rodríguez-Colman, M. J., Schewe, M., Meerlo, M., Stigter, E., Gerrits, J., Pras-Raves, M., Sacchetti, A., Hornsveld, M., Oost, K. C., Snippert, H. J., Verhoeven-Duif, N., Fodde, R., & Burgering, B. M. T. (2017). Interplay between metabolic identities in the intestinal crypt supports stem cell function. *Nature*, *543*(7645), 424–427. <https://doi.org/10.1038/nature21673>
- Rueden, C. T., Schindelin, J., Hiner, M. C., DeZonia, B. E., Walter, A. E., Arena, E. T., & Eliceiri, K. W. (2017). ImageJ2: ImageJ for the next generation of scientific image data. *BMC Bioinformatics*, *18*(1), 1–26. <https://doi.org/10.1186/s12859-017-1934-z>
- Sangiorgi, E., & Capecchi, M. R. (2008). Bmi1 is expressed in vivo in intestinal stem cells. *Nature Genetics*, *40*(7), 915–920. <https://doi.org/10.1038/ng.165>
- Sato, T., Clevers, H., Flier, L. G. van der, Clevers, H., Cheng, H., Leblond, C. P., Barker, N., Potten, C. S., Sangiorgi, E., Capecchi, M. R., Takeda, N., Montgomery, R. K., Powell, A. E., Buczacki, S. J., Snippert, H. J., Lopez-Garcia, C., Klein, A. M., Simons, B. D., Winton, D. J., ... Ledford, H. (2013). Growing Self-Organizing Mini-Guts from a Single Intestinal Stem Cell: Mechanism and Applications. *Science*, *340*(6137), 241–260. <https://doi.org/10.1126/science.1234852>
- Sato, T., Stange, D. E., Ferrante, M., Vries, R. G. J., van Es, J. H., van den Brink, S., van Houdt, W. J., Pronk, A., van Gorp, J., Siersema, P. D., & Clevers, H. (2011). Long-term expansion of epithelial organoids from human colon,

- adenoma, adenocarcinoma, and Barrett's epithelium. *Gastroenterology*, 141(5), 1762–1772. <https://doi.org/10.1053/j.gastro.2011.07.050>
- Sato, T., van Es, J. H., Snippert, H. J., Stange, D. E., Vries, R. G., van den Born, M., Barker, N., Shroyer, N. F., van de Wetering, M., & Clevers, H. (2011). Paneth cells constitute the niche for Lgr5 stem cells in intestinal crypts. *Nature*, 469(7330), 415–418. <https://doi.org/10.1038/nature09637>
- Sato, T., Vries, R. G., Snippert, H. J., van de Wetering, M., Barker, N., Stange, D. E., van Es, J. H., Abo, A., Kujala, P., Peters, P. J., & Clevers, H. (2009). Single Lgr5 stem cells build crypt-villus structures in vitro without a mesenchymal niche. *Nature*, 459(7244), 262–265. <https://doi.org/10.1038/nature07935>
- Sauer, B., & Henderson, N. (1988). Site-specific DNA recombination in mammalian cells by the Cre recombinase of bacteriophage P1. *Proceedings of the National Academy of Sciences of the United States of America*, 85(14), 5166–5170. <https://doi.org/10.1073/pnas.85.14.5166>
- Schepers, A., & Clevers, H. (2012). Wnt signaling, stem cells, and cancer of the gastrointestinal tract. *Cold Spring Harbor Perspectives in Biology*, 4(4), a007989. <https://doi.org/10.1101/cshperspect.a007989>
- Schindelin, J., Arganda-Carreras, I., Frise, E., Kaynig, V., Longair, M., Pietzsch, T., Preibisch, S., Rueden, C., Saalfeld, S., Schmid, B., Tinevez, J. Y., White, D. J., Hartenstein, V., Eliceiri, K., Tomancak, P., & Cardona, A. (2012). Fiji: An open-source platform for biological-image analysis. In *Nature Methods* (Vol. 9, Issue 7, pp. 676–682). Nature Publishing Group. <https://doi.org/10.1038/nmeth.2019>
- Schmidt, A., Tief, K., Foletti, A., Hunziker, A., Penna, D., Hummler, E., & Beermann, F. (1998). lacZ transgenic mice to monitor gene expression in embryo and adult. *Brain Research Protocols*, 3(1), 54–60. [https://doi.org/10.1016/S1385-299X\(98\)00021-X](https://doi.org/10.1016/S1385-299X(98)00021-X)
- Schuijers, J., Junker, J. P., Mokry, M., Hatzis, P., Koo, B. K., Sasselli, V., van der Flier, L. G., Cuppen, E., van Oudenaarden, A., & Clevers, H. (2015). Ascl2 acts as an R-spondin/wnt-responsive switch to control stemness in intestinal crypts. *Cell Stem Cell*, 16(2), 158–170. <https://doi.org/10.1016/j.stem.2014.12.006>
- Schulz, E., Klampfl, P., Holzapfel, S., Janecke, A. R., Ulz, P., Renner, W., Kashofer, K., Nojima, S., Leitner, A., Zebisch, A., Wölfler, A., Hofer, S., Gerger, A., Lax, S., Beham-Schmid, C., Steinke, V., Heitzer, E., Geigl, J. B., Windpassinger, C., ... Sill, H. (2014). Germline variants in the SEMA4A gene predispose to familial colorectal cancer type X. *Nature Communications*, 5(1), 1–11. <https://doi.org/10.1038/ncomms6191>
- Schwank, G., Andersson-Rolf, A., Koo, B. K., Sasaki, N., & Clevers, H. (2013). Generation of BAC Transgenic Epithelial Organoids. *PLoS ONE*, 8(10), 6–11. <https://doi.org/10.1371/journal.pone.0076871>

- Schwank, G., Koo, B. K., Sasselli, V., Dekkers, J. F., Heo, I., Demircan, T., Sasaki, N., Boymans, S., Cuppen, E., van der Ent, C. K., Nieuwenhuis, E. E. S., Beekman, J. M., & Clevers, H. (2013). Functional repair of CFTR by CRISPR/Cas9 in intestinal stem cell organoids of cystic fibrosis patients. *Cell Stem Cell*, *13*(6), 653–658. <https://doi.org/10.1016/j.stem.2013.11.002>
- Serra, D., Mayr, U., Boni, A., Lukonin, I., Rempfler, M., Challet Meylan, L., Stadler, M. B., Strnad, P., Papasaikas, P., Vischi, D., Waldt, A., Roma, G., & Liberali, P. (2019). Self-organization and symmetry breaking in intestinal organoid development. *Nature*, *569*(7754), 66–72. <https://doi.org/10.1038/s41586-019-1146-y>
- Shizuya, H., Birren, B., Kim, U. J., Mancino, V., Slepak, T., Tachiiri, Y., & Simon, M. (1992). Cloning and stable maintenance of 300-kilobase-pair fragments of human DNA in *Escherichia coli* using an F-factor-based vector. *Proceedings of the National Academy of Sciences of the United States of America*, *89*(18), 8794–8797. <https://doi.org/10.1073/pnas.89.18.8794>
- Shoshkes-Carmel, M., Wang, Y. J., Wangenstein, K. J., Tóth, B., Kondo, A., Massassa, E. E., Itzkovitz, S., & Kaestner, K. H. (2018). Subepithelial telocytes are an important source of Wnts that supports intestinal crypts. *Nature*, *557*(7704), 242–246. <https://doi.org/10.1038/s41586-018-0084-4>
- Sierra, J. R., Corso, S., Caione, L., Cepero, V., Conrotto, P., Cignetti, A., Piacibello, W., Kumanogoh, A., Kikutani, H., Comoglio, P. M., Tamagnone, L., & Giordano, S. (2008). Tumor angiogenesis and progression are enhanced by Sema4D produced by tumor-associated macrophages. *Journal of Experimental Medicine*, *205*(7), 1673–1685. <https://doi.org/10.1084/jem.20072602>
- Smeester, B. A., Slipek, N. J., Pomeroy, E. J., Bomberger, H. E., Shamsan, G. A., Peterson, J. J., Crosby, M. R., Draper, G. M., Becklin, K. L., Rahrmann, E. P., McCarthy, J. B., Odde, D. J., Wood, D. K., Largaespada, D. A., & Moriarity, B. S. (2020). SEMA4C is a novel target to limit osteosarcoma growth, progression, and metastasis. *Oncogene*, *39*(5), 1049–1062. <https://doi.org/10.1038/s41388-019-1041-x>
- Snippert, H. J., van der Flier, L. G., Sato, T., van Es, J. H., van den Born, M., Kroon-Veenboer, C., Barker, N., Klein, A. M., van Rheenen, J., Simons, B. D., & Clevers, H. (2010). Intestinal crypt homeostasis results from neutral competition between symmetrically dividing Lgr5 stem cells. *Cell*, *143*(1), 134–144. <https://doi.org/10.1016/j.cell.2010.09.016>
- Snoeck, V., Goddeeris, B., & Cox, E. (2005). The role of enterocytes in the intestinal barrier function and antigen uptake. In *Microbes and Infection* (Vol. 7, Issues 7–8, pp. 997–1004). Elsevier Masson SAS. <https://doi.org/10.1016/j.micinf.2005.04.003>
- Song, W., Cho, Y., Watt, D., & Cavalli, V. (2015). Tubulin-tyrosine ligase (TTL)-mediated increase in tyrosinated α -tubulin in injured axons is required for

- retrograde injury signaling and axon regeneration. *Journal of Biological Chemistry*, 290(23), 14765–14775. <https://doi.org/10.1074/jbc.M114.622753>
- Spit, M., Koo, B. K., & Maurice, M. M. (2018). Tales from the crypt: Intestinal niche signals in tissue renewal, plasticity and cancer. In *Open Biology* (Vol. 8, Issue 9). Royal Society Publishing. <https://doi.org/10.1098/rsob.180120>
- Sternberg, N., & Hamilton, D. (1981). Bacteriophage P1 site-specific recombination. I. Recombination between loxP sites. *Journal of Molecular Biology*, 150(4), 467–486. [https://doi.org/10.1016/0022-2836\(81\)90375-2](https://doi.org/10.1016/0022-2836(81)90375-2)
- Stevens, C. E., & Leblond, C. P. (1947). Rate of renewal of the cells of the intestinal epithelium in the rat. *The Anatomical Record*, 97(3), 373.
- Subramanian, V., & Feng, Y. (2007). A new role for angiogenin in neurite growth and pathfinding: Implications for amyotrophic lateral sclerosis. *Human Molecular Genetics*, 16(12), 1445–1453. <https://doi.org/10.1093/hmg/ddm095>
- Sun, T., Yang, L., Kaur, H., Pestel, J., Looso, M., Nolte, H., Krasel, C., Heil, D., Krishnan, R. K., Santoni, M. J., Borg, J. P., Bünemann, M., Offermanns, S., Swiercz, J. M., & Worzfeld, T. (2017). A reverse signaling pathway downstream of Sema4A controls cell migration via Scrib. *Journal of Cell Biology*, 216(1), 199–215. <https://doi.org/10.1083/jcb.201602002>
- Swiercz, J. M., Kuner, R., & Offermanns, S. (2004). Plexin-B1/RhoGEF-mediated RhoA activation involves the receptor tyrosine kinase ErbB-2. *Journal of Cell Biology*, 165(6), 869–880. <https://doi.org/10.1083/jcb.200312094>
- Takahashi, T., Fournier, A., Nakamura, F., Wang, L. H., Murakami, Y., Kalb, R. G., Fujisawa, H., & Strittmatter, S. M. (1999). Plexin-neuropilin-1 complexes form functional semaphorin-3A receptors. *Cell*, 99(1), 59–69. [https://doi.org/10.1016/S0092-8674\(00\)80062-8](https://doi.org/10.1016/S0092-8674(00)80062-8)
- Takeda, N., Jain, R., LeBoeuf, M. R., Wang, Q., Lu, M. M., & Epstein, J. A. (2011). Interconversion between intestinal stem cell populations in distinct niches. *Science*, 334(6061), 1420–1424. <https://doi.org/10.1126/science.1213214>
- Tamagnone, L., Artigiani, S., Chen, H., He, Z., Ming, G. L., Song, H. J., Chedotal, A., Winberg, M. L., Goodman, C. S., Poo, M. M., Tessier-Lavigne, M., & Comoglio, P. M. (1999). Plexins are a large family of receptors for transmembrane, secreted, and GPI-anchored semaphorins in vertebrates. *Cell*, 99(1), 71–80. [https://doi.org/10.1016/S0092-8674\(00\)80063-X](https://doi.org/10.1016/S0092-8674(00)80063-X)
- Tetteh, P. W., Basak, O., Farin, H. F., Wiebrands, K., Kretschmar, K., Begthel, H., van den Born, M., Korving, J., de Sauvage, F., van Es, J. H., van Oudenaarden, A., & Clevers, H. (2016). Replacement of Lost Lgr5-Positive Stem Cells through Plasticity of Their Enterocyte-Lineage Daughters. *Cell Stem Cell*, 18(2), 203–213. <https://doi.org/10.1016/j.stem.2016.01.001>

- Thaler, D. S., Stahl, M. M., & Stahl, F. W. (1987). Double-chain-cut sites are recombination hotspots in the red pathway of phage λ . *Journal of Molecular Biology*, 195(1), 75–87. [https://doi.org/10.1016/0022-2836\(87\)90328-7](https://doi.org/10.1016/0022-2836(87)90328-7)
- Tian, H., Biehs, B., Warming, S., Leong, K. G., Rangell, L., Klein, O. D., & de Sauvage, F. J. (2011). A reserve stem cell population in small intestine renders Lgr5-positive cells dispensable. *Nature*, 478(7368), 255–259. <https://doi.org/10.1038/nature10408>
- Toolan, H. W. (1953). Growth of Human Tumors in Cortisone-treated Laboratory Animals: The Possibility of Obtaining Permanently Transplantable Human Tumors. *Cancer Research*, 13(4–5), 389–394.
- Toyofuku, T., Nojima, S., Ishikawa, T., Takamatsu, H., Tsujimura, T., Uemura, A., Matsuda, J., Seki, T., & Kumanogoh, A. (2012). Endosomal sorting by Semaphorin 4a in retinal pigment epithelium supports photoreceptor survival. *Genes and Development*, 26(8), 816–829. <https://doi.org/10.1101/gad.184481.111>
- Toyofuku, T., Yabuki, M., Kamei, J., Kamei, M., Makino, N., Kumanogoh, A., & Hori, M. (2007). Semaphorin-4A, an activator for T-cell-mediated immunity, suppresses angiogenesis via Plexin-D1. *The EMBO Journal*, 26(5), 1373–1384. <https://doi.org/10.1038/sj.emboj.7601589>
- Tsuji, T., Sun, Y., Kishimoto, K., Olson, K. A., Liu, S., Hirukawa, S., & Hu, G. F. (2005). Angiogenin is translocated to the nucleus of HeLa cells and is involved in ribosomal RNA transcription and cell proliferation. *Cancer Research*, 65(4), 1352–1360. <https://doi.org/10.1158/0008-5472.CAN-04-2058>
- Valenta, T., Degirmenci, B., Moor, A. E., Herr, P., Zimmerli, D., Moor, M. B., Hausmann, G., Cantù, C., Aguet, M., & Basler, K. (2016). Wnt Ligands Secreted by Subepithelial Mesenchymal Cells Are Essential for the Survival of Intestinal Stem Cells and Gut Homeostasis. *Cell Reports*, 15(5), 911–918. <https://doi.org/10.1016/j.celrep.2016.03.088>
- van der Flier, L. G., & Clevers, H. (2009). Stem Cells, Self-Renewal, and Differentiation in the Intestinal Epithelium. *Annual Review of Physiology*, 71(1), 241–260. <https://doi.org/10.1146/annurev.physiol.010908.163145>
- van der Flier, L. G., Haegerbarth, A., Stange, D. E., van de Wetering, M., & Clevers, H. (2009). OLFM4 Is a Robust Marker for Stem Cells in Human Intestine and Marks a Subset of Colorectal Cancer Cells. *Gastroenterology*, 137(1), 15–17. <https://doi.org/10.1053/j.gastro.2009.05.035>
- van Es, J. H., van Gijn, M. E., Riccio, O., van den Born, M., Vooijs, M., Begthel, H., Cozijnsen, M., Robine, S., Winton, D. J., Radtke, F., & Clevers, H. (2005). Notch/ γ -secretase inhibition turns proliferative cells in intestinal crypts and adenomas into goblet cells. *Nature*, 435(7044), 959–963. <https://doi.org/10.1038/nature03659>

- van Es, M. A., Schelhaas, H. J., van Vught, P. W. J., Ticozzi, N., Andersen, P. M., Groen, E. J. N., Schulte, C., Blauw, H. M., Koppers, M., Diekstra, F. P., Fumoto, K., Leclerc, A. L., Keagle, P., Bloem, B. R., Scheffer, H., van Nuenen, B. F. L., van Blitterswijk, M., van Rheenen, W., Wills, A. M., ... van den Berg, L. H. (2011). Angiogenin variants in Parkinson disease and amyotrophic lateral sclerosis. In *Annals of Neurology* (Vol. 70, Issue 6, pp. 964–973). John Wiley & Sons, Ltd. <https://doi.org/10.1002/ana.22611>
- van Lidth de Jeude, J. F., Vermeulen, J. L. M., Montenegro-Miranda, P. S., van den Brink, G. R., & Heijmans, J. (2015). A Protocol for Lentiviral Transduction and Downstream Analysis of Intestinal Organoids. *Journal of Visualized Experiments*, 98. <https://doi.org/10.3791/52531>
- Varndell, I. M., Lloyd, R. v, Wilson, B. S., & Polak, J. M. (1985). Ultrastructural localization of chromogranin: potential marker for the electron microscopical recognition of endocrine cell secretory granules a. In *Histochemical Journal* (Vol. 17).
- Vintersten, K., Testa, G., Naumann, R., Anastassiadis, K., & Stewart, A. F. (2008). Bacterial artificial chromosome transgenesis through pronuclear injection of fertilized mouse oocytes. *Methods in Molecular Biology (Clifton, N.J.)*, 415, 83–100. https://doi.org/10.1007/978-1-59745-570-1_5
- Vlachogiannis, G., Hedayat, S., Vatsiou, A., Jamin, Y., Fernández-Mateos, J., Khan, K., Lampis, A., Eason, K., Huntingford, I., Burke, R., Rata, M., Koh, D. M., Tunariu, N., Collins, D., Hulkki-Wilson, S., Ragulan, C., Spiteri, I., Moorcraft, S. Y., Chau, I., ... Valeri, N. (2018). Patient-derived organoids model treatment response of metastatic gastrointestinal cancers. *Science*, 359(6378), 920–926. <https://doi.org/10.1126/science.aao2774>
- Vogelstein, B., Fearon, E. R., Hamilton, S. R., Kern, S. E., Preisinger, A. C., Leppert, M., Smits, A. M. m., & Bos, J. L. (1988). Genetic Alterations during Colorectal-Tumor Development. *New England Journal of Medicine*, 319(9), 525–532. <https://doi.org/10.1056/NEJM198809013190901>
- von Moltke, J., Ji, M., Liang, H. E., & Locksley, R. M. (2016). Tuft-cell-derived IL-25 regulates an intestinal ILC2-epithelial response circuit. *Nature*, 529(7585), 221–225. <https://doi.org/10.1038/nature16161>
- Wang, Xiaoliang, Zbou, C., Qiu, G., Fan, J., Tang, H., & Peng, Z. (2008). Screening of new tumor suppressor genes in sporadic colorectal cancer patients. *Hepato-Gastroenterology*, 55(88), 2039–2044. <http://www.ncbi.nlm.nih.gov/pubmed/19260473>
- Wang, Xiaosong, Kumanogoh, A., Watanabe, C., Shi, W., Yoshida, K., & Kikutani, H. (2001). Functional soluble CD100/sema4D released from activated lymphocytes: Possible role in normal and pathologic immune responses. *Blood*, 97(11), 3498–3504. <https://doi.org/10.1182/blood.V97.11.3498>

- Wang, Y., Pascoe, H. G., Brautigam, C. A., He, H., & Zhang, X. (2013). Structural basis for activation and non-canonical catalysis of the Rap GTPase activating protein domain of plexin. *ELife*, 2013(2). <https://doi.org/10.7554/eLife.01279.001>
- Weiner, H. L., Weiner, L. H., & Swain, J. L. (1987). Tissue distribution and developmental expression of the messenger RNA encoding angiogenin. *Science*, 237(4812), 280–282. <https://doi.org/10.1126/science.2440105>
- Whipple, R. A., Matrone, M. A., Cho, E. H., Balzer, E. M., Vitolo, M. I., Yoon, J. R., Ioffe, O. B., Tuttle, K. C., Yang, J., & Martin, S. S. (2010). Epithelial-to-mesenchymal transition promotes tubulin detyrosination and microtentacles that enhance endothelial engagement. *Cancer Research*, 70(20), 8127–8137. <https://doi.org/10.1158/0008-5472.CAN-09-4613>
- Williams-Hogarth, L. C., Puche, A. C., Torrey, C., Cai, X., Song, I., Kolodkin, A. L., Shipley, M. T., & Ronnett, G. v. (2000). Expression of semaphorins in developing and regenerating olfactory epithelium. *Journal of Comparative Neurology*, 423(4), 565–578. [https://doi.org/10.1002/1096-9861\(20000807\)423:4<565::AID-CNE3>3.0.CO;2-F](https://doi.org/10.1002/1096-9861(20000807)423:4<565::AID-CNE3>3.0.CO;2-F)
- Winberg, M. L., Noordermeer, J. N., Tamagnone, L., Comoglio, P. M., Spriggs, M. K., Tessier-Lavigne, M., & Goodman, C. S. (1998). Plexin A is a neuronal semaphorin receptor that controls axon guidance. *Cell*, 95(7), 903–916. [https://doi.org/10.1016/S0092-8674\(00\)81715-8](https://doi.org/10.1016/S0092-8674(00)81715-8)
- Witherden, D. A., Watanabe, M., Garijo, O., Rieder, S. E., Sarkisyan, G., Cronin, S. J. F., Verdino, P., Wilson, I. A., Kumanogoh, A., Kikutani, H., Teyton, L., Fischer, W. H., & Havran, W. L. (2012). The CD100 Receptor Interacts with Its Plexin B2 Ligand to Regulate Epidermal $\gamma\delta$ T Cell Function. *Immunity*, 37(2), 314–325. <https://doi.org/10.1016/j.immuni.2012.05.026>
- Witzgall, R., Brown, D., Schwarz, C., & Bonventre, J. v. (1994). Localization of proliferating cell nuclear antigen, vimentin, c-Fos, and clusterin in the postischemic kidney. Evidence for a heterogeneous genetic response among nephron segments, and a large pool of mitotically active and dedifferentiated cells. *Journal of Clinical Investigation*, 93(5), 2175–2188. <https://doi.org/10.1172/JCI117214>
- World Cancer Research Fund. (2018). Diet, nutrition, physical activity and colorectal cancer. *Continuous Update Project*, 1–62. dietandcancerreport.org
- Worzfeld, T., & Offermanns, S. (2014). Semaphorins and plexins as therapeutic targets. *Nature Reviews Drug Discovery*, 13(8), 603–621. <https://doi.org/10.1038/nrd4337>
- Worzfeld, T., Swiercz, J. M., Looso, M., Straub, B. K., Sivaraj, K. K., & Offermanns, S. (2012). ErbB-2 signals through Plexin-B1 to promote breast cancer metastasis. *Journal of Clinical Investigation*, 122(4), 1296–1305. <https://doi.org/10.1172/JCI60568>

- Xia, J., Swiercz, J. M., Bañón-Rodríguez, I., Matković, I., Federico, G., Sun, T., Franz, T., Brakebusch, C. H., Kumanogoh, A., Friedel, R. H., Martín-Belmonte, F., Gröne, H. J., Offermanns, S., & Worzfeld, T. (2015). Semaphorin-Plexin Signaling Controls Mitotic Spindle Orientation during Epithelial Morphogenesis and Repair. *Developmental Cell*, 33(3), 299–313. <https://doi.org/10.1016/j.devcel.2015.02.001>
- Xiao, K., Liu, Q., Peng, G., Su, J., Qin, C. Y., & Wang, X. Y. (2020). Identification and validation of a three-gene signature as a candidate prognostic biomarker for lower grade glioma. *PeerJ*, 2020(1). <https://doi.org/10.7717/peerj.8312>
- Yan, H., Wu, L., Shih, C., Hou, S., Shi, J., Mao, T., Chen, W., Melvin, B., Rigby, R. J., Chen, Y., Jiang, H., Friedel, R. H., Vinuesa, C. G., & Qi, H. (2017). Plexin B2 and Semaphorin 4C Guide T Cell Recruitment and Function in the Germinal Center. *Cell Reports*, 19(5), 995–1007. <https://doi.org/10.1016/j.celrep.2017.04.022>
- Yan, K. S., Chia, L. A., Li, X., Ootani, A., Su, J., Lee, J. Y., Su, N., Luo, Y., Heilshorn, S. C., Amieva, M. R., Sangiorgi, E., Capecchi, M. R., & Kuo, C. J. (2012). The intestinal stem cell markers Bmi1 and Lgr5 identify two functionally distinct populations. *Proceedings of the National Academy of Sciences of the United States of America*, 109(2), 466–471. <https://doi.org/10.1073/pnas.1118857109>
- Yang, Q., Bermingham, N. A., Finegold, M. J., & Zoghbi, H. Y. (2001). Requirement of Math1 for secretory cell lineage commitment in the mouse intestine. *Science*, 294(5549), 2155–2158. <https://doi.org/10.1126/science.1065718>
- Yoshioka, N., Wang, L., Kishimoto, K., Tsuji, T., & Hu, G. F. (2006). A therapeutic target for prostate cancer based on angiogenin-stimulated angiogenesis and cancer cell proliferation. *Proceedings of the National Academy of Sciences of the United States of America*, 103(39), 14519–14524. <https://doi.org/10.1073/pnas.0606708103>
- Youming, Z., Frank, B., Joep, M., & Francis, S. (1998). A new logic for DNA engineering using recombination in *Escherichia coli*. *Nature Genetics*, 20(2), 123–128. <https://doi.org/10.1038/2417> PM - 9771703 M4 - Citavi
- Yu, D., Ellis, H. M., Lee, E. C., Jenkins, N. A., Copeland, N. G., & Court, D. L. (2000). An efficient recombination system for chromosome engineering in *Escherichia coli*. *Proceedings of the National Academy of Sciences of the United States of America*, 97(11), 5978–5983. <https://doi.org/10.1073/pnas.100127597>
- Yu, W., Goncalves, K. A., Li, S., Kishikawa, H., Sun, G., Yang, H., Vanli, N., Wu, Y., Jiang, Y., Hu, M. G., Friedel, R. H., & Hu, G. (2017). Plexin-B2 Mediates Physiologic and Pathologic Functions of Angiogenin. *Cell*, 171(4), 849–864.e25. <https://doi.org/10.1016/j.cell.2017.10.005>

- Zhou, H., Kann, M. G., Mallory, E. K., Yang, Y. H., Bugshan, A., Binmadi, N. O., & Basile, J. R. (2017). Recruitment of Tiam1 to Semaphorin 4D Activates Rac and Enhances Proliferation, Invasion, and Metastasis in Oral Squamous Cell Carcinoma. *Neoplasia (United States)*, 19(2), 65–74. <https://doi.org/10.1016/j.neo.2016.12.004>
- Zielonka, M., Xia, J., Friedel, R. H., Offermanns, S., & Worzfeld, T. (2010). A systematic expression analysis implicates Plexin-B2 and its ligand Sema4C in the regulation of the vascular and endocrine system. *Experimental Cell Research*, 316(15), 2477–2486. <https://doi.org/10.1016/j.yexcr.2010.05.007>

Academic Teachers

My academic teachers in Marburg were:

Dr. Till Adhikary, Prof. Dr. Stefan Bauer, Prof. Dr. Uta-Maria Bauer, Dr. Dominique Brandt, Prof. Dr. Alexander Brehm, PD Dr. Cornelia Brendel, Prof. Dr. Frank Czubayko, Prof. Dr. Dr. Jürgen Daut, Prof. Dr. Hans-Peter Elsässer, PD Dr. Barbara Fritz, Prof. Dr. Karl-Heinz Grzeschik, Dr. Jörg Hänze, Prof. Dr. Ralf Jacob, Prof. Dr. Matthias Lauth, Prof. Dr. Roland Lill, Prof. Dr. Michael Lohoff, Prof. Dr. Andrea Maisner, Dr. Jacqueline Mermoud, Dr. Wiebke Milani, Prof. Dr. Roland Moll, Prof. Dr. Rolf Müller, Dr. Sabine Müller-Brüsselbach, Prof. Dr. Dominik Oliver, Prof. Dr. Axel Frieder Pagenstecher, Prof. Dr. Sabine Pankuweit, Prof. Dr. Timothy D. Plant, PD Dr. Regina Preisig-Müller, Dr. Ansgar Schmidt, Prof. Dr. Thorsten Stiewe, Prof. Dr. Guntram Suske, PD Dr. Reiner Westermann, Prof. Dr. Thomas Worzfeld, Dr. Christian Wrocklage.

Danksagung

An dieser Stelle möchte ich mich bei all denen bedanken, die mich während meiner Promotionszeit am Pharmakologischen Institut der Philipps-Universität in Marburg auf unterschiedlichste Weise unterstützt haben:

Herrn Prof. Dr. Thomas Worzfeld danke ich für die Möglichkeit, meine Doktorarbeit unter seiner Führung anfertigen zu können, seine Unterstützung war vielseitiger Natur und von unschätzbarem Wert. Insbesondere für die fachliche Anleitung und Diskussion, Konferenzteilnahmen, das Ermöglichen wichtiger Kooperationen, sowie die Durchsicht dieser Arbeit möchte ich mich herzlich bedanken.

Den Mitarbeitern und Kollegen des Pharmakologischen Instituts möchte ich meinen Dank ausdrücken für die zweifellos einzigartige Arbeitsatmosphäre, anregende Diskussion und technische Unterstützung.

Für die fruchtbare Zusammenarbeit bei der Etablierung der humanen Organotide bedanke ich mich bei der Abteilung für Viszeral-, Thorax- und Gefäßchirurgie des Universitätsklinikums Marburg unter Leitung von Herrn Prof. Dr. Detlef K. Bartsch, sowie den Mitarbeitern des Instituts für Pathologie des Universitätsklinikums Marburg unter der Leitung von Prof. Dr. Roland Moll. Insbesondere Herr PD Dr. Leif Schiffmann war eine treibende Kraft.

Weiterhin gebührt mein Dank unseren Kooperationspartnern des Max-Planck-Instituts für Herz- und Lungenforschung in Bad Nauheim für die Zusammenarbeit bei der Zucht des Alpi-Cre2 Mausstamms. Ferner danke ich Herrn Dr. Mario Looso für die Zusammenarbeit.

Herrn Prof. Dr. Hermann-Josef Gröne danke ich für die Gelegenheit, in seinem Labor die smRNA FISH-Methode zu erlernen, die für diese Arbeit von zentraler Bedeutung war.

Michael Mazzola danke ich für die Überlassung der Angiogenin-Knockoutproben, sowie für seinen Einsatz bei der Überwindung der Versandschwierigkeiten.

Meinen Doktoranden-Kolleginnen und Kollegen möchte ich danken für all die guten Zeiten, die wir gemeinsam erlebt haben. Ivana, Jessi, Javier und Carsten, jeder von euch auf seine Art hat diesen Abschnitt zu etwas Besonderem gemacht.

Meiner Partnerin Janin möchte ich für das entgegengebrachte Vertrauen in dieser Zeit danken. Ihr Verständnis hat mir stets ein Gefühl der Sicherheit gegeben, das vieles leichter gemacht hat.

Meinen Eltern und Geschwistern danke ich herzlich für ihre Unterstützung, ihr Verständnis und ihre Geduld während meines Werdegangs, ohne die diese Arbeit so nicht möglich gewesen wäre.